CR 73162

PLANET GEOMETRIC CENTER TRACKER

VOLUME I

By W. H. Alff, A. R. Kraemer, and E. G. Fleenor

31 August 1967

PREPARED UNDER CONTRACT NO. NAS 2-2485 BY

LOCKHEED MISSILES & SPACE COMPANY

SUNNYVALE, CALIFORNIA

FOR

AMES RESEARCH CENTER
NATIONAL AERONAUTICS AND SPACE ADMINISTRATION

PLANET GEOMETRIC CENTER TRACKER

VOLUME I

By W. H. Alff, A. R. Kraemer, and E. G. Fleenor

31 August 1967

PREPARED UNDER CONTRACT NO. NAS 2-2485 BY

LOCKHEED MISSILES & SPACE COMPANY

SUNNYVALE, CALIFORNIA

FOR

AMES RESEARCH CENTER
NATIONAL AERONAUTICS AND SPACE ADMINISTRATION

TABLE OF CONTENTS

VOLUME I

FOREWORD

This final report was prepared by Lockheed Missiles and Space Company, for the National Aeronautics and Space Administration, Ames Research Center, under Contract NAS 2-2485. This research is basically advanced sensor development and was conducted over the period from October 1964 to July 1967.

A B S T R A C T

PLANET GEOMETRIC CENTER TRACKER

The tracker locates the geometric center of Mars, Venus, or Jupiter with angular accuracy on the order of 1 arc second, regardless of whether the planet appears gibbous or crescent-shaped. The tracker functions over the full range of illuminations and radii for these three planets. The basic scheme involves the use of a roulette type circular scan, constrained to be circular, around the planet's edge and evaluation of the harmonic content of the signal generated by the tracker detector, an image dissector.

The expected performance of the tracker was analyzed using an analog simulator and digital computer. The predicted performance exceeded all requirements. The actual performance was determined with the breadboard tracker using an LMSC 40-foot collimator with focal plane translation of planet masks to simulate actual planet geometry. The tracker performed almost as well as predicted and the results firmly establish the practical basis for this technique to be used in operational hardware.

Lockheed
MISSILES
& SPACE
COMPANY

30 August 1967

TECHNICAL DESCRIPTION OF THE PLANET GEOMETRIC CENTER TRACKER

Lockheed Missiles and Space Company has recently completed a breadboard development fixed price contract for NASA/Ames Research Center for a Planet Geometric Center Tracker.

The tracker locates the geometric center of Mars, Venus, or Jupiter with angular accuracy on the order of 1 arc second, regardless of whether the planet appears gibbous or crescent-shaped. The tracker functions over the full range of illuminations and radii for these three planets. The basic scheme involves the use of a roulette type circular scan, constrained to be circular, around the planet's edge and evaluation of the harmonic content of the signal generated by the tracker detector, an image dissector.

The expected performance of the tracker was analyzed using an analog simulator and digital computer. The predicted performance exceeded all requirements. The actual performance was determined with the breadboard tracker using an LMSC 40-foot collimator with focal plane translation of planet masks to simulate actual planet geometry. The tracker performed almost as well as predicted and the results firmly establish the practical basis for this technique to be used in operational hardware.

The operating characteristics of the breadboard tracker are as follows:

Field of View	4.5 x 4.5 minutes	Tracking Rate	15 arc sec./sec.
Error Signal Slope	180 mv/arc sec.	Offset Error	0.2 to 1.5 arc seconds depending on illumination and planet shape
Noise Equivalent Angle	0.17 arc sec.		
Linear Slope Limits	$\pm$ 2.25 arc min.		

The research breadboard was carried to a state of completion where it is possible to construct an engineering model planet tracker without difficulty. For example, optical, mechanical, and electronic designs are now available to generate the design of an engineering model. The engineering model of a flight configuration tracker could have all of the above performance characteristics; its estimated weight, power consumption, and size are 20 pounds, 5 watts, and 8.5 inches diameter x 13.5 inches long, respectively.

The original objective of the planet tracker was for long range pointing. Additional possible applications are pointing laser beams for communication purposes, approach guidance, and lunar and earth horizon sensing. The basic tracker design is flexible enough to allow reconfiguration to meet these applications easily.

SYMBOLS

SYMBOL	UNIT
A	ampere
cm	centimeter
c/s	cycles per second
^{o}C	degrees Centigrade
^{o}K	degrees Kelvin
ft.	feet
in.	inch
uA	microampere
uV	microvolt
mil	.001 inch
mA	milliampere
ms	millisecond
mV	millivolt
nA	nanoampere
"	second (angle)
s	second (time)
V	volt
NEB (f)	noise equivalent bandwidth
S/N	signal to noise ratio
d.u.	decentration unit (0.1 planet radius)
NEA	noise equivalent angle
FOV	field of view

Section 1
INTRODUCTION

This introductory section describes in general terms the project requirements, the achieved results, both analytical and experimental, and the final report structure. Necessary definitions and nomenclature are provided to aid the reader in understanding the report contents.

The purpose of the Precision Planet Tracker developed at Lockheed Missiles and Space Company, under Contract NAS 2-2485 to the National Aeronautics and Space Administration, Ames Research Center, is to locate the geometric center of certain planets (Mars, Venus, Jupiter) with high angular accuracy, on the order of seconds of arc, under varying illumination conditions. For example, in a typical operation, the planet tracker would provide attitude error signals to point precisely an earth orbiting experimental package in the direction of a given planet. Accuracies of better than 1.6 arc seconds have been achieved for planets subtending angles from 10 to 60 arc seconds under illumination conditions varying from 1/2 to full illumination.

The tracking of the geometric center rather than the illumination center of a planet is particularly significant for these reasons:

1. For long experiment exposure times relative to a particular point on a planet, the illumination center may move several arc seconds relative to the geometric center, causing the image to smear.
2. A particular point on a given planet can always be reacquired at a later time regardless of the planet illumination.
3. Precise spatial mapping can be performed by biasing the planet tracker away from the geometric center.
4. For experiments having loose roll control, motion about the geometric center would be more tolerable than motion about the illumination center.
5. The geometric center of a planet is a more precisely known astronomical reference than the illumination center.

The planet tracker program was based on LMSC Proposal 893537 (Ref. 1.1), and the resulting subcontracts, NAS 2-2485 and NAS 2-2485 F/O (Ref.1.2 and 1.3), and had these general objectives:

- Compilation of planet illumination and radiation data.
- Trade-off analyses of various tracking schemes, including infrared and visible radiometric and edge tracking concepts.

- Generation of detailed tracker design.
- Fabrication of breadboard tracker.
- Experimental verification of tracker performance.
- Design, fabricate, and test planet simulator.
- Perform optimization analysis to determine theoretically maximum tracker performance.
- Write final report.
- Participate in visits to various NASA centers, describing the program results.

The program proceeded generally along the paths suggested by the preceding work items. We were committed to consider visible edge tracking according to the general concepts specified in the proposal, unless it were clearly shown, by virtue of some of the preliminary analyses, that other techniques would be superior. Infrared edge tracking techniques and visible and infrared radiometric balance techniques were evaluated in the early phases of the program. The basic concept, reduced to breadboard hardware, was essentially as originally intended and proposed, i.e., visible edge tracking based on a determination and selection of certain harmonics which were maximized or minimized at tracking null.

The program proceeded normally for a research breadboard hardware program. For example, the computer evaluation of the harmonic content of various error signals provided results which initially did not correlate in detail with the results obtained on the analog simulator and by mathematical analysis. The computer analysis was iterated three times before complete agreement was obtained. This report describes the accomplished activities as though they were accomplished in a logical routine chronological fashion, although it is clear that the actual sequence of events included many redesigns, re-evaluations, and modifications in both the analysis and hardware areas.

As an aid to understanding the material presented in the following sections, certain definitions and nomenclature should be understood.

- Crescent Planet: The apparent shape of the planet when the sun is illuminating the planet from behind; for this condition, the planet can appear as a thin crescent-shaped sliver. The planet appears to be composed of a semicircular segment and an elliptical segment in concave form.
- Gibbous Planet: This condition of illumination is essentially complementary to the condition of crescent illumination. Here the planet, as seen by the observer, is nearly completely illuminated with the exception of one edge where the projection of the terminator as seen by the observer is elliptical. The planet appears to be composed of a semicircular segment and an elliptical segment in convex form.

- Roulette Scanning Pattern: The scan pattern used in the final version of the planet tracker is a roulette pattern which appears as a series of connected small circular spirals formed around the circular part of the planet edge.
- Decentration Unit: The angular separation between the geometric center of the scan pattern is specified in terms of decentration units. One decentration unit is that angular distance where the scan pattern center is separated from the planet's geometric center by one tenth of the planet radius. The magnitude of a decentration unit in arc seconds depends on the planet being tracked.

This report is organized as follows:

The section immediately following this one is Section 2, the Summary, which is designed to present to the reader all essential points concerning the program and its results.

Section 3 contains a summary of Planet Characteristics which have been compiled through interactions with various astronomers and through evaluation of the literature. Planet illumination characteristics, size and shape, color temperature, and black body temperatures are discussed with emphasis on the planet tracking applications.

Section 4 contains the results of a short study on various Planet Tracking Techniques. Included in this section are the general trade-offs between energy balance and edge tracking approaches in both the visible and infrared parts of the spectrum. Several edge tracking approaches are considered and one visible edge tracking approach is selected as being the most promising. It is this approach and its evolutions which are explored more thoroughly in the subsequent sections of the report.

Section 5 is titled General Tracker Design Considerations, and treats several particular cases of visible edge tracking schemes which take the reader through the various design iterations leading to the final configuration. It is based on material contained in the preceding section, Section 4, and treats the visible edge tracking approach in greater detail and explores several possible ways of achieving the technical objectives. It contains information on the various computer, analog simulator, and mathematical analyses which were used to refine and modify the block diagram.

Section 6 describes the Detail Instrument Design. By this stage of the program and report, we have concluded that a specific design approach is a satisfactory solution to the technical objectives. This section describes the final electronic, mechanical, and optical approaches in technical detail. Several changes to the final design are discussed in this section, which result from evaluation of breadboard tests on various electronic sub-assemblies. However, these changes are not of major significance and the concept remained unchanged.

Performance Tests are described in Section 7, which also includes descriptions of test planning, test procedures, and test instrumentation. The actual test results are compared to the tracker's predicted performance. In particular, signal to noise ratios are determined from Mars, Venus, and Jupiter along with tracker linearity and noise equivalent angle.

Section 8 discusses the conclusions, provides several overall comments, and makes specific recommendations concerning possible follow-on programs and describes potential uses.

Volume II contains the results of the edge tracking optimization study which resulted from a follow-on contract, Reference 1.3.

SECTION 2
SUMMARY

This section provides a general chronology of the program and summarizes the technical aspects.

The RFP requirements were that a research breadboard tracker be developed which would locate the geometric center of Mars, Venus, or Jupiter with high angular accuracy, on the order of 1 second of arc, regardless of planet illumination. The requirement is that the geometric center be located whether the planet appears in circular or gibbous form. As originally intended, the tracker would have its eventual application in pointing an astronomical observatory to any geometric location on the planet with high pointing accuracy. The RFP also required that a trade-off analysis be accomplished between various visible and infrared radiometric energy balance techniques before detailed tracker design and breadboard tests were begun.

The original concept proposed by LMSC has remained essentially unchanged, although its implementation was considerably more complex than originally envisioned. The basic scheme proposed used an image dissector (an imaging detector where a small aperture, behind which are electron multipliers, is electronically scanned across the image) scanning along the circular edge of the planet in a roulette pattern. The scanning pattern is generated by imposing on the x and y deflection plates of the image dissector, sinusoidal voltages 90° out of phase, the resulting pattern is circular with smaller scanning circles superimposed on the edge of the larger circle. The reader is referred to the photographs of Figures 6.1, 6.2, 6.3, and 6.4. The larger scanning circle is generated by sinusoidal waveforms of frequency W_0, and the smaller circles are generated by sine waves at frequency nW_0. There are (n-1) loops in a complete scan. The resulting video signal out of the image dissector has principal frequency components at W_0 and $(n-1)W_0$.

The proposed tracking scheme accomplishes the search function by expanding and contracting the size of the larger scan circle until a planet crossing signal is obtained and then phase detecting the signal with respect to the x and y W_0 drive voltages. The center of the scan pattern is then moved in the direction of the planet. We proposed to fine track the planet by examination of the second harmonics of the $(n-1)W_0$ component. The output waveform is a symmetrical square wave at a frequency of $(n-1)W_0$ for coincidence of the center of a circular planet image and the center of the scan circle. For small decentrations, the square wave is pulse width modulated and the resulting output contains finite second harmonic voltages. Thus, by nulling the second harmonic, the scan would be accurately centered on the planet's center.

For gibbous planets, when the scan center and planet center were coincident, the second harmonic signal would also be zero because there would be no pulse width modulation with the exception of those few pulses where the circular horizon and the gibbous terminator met. It was felt that the second harmonic contribution from these pulses would not be significant. These preceding paragraphs, then, summarize the originally proposed design.

To satisfy contractual requirements, analyses were performed to determine the validity of the proposed approach compared to infrared and visible energy balance schemes. The results of the investigations indicated that the logic associated with locating the planet center from its illumination centroid would be extremely complex. Evaluation of the infrared approach indicated that insufficient energy would be available within the aperture size constrained by tracker size and volume. It was therefore concluded that visible edge tracking was the best approach.

The design concept for visible edge tracking was examined in detail through three complementary approaches. The first involved the derivation and hand-calculation of the harmonic content of the video signal. The second involved analyses performed on the digital computer. The third involved the use of an analog simulator. This last technique proved to be extremely valuable in the actual design and testing of the planet tracker electronics. Each of these techniques is briefly discussed in the following paragraphs.

The hand calculation approach involved classical Fourier waveform analyses with a desk calculator being used to compute the magnitude of the various harmonics for given decentrations. This technique provided immediate results, but was, of course, tedious and calculations were soon performed using large digital computers based on established Fourier analysis programs. Large quantities of data were generated, but this part of the activity was dogged by minor programming errors, some of which only gave erroneous results for certain extreme cases.

The third approach utilized an analog simulator which consists of an oscilloscope, scope camera housing, and photomultiplier. Masks simulating planet shapes are placed on the face of the cathode ray tube and the oscilloscope beam is deflected by the same x-y voltages that are applied to the Reconotron. The oscilloscope beam then crosses the edge of the mask in the same way that the Reconotron beam crosses the edge of a planet image. The photomultiplier reads the light output and provides a video signal. This signal is exactly the same signal as the signal at the Reconotron output. Therefore, the analog simulator accurately simulates the planet tracker optics and Reconotron.

Data relating harmonic content to decentration for various planet sizes and shapes are generated by each of the three methods and the results compared. Small, but significant, differences were found between the digital computer results and the analog simulator data. Careful examination of the data showed that there were errors in the computer program. The results of the

final data showed clearly that the proposed tracking scheme would not work and that it was possible and even likely that false nulls would be obtained for the $2(n-1)W_0$ component which would indicate that the scan pattern center and the planet center were coincident when, in fact, they were not. The cause arises from some of the subtle interactions between the beam and the planet edge, and is particularly significant for gibbous planets. Using the computer results, where the harmonic content of the first 40 harmonics were plotted as a function of x and y decentration for various gibbosities, it was determined that additional logic would be needed to locate the planet center unambiguously.

This logic took the form of additional modulation of the scan pattern (slither, both fine and coarse) and examination of the nulls and peaks of several harmonics.

The details are too involved to be discussed here, but briefly it was determined that for all cases of planet size and shapes considered, the $(n-1)^{th}$ harmonic had a peak while the $2(n-1)-1^{th}$ harmonic had a minimum for coincidence of scan center and planet center. The problem is in determining whether the peak is a true maximum or a secondary peak. Verification that the peak is a maximum is done by electronically displacing the scan center through the application of coarse and fine slither voltages and then examining the way the amplitude of the $(n-1)^{th}$ harmonic changes. The reader is referred to Section 5 for a more detailed explanation. The addition of these modulation voltages made possible the successful performance of the tracker.

The versatility of the analog simulator enabled the entire planet tracker electronic design to be accomplished and tested without the Reconotron. This was particularly important because the Reconotron was late in delivery. Output voltages from the analog simulator photomultiplier were fed directly into the planet tracker preamp and other circuits were required to function as they would in the planet tracker itself; thus, when the Reconotron was received, practically all the electronics, with the exception of those few circuits that were unique to the Reconotron, had already been checked out.

Some difficulty was encountered in obtaining a Reconotron which met our specifications. Reconotrons available in 1965 had, according to the data sheet, excellent linearity. However, linearity was defined in terms of radial line segments through the center of the face plate. In fact, the tubes generally suffered from pincushion distortion, and the definition of linearity does not provide an assessment of this type of distortion. With the cooperation of CBS Laboratories, we eventually obtained a tube with linearity which was satisfactory and was considerably better than the worst case linearity they quoted.

When the Reconotron arrived, it was assembled within the electronics and the system debugging began. Electronic compatibility was obtained through electronic bench checks, after which the assembled electronics with the Reconotron was coupled to the optical system. The optical system is fairly straightforward and consists of a Zoomar objective 5" in diameter and 40." focal length. The Zoomar's image is magnified by a small Luminar relay lens which provides a magnification of 10 times. The Luminar image falls directly on the face plate of the Reconotron. Both the Luminar and the Reconotron are mounted on x-y slides so that optical adjustments and alignments and data acquisition is facilitated. The assembled planet tracker was stimulated using a 40-foot collimator with planet masks at its focal point. The source mount included a tungsten ribbon filament lamp, the masks in the mask holder, and a slide to allow translating the mask to provide planet motion. The performance of the completed planet tracker was evaluated using this setup.

The actual performance of the tracker was such that, with a 10-cycle output bandwidth, the logic circuits function properly with a S/N of 10. Under this condition, an output linearity of $\pm$ 1.6 arc seconds can be expected. In the present breadboard configuration, Venus will far exceed the required signal to noise ratio and Mars provides a marginal signal to noise ratio. Jupiter cannot be tracked because the calculated signal to noise ratio using all the existing components (Degradation in the resolution of the Reconotron and the transmission losses in the optical system degrade the signal to noise ratio) is only two to one. Several alternatives are available which will allow the tracker to perform its function. For example, obtaining a Reconotron with the advertised resolution and reducing the system bandwidth sufficiently that the required signal to noise ratio can be obtained.

Based on inputs provided by LMSC's AAP team, it is felt that one-cycle output bandwidths are not unreasonable. The breadboard tracker will meet all requirements with a one-cycle output bandwidth. Performance improvements which allow utilization of the bandwidth on the order of three cycles per second are possible with better Reconotron resolution. It was felt that these improvements are completely within the current state of the art.

We conclude that there is no doubt that locating the geometric center of Mars, Venus, and Jupiter under all conditions of illumination is entirely feasible. The completed program provides the basis for accomplishing a detailed design which will meet the requirements for precision pointing. The program also provides the basis for activity extension in the areas of tracker refinements. One of the advantages of this tracking scheme is its flexibility. It is possible, with slight modification, to measure planet radius, gibbosity, and location of the terminator. Current applications emphasize optical approach guidance and possibly earth or lunar horizon sensing. This tracking scheme probably allows for relatively easy adaptability to these applications.

Section 3

PLANET RADIATION CHARACTERISTICS

3.1 INTRODUCTION AND SUMMARY

This section contains a compilation of data on planetary radiation characteristics obtained from the literature and from recent conversations with planetary astronomers. This information is essential to the successful design of a precision planet tracker whether it operates in the infrared or visible regions of the spectrum, whether it imploys edge tracking or radiometric balance.

Of the three planets considered in detail, Venus is brightest with a visual magnitude of about -4, Jupiter is next brightest with a visual magnitude of about -2, and Mars is dimmest with a visual magnitude ranging from +.5 to about -2 for the range of orbital locations considered. For edge tracking sensors, it is important to consider the illumination (lumens per square centimeter) from an elemental planetary area (for example, 1 square arc second). For this situation, Venus provides the highest illumination level, with Mars being less bright, and Jupiter being least bright. The approximate illumination levels are 6×10^{-11}, 5×10^{-12}, and 1.2×10^{-12} lumens per square centimeter for a square arc second area respectively.

Planetary infrared radiation characteristics are less well determined. Planets may have temperature gradients which may cause difficulties for infrared trackers employing radiation balance techniques. Calculations are provided which show essential agreement between published color temperature radiation for Mars, Venus, and Jupiter, and our calculations for effective temperature. This agreement allows the use of existing LMSC computer programs based on effective temperature.

TABLE 3.1

PLANET	SEMI-MAJOR AXIS OF ORBIT A.U.	SIDEREAL PERIOD (DAYS)	ECCENTRICITY e	INCLINATION TO ELLIPTIC	SEMI-DIAMETER (EQUATORIAL) arc sec.	
					At 1 A.U	At Mean conjunction or opposition
Mercury	0.39	87.9	0.205	$7^{\circ}00'$	3.34	5.45
Venus	0.72	224.7	0.006	3 23	8.43	30.5
Earth	1.00	365.2	0.016		8.80	
Mars	1.52	686.9	0.093	1 51	4.68	8.94
Jupiter	5.20	4332.5	0.048	1 18	98.47	23.43
Saturn	9.55	10759.2	0.055	2 29	83.33	9.76
Uranus	19.2	30685	0.047	0 46	32.8	1.80
Neptune	30.1	60188	0.008	1 46	30.7	1.06
Pluto	39.5	90700	0.249	17 10	4.1	0.11

3.2 GENERAL PLANET CHARACTERISTICS

TABLE 3.2

PLANET	ρ	Q	A	Magnitude m_v		$\pi\Delta$	$B-V$	Variation of phase	with =
Mars	.14	1.07	.15	-1.98	0	.798	+ 1.41	-1.41 + 5 log	+ 0.01420
Venus	.85	1.0	.85	-4.22	E	.500	+ 0.79	-4.3 + 5 log	+ 0.000
Jupiter	.41	1.4	.58	-2.50	0	21.9	+ 0.6	to .00024	- 0.0000006
								-9.1 + 5 log	+ 0.015

ρ = ratio of planet brightness at $\alpha = 0$ to brightness of perfectly diffusing disk with same position and apparent size as the planet. Then

$$\log (\rho) + \log \phi(\alpha) = 0.4 (m_{sun} - m_{planet}) + 2 \log (r\Delta / \text{radius of planet in Au})$$

when Q is unknown because the α range is small, ρ is sometimes called the albedo.

$Q = 2\int_0^{\pi} \phi(\alpha) \sin\alpha \, d\alpha$ is a factor that represents the phase law. We have the following cases:

Lambert law (perfect diffusion)	$Q = 1.50$
Lommel-Seeliger law	$Q = 1.64$
Metallic reflection	$Q = 4.00$
$\phi(\alpha) = 1/2(1+\cos\alpha)$ (i.e., α illuminated area)	$Q = 2.00$

A = pQ = Bond albedo = ratio of total light reflected from a sphere to total light incident on it.

α = phase angle = angle between sun and earth seen from planet.

r = sun-planet distance in Au.

B-V = color index.

Δ = earth-planet distance in Au.

3.4 VARIATION OF THE ILLUMINATION RECEIVED FROM VENUS, MARS, AND JUPITER

The apparent visual magnitude of each of the planets depends upon the angular position and distance of the planet relative to the sun and earth. The magnitude variations and extremes were determined for Venus, Mars, and Jupiter from equations given by C. V. Allen in "Astrophysical Quantities, Second Edition" (Ref. 3.1, page 145). To simpliiy the calculations, both the orbital eccentricity and inclination to the ecliptic were assumed to be zero for each of the planets. The magnitude of Venus was found to vary between -3.34 m_v at the dimmest to -4.37 m_v at its brightest. Mars has a magnitude variation from $+1.61$ m_v to -1.90 m_v and Jupiter varies from -1.52 m_v to -2.42 m_v. Figure 3-1 shows the planet magnitudes plotted as a function of the angle between planet and earth as seen from the sun. The program requirements are that Mars, Venus, and Jupiter must be considered whenever their angular diameter is greater than 10 seconds of arc and whenever they are at least 50% illuminated. These ranges of angular diameter and illumination are shown in Figure 3-1.

Since the instantaneous field of view of an edge tracker is small, consideration must also be given to changes of the phase of illumination (i.e., crescent, gibbous, or full) and to the apparent angular diameter of the target planet. The apparent angular size of each planet was calculated for various orbital positions relative to the earth, and the values of visual magnitude corresponding to each position were converted to lumens/cm^2 received outside the earth's atmosphere. The phase angle of the planet and the apparent angular size were used to calculate the area of the illuminated portion of the planet in square are seconds. Figure 3.2 shows the variation in illumination received from a one square arc second area from each of the planets. Illumination per unit area of source is plotted against planet radius to illustrate both changes in energy level and angular size of the planets. As in Figure 3.1, the range of values of angular diameter and illumination are shown in Figure 3.2.
In addition to phase, size, and magnitude, consideration must be given to the spectral characteristics of the detector and the planets. In the visual region, the color temperature of Venus is 4470°K, Jupiter 6520°K, and Mars 3780°K. Calculations in Section 4, Planet Tracking Techniques, are made to determine the absolute response of various photo detectors (S-5, S-11, S-20) to the planets based on actual magnitudes and color temperatures.

3.5 SPECTRAL CONSIDERATIONS

The illumination received from the planets is reflected energy from the sun modified by the reflection and absorption characteristics of each planet. The variations of illumination received from the planets Mars, Venus, and Jupiter as a result of changes in visual magnitude and apparent angular size were considered in the previous section, Section 3.4. The values given in Figure 3.2 refer to the energy in the astronomical visual region and define the energy relative to that from a reference star which is said to have an apparent visual magnitude of zero ($m_v = 0$). To the human eye the reference Type A0 star provides an illumination of 2.65×10^{-10} lumens-cm^{-2} outside the

MAGNITUDE CHANGES OF THE PLANETS

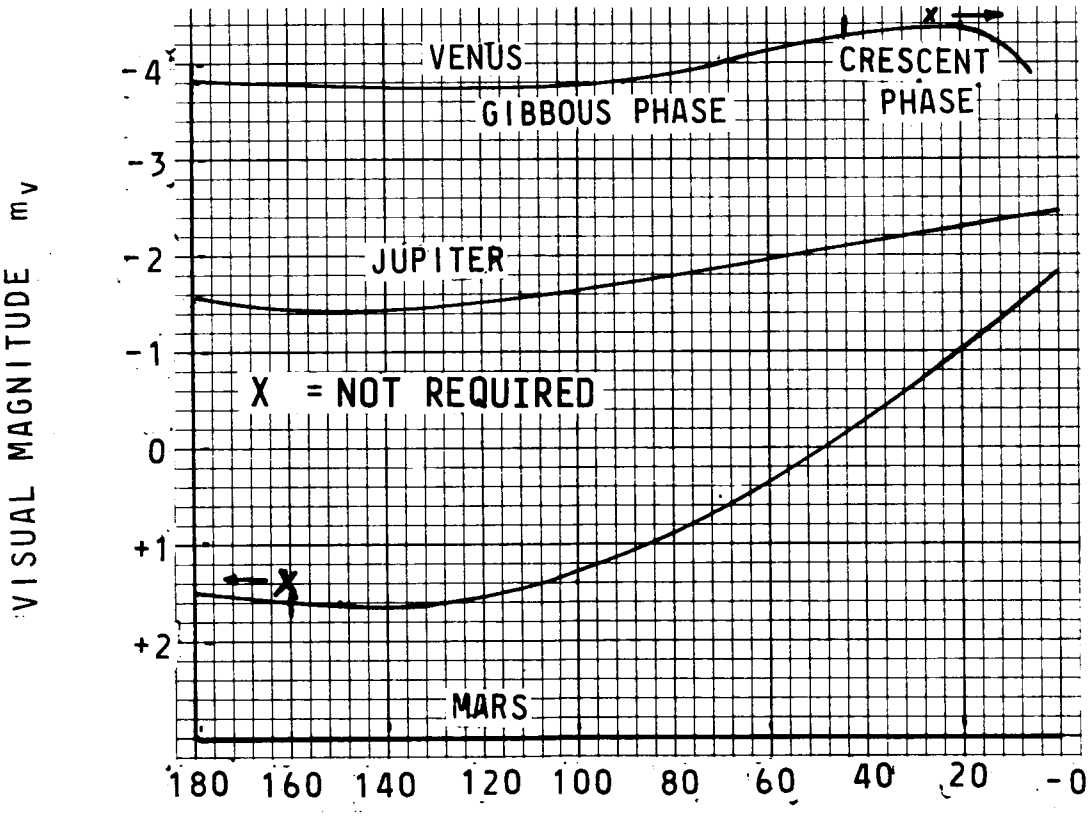

FIGURE 3.1

ILLUMINATION RECEIVED FROM EQUAL AREAS OF THE PLANETS

FIGURE 3-2

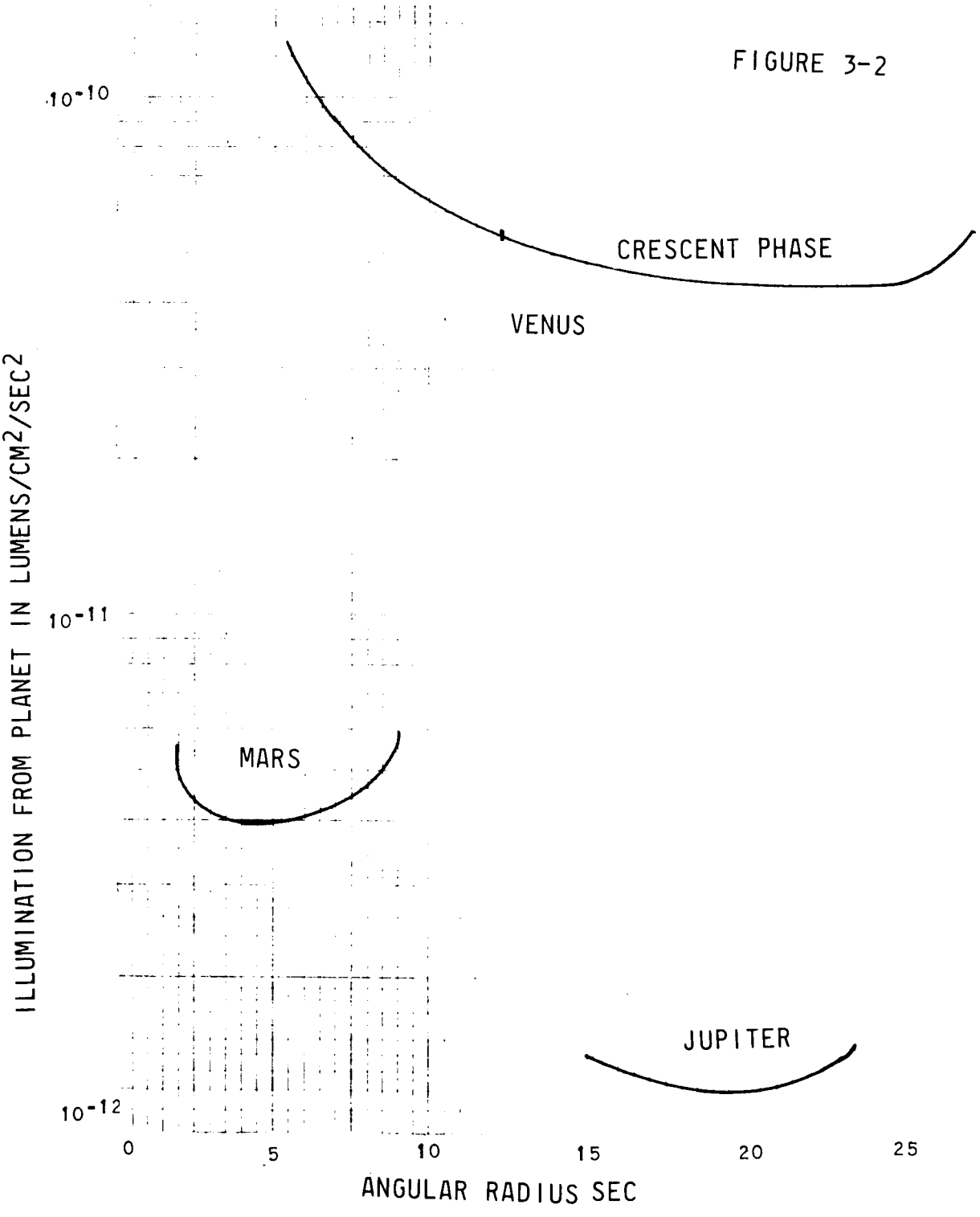

earth's atmosphere (Ref. 3.1).

To determine the response to planet energy by detectors having spectral sensitivity outside the spectral region of measurement, it is necessary to determine both the spectral characteristics of the planets and their absolute energies. This can be achieved by measuring the absolute amounts of energy from the source in two separate intervals. The spectral intervals generally used for this purpose (Ref. 3.1) are illustrated in Figure 3.3. These two intervals are generally referred to as the B and V curves.

The B-V corrections listed in Ref. 3.1 for each planet relate to the relative response to the source of the V and B curves shown in Figure 3.3. The color temperature of the planets based on B-V values were computed as: Jupiter - 6520°K; Venus - 5570°K; and Mars - 3780°K.

The spectral characteristics of the reference A0 star must also be known. Based on the B-V correction, an A0 star would have a color temperature of 15400°K. Since, however, the color temperature actually refers to the apparent shape of the envelope of the energy rather than to the smoothed flux which would be seen by a detector, the temperature is assumed to be 11000°K. This assumption is in good agreement with references 3.2 and 3.3, Keenan and Lamore, and yields radiance levels about 2 percent lower than that obtained using the color temperature.

The absolute energy distributions from zero magnitude 11000°K, 6520°K, 5570°K, and 3780°K black body sources are shown in Figure 3.3. The curve for A0 was determined by equating the value of luminous flux from an $m_v = 0$ star to the integral with respect to wavelength of the product of the absolute response curve of the eye (K 680 lumens/watt) and the energy curve for an 11000°K black body with an unknown absolute value (C_1 $H_{2\ 11000°K}$) and solving for the constant C_1.

$$\text{I.e.,} \quad C_1 = \frac{2.65 \times 10^{-10} \text{ lumens - cm}^{-2}}{680 \text{ lumens-watt}^{-1}} = 5.01 \times 10^{-17}$$
$$\qquad\qquad {}_{o}K\ H_{11000K}$$

The absolute energy curves for zero magnitude sources at the color temperature of each planet were found in a similar manner by using the relative astronomical visual curve (V_2) and equating the integrals

$$C_1 \int_o^\infty V_\lambda H_{\lambda\ 11000k} = C_2 \int_o^\infty V_\lambda H_{\lambda 6520}\, d\lambda$$

$$= C_3 \int_o^\infty V_\lambda H_{\lambda 5570}\, d\lambda$$

$$= C_4 \int_o^\infty V_\lambda H_{\lambda 3780}\, d\lambda$$

SPECTRAL CONSIDERATIONS

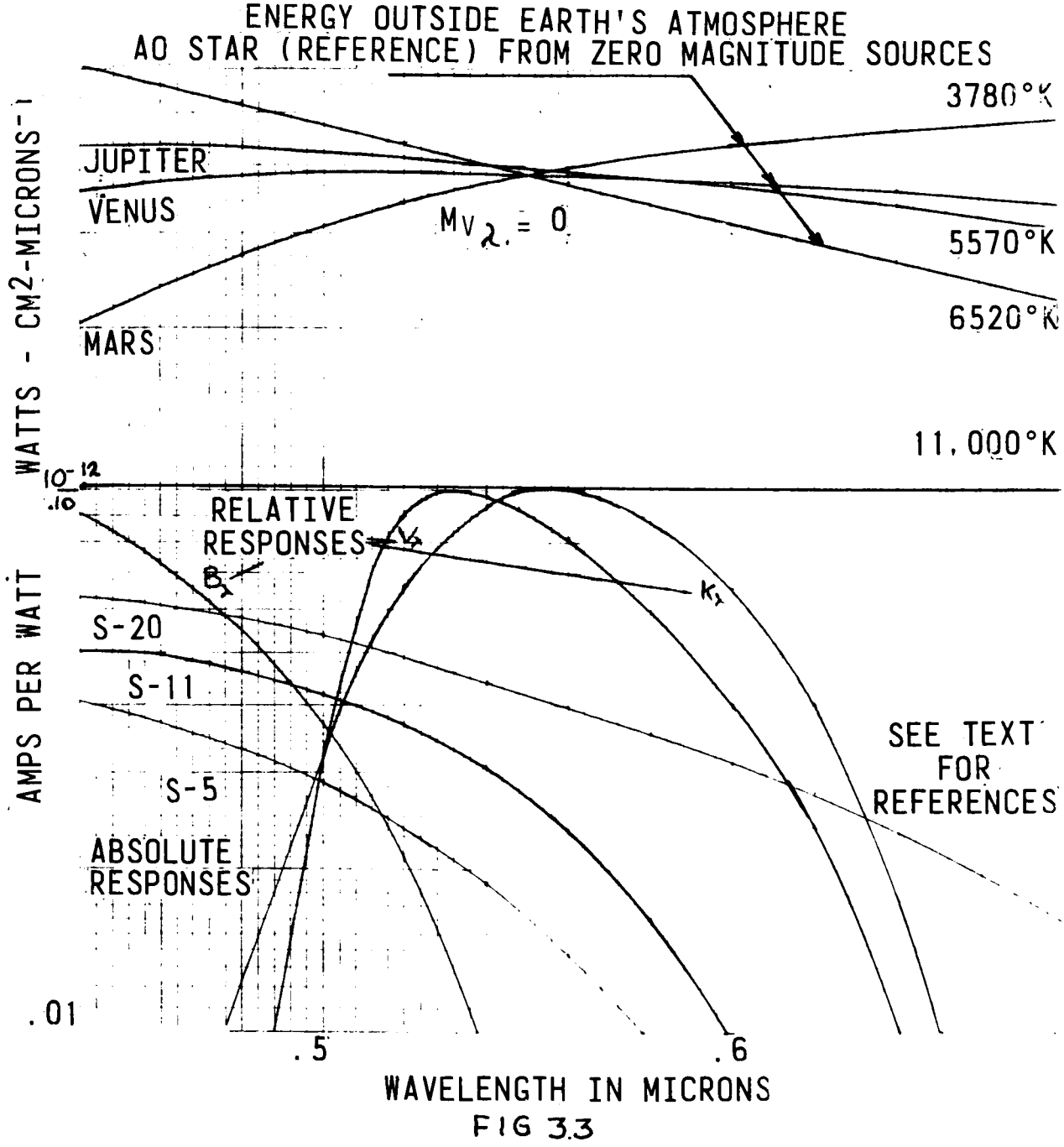

FIG 3.3

and solving for C_2, C_3, and C_4.

$$C_2 = 2.89 \times 10^{-16}; \quad C_3 = 5.60 \times 10^{-16}; \quad C_4 = 5.20 \times 10^{-15}$$

It should be noted that when derived in this manner, if H_2 is watts $-cm^{-2}$ micron^{-1} radiated from a source, the values $c_m H_{2T}$ (as shown in Figure 1) are illumination in watts $-cm^{-2}$ - micron^{-1} received outside the earth's atmosphere.

The $m_v = 0$ values can be converted to the minimum level of illumination per arc second using values taken from the curves in Figure 3.2 by multiplying by the ratio of minimum lumens - cm^{-2} - arc sec^{-2} to the Reference 2.65×10^{-10} lumens - cm^{-2}.

The resulting ratios are:

Jupiter	4.56×10^{-3} arc sec^{-2}
Venus	1.59×10^{-1} arc sec^{-2}
Marx	1.56×10^{-2} arc sec^{-2}

These values are applied in Section 4 where the absolute spectral responses of various photodetectors are integrated together with the spectral characteristics of planets based on the information in this section.

3.6 GIBBOUS PHASES OF MARS, VENUS, AND JUPITER

A planet enters the gibbous illumination phase when the angle between the observer and the sun as measured from the planet begins to depart from 0 degrees. As the angle increases to 90 degrees, the planet, as seen by the observer, is illuminated on only one half of its apparent disk. We are concerned, for the purposes of this study, with the "gibbousity" of Mars, Venus, and Jupiter because the existence of a non-circular planet or a planet whose illumination characteristics depart only slightly from circularity may cause an edge seeking sensor to seek false nulls away from the geometric center of the planet. These points will be explored in detail in Section 5, General Tracker Design Considerations, where the harmonic content of the error signal for an edge tracker under various conditions of gibbousity are examined.

Figure 3.4 shows the gibbousity of Mars, Venus, and Jupiter as a function of planet radius. We are required to consider Mars only when its angular diameter is greater than 10 arc seconds. This situation is shown in the figure. The ratio A/B is the ratio of the angular radius of the gibbous half of the planet to the actual planet radius. Venus has the largest departure from circularity and Jupiter the least.

Of the three planets considered, only Venus becomes crescent (less than 50% illuminated), since Mars and Jupiter are both exterior planets (i.e., have orbital radii greater than that of the earth).

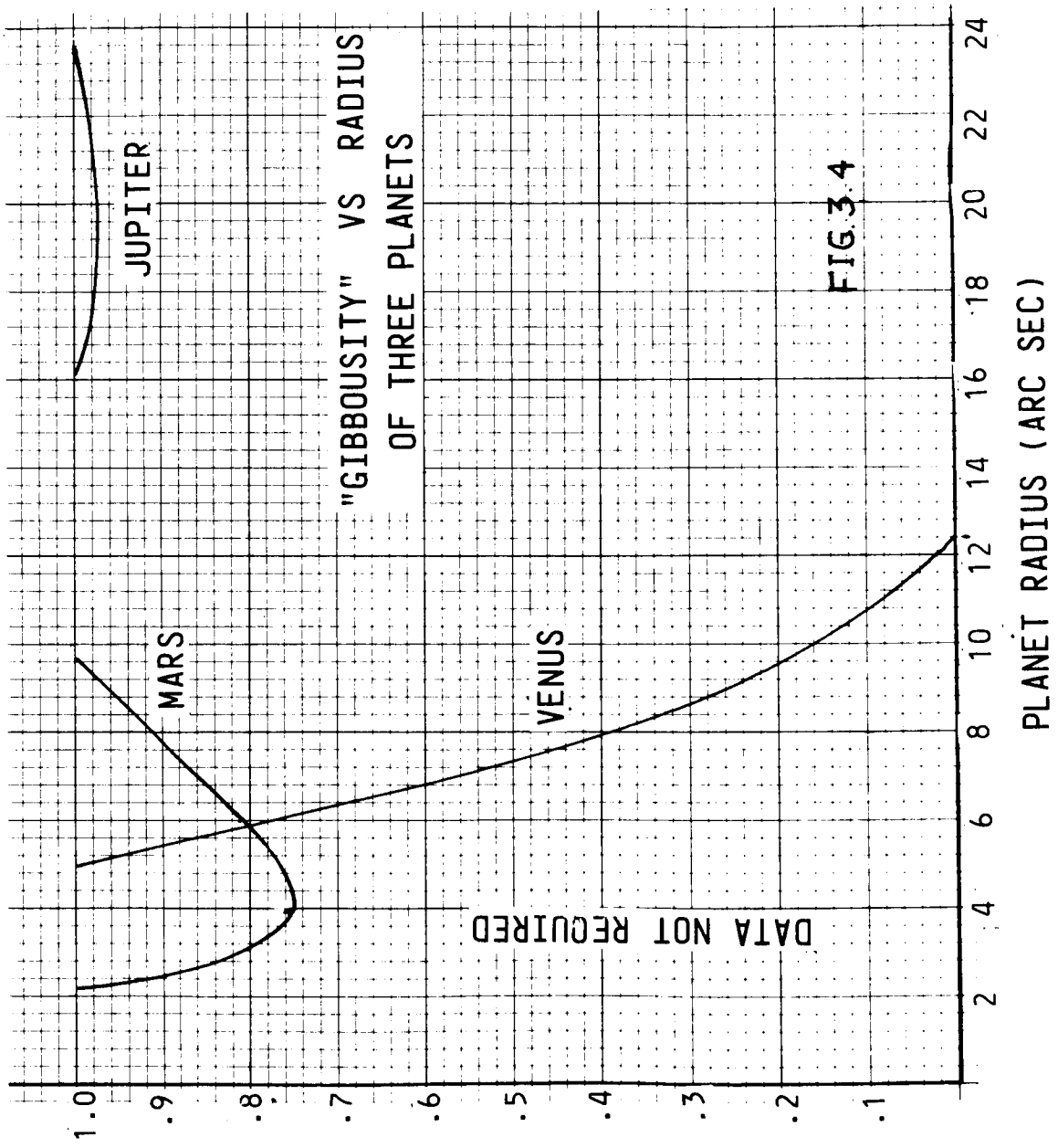
"GIBBOUSITY" VS RADIUS
OF THREE PLANETS
FIG 3.4
JUPITER
MARS
VENUS
DATA NOT REQUIRED
PLANET RADIUS (ARC SEC)
1.0
.9
.8
.7
.6
.5
.4
.3
.2
.1
2
4
6
8
10
12
14
16
18
20
22
24

FIGURE 3.4

3.7 ADDITIONAL DATA OBTAINED FROM VARIOUS OBSERVATORIES

In December 1964, discussions were held with both Dr. C. P. Kuiper and Dr. J. F. Low of the University of Arizona concerning planet spectral and spatial characteristics. Dr. Kuiper was asked for data concerning spectral and spatial data in the visible and Dr. Low for infrared data.

In the visible region of the spectrum, Dr. Kuiper referred to the data in Vol. III of Planets and Satellites (Ref. 3.4) as the only "good data available." For our purposes the data is somewhat limited, however, general trends are discussed which will assist in determining the proper spectral interval for a visible system. In general, the data consists of a series of photographs of Mars, Jupiter, and Venus. Some of the photos are in color and some are in black and white. The latter were taken with red, blue, and yellow photographs. Details in the photos were, in general, poor. Reprints were obtained from the Mount Wilson Observatory.

Investigation of the Mars photographs from both sources shows that many large cloud-like structures are visible in the red and orange portions of the spectrum, while in the blue region the contrast from the clouds becomes definitely decreased and in one case almost eliminated, thus providing an almost uniformly illuminated target. This effect arises from Rayleigh scattering from the Martian atmosphere. Additional data concerning the variation of the brightness of Mars with rotational phase further indicates uniformity in the blue region of the spectrum. As a result of reviewing this data, it is concluded that operation in the blue region of the spectrum is desirable to assure uniformity of the edge in the case of Mars.

Planet temperature information was obtained from Dr. F. G. Low. In general, Dr. Low also referenced the work by Pettit in Kuiper's book (Ref.3.4) as the best source of planet temperature data with the exception of Saturn. The temperature of Saturn has recently been measured by Dr. Low with a Ge Bolometer in the 8 - 14 micron region. He obtained a temperature of $93^{\circ}K$ which is about 30° lower than that reported in the literature.

A summary of the Pettit data is provided below:

	Max. $^{\circ}K$	Min. $^{\circ}K$	
Venus	240°	235°	
Mars (Polar Cap)	221°	211°	
Jupiter	149°	?	
Saturn	125°	93°	(F. Low Data)

As a general note, it should be pointed out that for Mars the temperature variation across the surface from the south polar cap to the limb varies with $221^{\circ}K$ and $274^{\circ}K$ which could give serious troubles in locating the geometric center of the planet with an infrared radiometric balance tracker.

3.8 COMPUTER BASED RADIOMETRIC CALCULATIONS

From the early stages of the program, we planned to use existing computer programs to perform the radiometric calculations used to predict the performance of various sensors. As information on the detailed illumination and radiation characteristics of the planets was obtained, the question arose concerning the applicability of existing computer programs based on integration of black body functions to the calculation of tracker performance. The question is basically, how well do planetary radiation characteristics in terms of color temperature fit into existing computer programs which are written in terms of effective temperature? The analysis, which is summarized for the case of Mars in the following paragraphs, showed that the assumption that the color temperature and effective temperatures are equal, is satisfactory for Mars, Venus, and Jupiter for the purposes of this program.

The following paragraphs show the calculation for Mars in detail:

$$m_v = -1.98$$

$$B\text{-}V = 1.41$$

$$Tc = 3780^{\circ}K$$

$$\int V_\lambda \; f_\lambda \; d\lambda = 2.04 \times 10^{1} \text{ watts/cm}^2 \text{ ster.}$$

where $f\lambda$ is radiation from a $3780^{\circ}K$ blackbody and $V\lambda$ is from Ref. 3.1, page 191.

$$m_v = -2.5 \; 19 \log\left(\int V_\lambda \; f_\lambda \; d\lambda\right) - 14.08$$

let $x = \int V_\lambda F_\lambda \, d\lambda$

$$-1.98 = -2.5 \log (X) - 14.08$$

$$X = 1.45 \times 10^{-12} \text{ watts/cm}^2$$

Ratio of calculation by computer to that from m_v calculation.

$$R = \frac{1.45 \times 10^{-12}}{2.04 \times 10^{1}} = 2.22 \times 10^{-14}$$

If we assume $Tc = Tc$

$$BC = -42.5 + 10 \log (3780) + \frac{28000}{3780}$$

$$BC = +1.05$$

$$m_{bol} = m_v - BC$$

$$m_{bol} = -1.98 - 1.05 = -3.04$$

$$m_{bol} = 2.51 \log \frac{2.52 \times 10^{-12}}{H}$$

$$H = 4.08 \times 10^{-11} \text{ watts/cm}^2$$

Total power received from 3780°K blackbody

$$= 1.2 \times 10^{3} \text{ watts/cm}^2$$

$$H_1 = 1.2 \times 103 \cdot R = 1.2 \times 10^{3} \cdot 2.22 \times 10^{-14} =$$

$$H_1 = 2.67 \times 10^{-11} \text{ watts/cm}^2$$

$$H_1 = H$$

The approximate equality, when considered with program objectives and the uncertainty in the source data, shows that the assumption of the equality of the effective temperature and the color temperature is satisfactory and that new computer programs based on color temperature need not be written.

Similar calculations were performed for Jupiter and Venus which yielded equivalent agreement for each planet. Color temperature information from Reference 3.1 is summarized below:

$$B\text{-}V = 7300^{\circ}/Tc - 0.52$$

where Tc is color temperature - visible continuum

Mars B-V = +1.41
1.41 = 7300°/Tc -0.52
Tc = 3780°K

Jupiter B-V = +0.6
0.6 = 7300°/Tc -0.52
Tc = 6520°K

Venus B-V = 0.79
0.79 = 7300°K/Tc -0.52
Tc = 5570°K

3.9 COMMENTS

The material compiled in this section provides the basis for the following comments.

1. An edge tracking sensor operating in the visible will have the most difficulty tracking Jupiter because of its small radiation level per unit area.
2. Infrared radiometric balance trackers may have considerable difficulty overcoming temperature gradients existing on a planet such as Mars, for example, in addition to considerable uncertainty, even now, concerning the existence and magnitude of these gradients. In the absence of better source information, it appears that no definitive specification for an infrared radiometric balance planet tracker can be written.

Section 4

PLANET TRACKING TECHNIQUES

4.1 INTRODUCTION AND SUMMARY

One of the contractual requirements involved investigation of tracking schemes other than visible edge tracking. The additional techniques considered were infrared edge tracking and infrared and visible radiometric or photometric balance techniques. This section describes the analyses conducted and concludes that infrared techniques are not as practical as visible techniques. Specifically, infrared radiometric balance approaches are limited by available signal to noise ratio. Infrared edge tracking schemes do not appear practical either, also because of the low energies available. We could not configure conceptually a visible photometric balance approach which could accurately and consistently locate the geometric center with anywhere near the angular accuracy required. The technique which provides most promise is the visible edge tracking approach which is able to locate the geometric center consistently, even with partial illumination of the planet.

4.2 INFRARED PLANET TRACKERS FOR HIGH ANGULAR ACCURACY

Introduction and Summary

One of the contractual requirements for NASA Contract NAS 2-2485 is that the feasibility of infrared trackers be investigated. A system study of the parameters involved shows that a planet tracker able to track planet edges is theoretically feasible if the full 38-inch aperture were available. Practically, however, development of such a tracker would require a significant advance in detector manufacturing techniques to manufacture a detector array of the necessary size and complexity. Further difficulties encountered with chopping of the incident bundle lead to the conclusion that high accuracy infrared planet trackers are not practical at this time.

In general, infrared trackers of the required type can be divided into three categories, namely, electronic scan, mechanical scan, and multiple detector types. In order to operate from planet emission, the detecting element must operate in the spectral region dictated by the planet temperature. For the worst case analysis, the lowest temperature involved is about 150°K. Temperatures in this region require infrared detectors operating at wavelengths greater than 20 microns.

4.2.1 Electronic Scanning Systems

The only uncooled electronic scanning device currently commercially available for operating in this spectral region is the Westinghouse Thermicon (Ref. 4.1). This device utilizes a vidicon gun and a special thermally sensitive retina.

Current types of this tube use magnetic sweeps which limit the desirability of its use for the tracker application because of weight and power requirements. Although the detail specifications for the tube are classified, it can be said that the sensitivity of the tube is too low for planet tracking.

A second type of electronic scan although not commercially available has been made by Philco and is called Filterscan (Ref. 4.2). This system utilizes a single element detector behind a special electronic shutter. The shutter operates in such a manner that the scanning of a target results in a negative contrast type of signal. Scan rates are readily adjustable so the sensitivity of this type of system is identical to that of any single element detector system if background radiation is properly considered, thus the data in subsequent sections should suffice.

4.2.2 Single/Multiple Detector Arrays

In order to determine the feasibility of utilizing either scanning or stationary detector arrys, it is required that the proper detector be selected to match the target temperature. The general method used to select the proper infrared detector and determine the associated signal to noise ratio is discussed in the following paragraphs.

4.2.2.1 Signal to Noise Ratio Calculation Procedure

The signal to noise ratio of a passive electro-optical planet tracker can be specified as

$$S/N = \frac{P_D}{NEP} \tag{1}$$

where

P_D = Signal power incident on the detector

NEP = Detector noise equivalent power.

The effective signal power incident on the detector, P_D, can also be expressed as:

$$P_D = \frac{Ao\, A_D \eta M}{F^2} \times \int_o^{\lambda} N(\lambda) R(\lambda) d \tag{2}$$

where

Ao = System Aperture Area

A_D = Detector area

F^D = Focal Length

η = Optical Efficiency

M = Modulation Efficiency

$N(\lambda)$ = Planck's Radiation Equation

$R(\lambda)$ = Relative detector wavelength reaponse

Typically detector manufacturers do not specify relative response, instead data for D* is normally published where

$$D^*_\lambda = \frac{A_D^{1/2}\,\Delta F}{NEP_\lambda} \tag{3}$$

where Δ f is the measuring bandwidth.

However,

$$\frac{\int_0^\lambda N(\lambda)\,D^*(\lambda)\,d\lambda}{D^*_{\lambda PEAK}} = \int_0^\lambda N(\lambda)\,R(\lambda)\,d\lambda \tag{4}$$

Substitution of (4) and (3) in (1) yields

$$\frac{S}{N} \qquad \frac{A_o A_D^{1/2}}{F^2 \Delta F} \int_0^\lambda N(\lambda)\,D^*_\lambda\,d\lambda \tag{5}$$

The integral has been computer calculated for typical planet temperatures and typical infrared detectors. Data for infrared detectors was obtained from Space/Aeronautics (Ref. 4.3).

4.2.2.2 IR/OAO Planet Tracker Signal-to-Noise Ratios

The aperture area Ao available for the IR/OAO could feasibly be as large as 38 inches in diameter; however, since the system previously requested (Ref. 4.4) had a nominal aperture of six inches in diameter, this size has been used for the following calculations for comparison.

Typical sizes for small infrared detectors which are currently available are about 0.1 mm or .004 inch square, thus for an instantaneous field of view of one second, a focal length of 825 inches is required. Assuming an optical efficiency of 70% and a modulation efficiency of 40%, equation (5) becomes

$$S/N = 1.18 \times 10^{-7}$$

Based on the above calculations, the following signal-to-noise ratios are obtained using the types of detectors indicated:

	(20°K) Ge,Si,Au	Ge,Si,Zn	Ge,Si,Au	Te	Ge,Cd	GeAu	InSb
Venus	.62	.45	.039	.007	3.1	.90	.022
Mars	.45	.36	.028	.056	2.5	.06	.013
Jupiter	.016	.03	10^{-3}	10^{-6}	.34	10^{-3}	10^{-5}

All of the above detectors require cooling in the region of 20 to 60°K except the Te and InSb detectors which operate at 77°K.

Similar calculations for room temperature Ge immersed thermistors yield S/N ratios of .51, .32, and 10^{-2} for Venus, Mars, and Jupiter, respectively. For the purpose of this calculation D* was calculated from Ref. 4.5 and it was

further assumed that the response cut off at 20 microns.

If the total 38 inch aperture were available, the overall signal-to-noise ratio would be increased by $(38/6)^2 = 40$ which would make operation realizable providing implementation is feasible with the cadmium doped Germanium detector.

Assuming that the total aperture is available, two different detection schemes can be visualized. The first of these would utilize a detector array similar to that discussed in the original planet tracker proposal while the second would use a linear array and auxiliary scanning mirror. Both of these systems have one common feature, namely they operate on a time sharing basis with the proposed IR/OAO spectrometer. This can be achieved with relative simplicity by aluminizing the back surface of the spectrometer chopper so that during the spectrometer off period the energy incident on the rear of the chopper is reflected to a tracker detector array as shown in Figure 4-2.

The linear detector array should cover the total field of view 270" in one dimension. To provide the proper characteristics the array should be divided into 200 elements, each corresponding to a one second square field of view (.004 x .004 in.) and approximately seven additional collinear detectors element on each end of the array. These latter detectors would have a field of view of about one by five seconds. The layout in the focal plane region is described in the accompanying sketch.

The oscillating mirror would oscillate at about 250 cps, with an amplitude of 2' 15" so that the field of view swept out would then be 4' 30" square.

Target location can be obtained along one axis from detector location and along the other axis from the signal characteristics. If the image is positioned so that the planet is at the center of the field of view and the mirror is vibrated at 250 cps with a peak to peak amplitude of 4 minutes about null position, the image spot will be swept back and forth over the detector array, and a 500 cps square wave detector output will result. If the position of the image is at either edge of the array, a 250 cps square wave detector output will result. A Fourier analysis of the detector output shows that the amplitudes of the 250 cps and 500 cps signal components vary as a function of image null position. The relative amplitude of the 250 cps component increases almost linearly with the relative movement of the image null position. This signal component would then be used as an input to a servo system which would position the vibrating mirror so as to maintain the image near the center of the detector. Target location can then be determined from mirror position.

In all cases many detectors would see the target on each scan. It is desirable to locate only the channels intersecting the planet limb. This can be accomplished by electronically scanning across the array to locate the two end detectors generating a signal and only processing the data from the two channels concerned.

Comparison of the above approach with the array discussed in the original proposal LMSC 893537 yields the following important points.

1. The detector array originally discussed in LMSC 893537 utilized 64 detectors. The present system utilizes 214 detectors, which is a disadvantage both with respect to detector packaging and the complexity of the electronics. However, it should be possible to locate edges accurately with the large array.

2. The linear array has the further advantage in that it has the capability of locating the geometric center of the target providing extremely cold and resulting poor S/N ratios do not exist at the edge.

3. The linear array has several disadvantages. Probably the major disadvantage is that scanning of the field of view as suggested can lead to generation of spurious background signals. Ideally those signals can be eliminated but practically they are extremely difficult to eliminate. This arises because the mirror energy from surrounding objects can be reflected on the detector and cause spurious signals. Stops and baffles can minimize this problem, but to be completely successful, all the stops must have the same temperature emissivity product, which can pose a difficult problem.

4. Either system to operate properly would require the full aperture. This can only be accomplished with the 45° beam splitter shown in the sketch. Such a system automatically blocks out a certain amount of energy from the spectrometer slit. Depending on the actual dimensions this could be as much as 50%, which could impose S/N problems at the spectrometer output.

5. The actual manufacture of either array, or IR detectors, is extremely difficult and possibly impossible unless photo etch techniques could be utilized. Photo etch techniques for similar detectors are under development by Honeywell at this time.

In summary, it is feasible to develop an infrared planet tracker using a 38 inch aperture and a cadium doped detector array; however, detector development would probably require an advance in the state-of-the-art. Cooling requirements would be relatively severe for long term application. With proper design the tracker could locate the planet edges rather than the thermal centroid.

4.3 PRECISION PLANET TRACKERS OPERATING IN THE VISIBLE SPECTRUM

The requirement for tracking the geometric center of planets which can appear in crescent or gibbous phase cannot be met by any reasonable combination of photometric balance schemes. This statement is based on interaction with personnel at NASA/Ames Research Center and on discussions among ourselves and with our colleagues, both inside and outside of LMSC. No one has been able to suggest a simple configuration which could overcome the drastic changes in illumination centroid relative to the geometric center of the three planets we were considering. Simple geometrical calculations show that

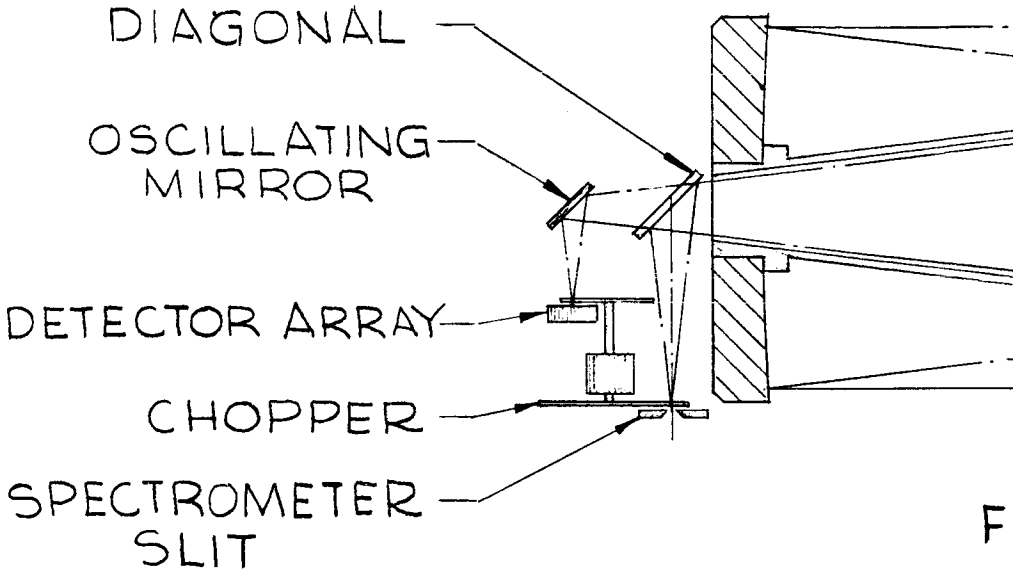

F

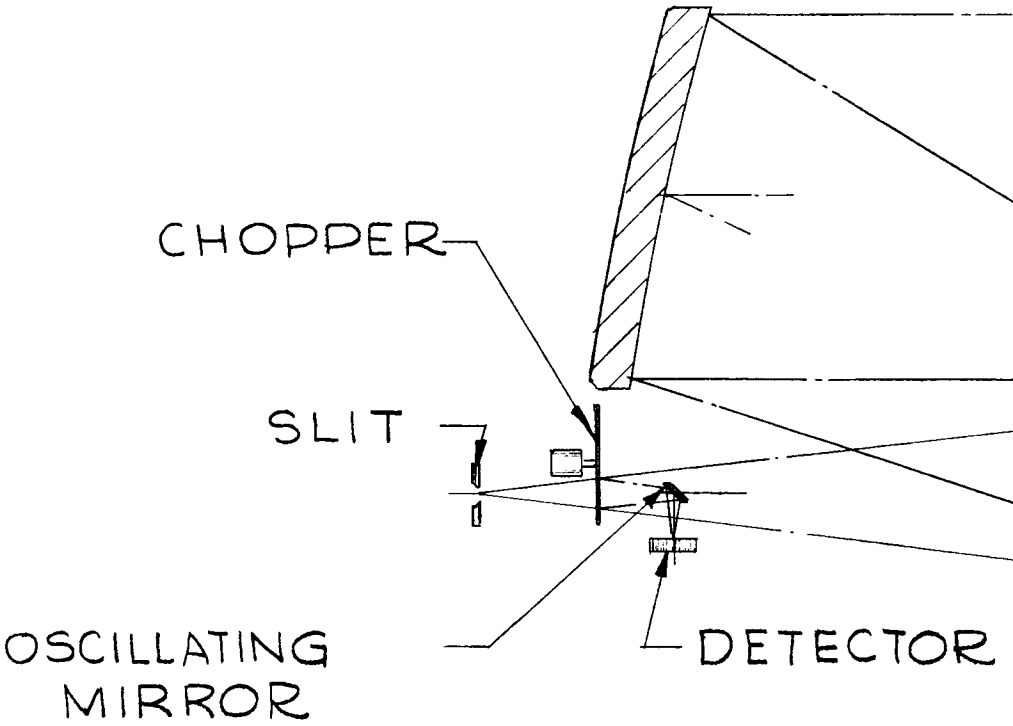

F

4-6-A

INFRARED

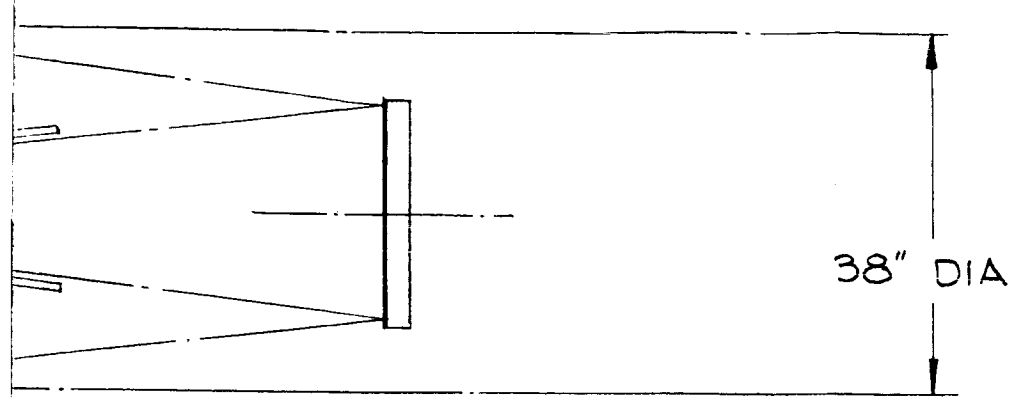

IG 4.1

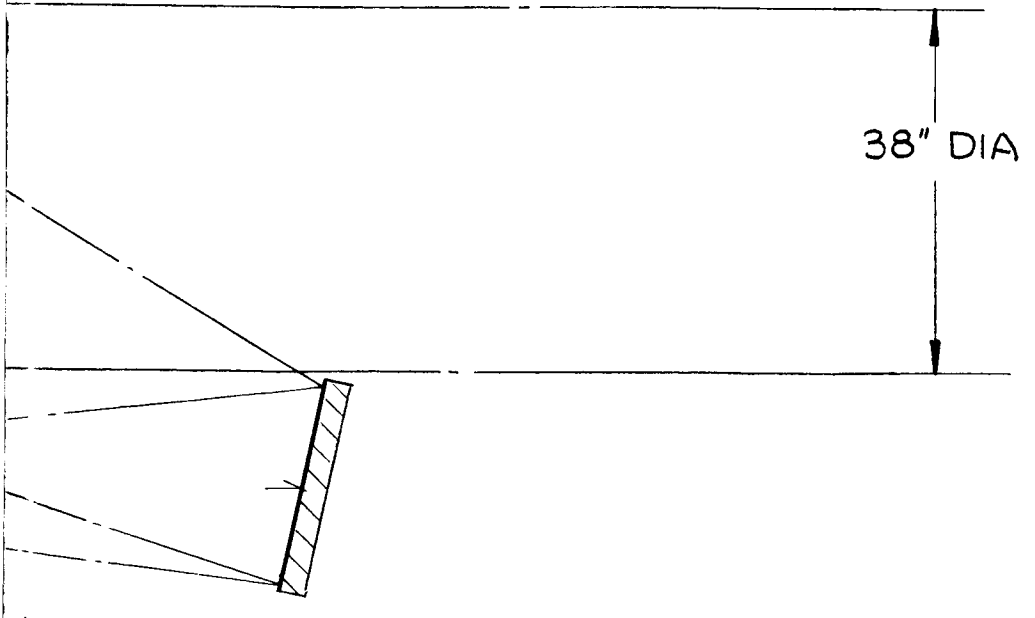

ARRAY

FIG. 4.2

4-6-B

9-6-C

PLANET TRACKER

an energy balancing method could result in a geometric center location error of more than 12 arc seconds for a 50% illuminated planet subtending 60 arc seconds. Schemes which came closest involved the use of multiple detectors and complicated logic to construct circular arc segments and then find the center of the arc segment. These schemes appear to be particularly vulnerable to tracking the gibbous edge of a planet and yielding false center information. For these reasons, the approach was not considered any further after the initial investigation because of the small probability of a feasible solution.

4.4 SPECTRAL CHARACTERISTICS OF PLANETARY RADIATION AND VISIBLE DETECTORS

Section 3, Planet Characteristics, discussed the influence of the spectral description of planetary radiation on the energy available for planet tracking. The following paragraphs of this subsection are based on the results of Section 3.5, and extend that analysis with c onsideration of the absolute spectral response of various photo-emissive detectors such as photomultipliers.

The absolute spectral responses of the photocathodes (Ref. 4.6) available for the CBS Reconotron (S-5, S-11, and S-20) are also shown in Figure 3.3. A computer was used to determine the integrals over discrete wavelength intervals of the products of each of the photocathode sensitivity curves and black body radiation at 6520°K, 5570°K, and 3780°K. The computed values were converted to absolute response to minimum planet energy by multiplying by the appropriate illumination ratios and c_m constant. Since the computer program used H_2 in terms of watts - cm^{-2} $micron^{-1}$ - steradian, an additional factor of steradians was used in the conversion.

The resulting values for intervals in the 0.4 to 0.8 micron region are summarized in Table 4.1 in units of 10^{-16} amps - cm^{-2} - arc sec^{-2}. This table shows that the S-20 cathode will provide the highest response to each of the planets for any wavelength interval from 0.4 to 0.8 microns. It will be remembered that the planet spectral calculations are based on color temperature rather than the temperature associated with the smoothed flux. Such temperatures would be lower than the color temperatures and would yield results for which the S-20 improvement over S-5 or S-11 would be even greater. If the lower temperatures are correct, it is estimated that at most the values listed for S-20 in Table 4.1 are approximatly 1 percent high for Mars, 6 percent high for Venus, and 7 percent high for Jupiter. The values listed for S-5 would, however, be more than 2.5 times too high. Thus, although the actual best temperature for each planet is uncertain, the temperature chosen clearly indicates the superiority of the S-20 response, and the results for that response are used in the calculations below.

The proposed planet tracker has an aperture area of 129 cm^2 and has an effective focal length of 400 inches. Taking into account the reflection losses from five surfaces, the overall optical efficiency is assumed to be 90.2% or .98% per surface. The effective collecting area is therefore 116.2 cm^2. The instantaneous field of view is assumed to be a .002 inch diameter circle at the photocathode and is equivalent to 0.636 $arcsec^2$.

Using the minimum illumination from Jupiter as 2.23×10^{-16} amps - cm^{2} - $arcsec^{-2}$ over the 0.4 to 0.8 micron region (from Table 4.1), the actual planet tracker signal at the photocathode would be:

$$2.23 \times 10^{-16} \text{ amps} - cm^{-2} - arcsec^{-2} \times 116.2\ cm^{2} \times .636\ arcsec^{2} =$$

$$165 \times 10^{-16} \text{ amps} = 1.65 \times 10^{-14} \text{ amps}$$

TABLE 4.1

Absolute photocathode response to minimum illumination per square arc second received from each planet.

	.4-.5 u	.5-.6 u	.6-.7 u	.7-.8u	.4 u - .8u
VENUS					
S-20	34.6	25.8	12.5	3.0	75.9
S-11	27.2	16.4	1.3	---	44.9
S-5	21.6	10.3	.7*	---	32.6
MARS					
S-20	2.06	2.47	1.66	.50	6.69
S-11	1.63	1.53	.17	---	3.33
S-5	1.28	.95	.08*	---	2.31
JUPITER					
S-20	1.19	.72	.34	.08	2.23
S-11	.93	.49	.04	---	1.46
S-5	.75	.31	.02*	---	1.08

* .6 u - .65 u

$$1.0 = 10^{-16} \text{ amps} - cm^{-2} - arcsec^{-2}$$

This value of signal current is shown to provide an adequate signal to noise ratio in following sections.

4.5 EXAMINATION OF ROULETTE PATTERNS FOR PLANET IMAGE SCANNING

The preceding subsections concluded that infrared tracking is not feasible and that visible photometric balance systems were likewise not feasible. This subsection discusses a particular form of planet edge tracking. The roulette pattern forms the basis for the proposed planet tracker concept. The equations for the generation of the particular scan pattern used have been previously discussed and are shown in Figure 4.3. This section describes how the

roulette pattern may take on various forms.

Figure 4.3 is plotted using this nomenclature: n is the ratio of the dither frequency fo the fundamental scan frequency and $C = \frac{A}{B}$, where A is the amplitude of $\sin w_o t$ component and B is the amplitude of $\sin n w_o t$. Voltages at the fundamental frequency drive the scan around the edge of the planet. Voltages at the dither frequency drive it across the edge of the planet.

The straight line in Figure 4.3 is the boundary between the areas where the pattern is looped and where the pattern is unlooped or open. Each of these patterns, while they appear basically different, one appearing as a gear tooth and the other as an epi-cycle, are each a case of the general roulette pattern. For a given n either pattern may be obtained by varying $\frac{A}{B}$. Further, for a given $\frac{A}{B}$ one can vary n to obtain either pattern.

Figures 4.4 and 4.5 show roulette patterns for various values of n and C. These values of n and C are shown in Figure 4.3 as numbered points corresponding to the numbers of the photographs in Figures 4.4 and 4.5. The special cases of the general roulette pattern are clearly demonstrated.

Of special interest is Photograph 20 on Figure 4.5. It was obtained by increasing B in Photograph 19 until the scan lines intersected in a point. The intersection is not precisely a point, indicating that there is a small amount of residual phase shift. Photograph 22 represents a similar situation where n = 10.

Photograph 21, on careful inspection, demonstrated that the phase modulation scheme of frequency shifting the basic drive voltages and then re-adding them produces an expanding and shrinking circle. The photograph is for the case where B = 0. Note that the scan is actually a spiral scan. Additional photographs have been taken for non-zero B.

These illustrations of angle modulation are not intended to show any advantage over amplitude modulation, but are provided to form a basis for comparison between the two.

4.6 FUNDAMENTAL LIMITATIONS OF PLANET TRACKER ACCURACY

For the purpose of these calculations, Jupiter has been utilized because it presents the worst possible target. Several data processing techniques are discussed and the implications on signal to noise and accuracy are discussed. This subsection expands the signal level calculations of Section 4. and involved calculations of signal to noise ratios and the ratio of the dither frequency to the scan circle.

In considering the performance of the present planet tracker concept and variations from it, certain fundamental limits of performance have been investigated. They are (1) the number of photons incident on the detector

$x = A \sin \omega_o t + B \sin N \omega_o t$ $\quad y = A \cos \omega_o t + B \cos N \omega_o t$

#1

N = 5 C = 5

#2

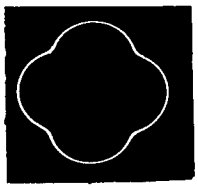

N = 5 C = 10

$\omega_o = 2\pi\ 100$ $\quad C = A/B$

#3

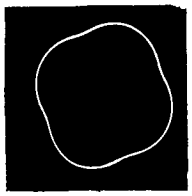

N = 5 C = 15

#4

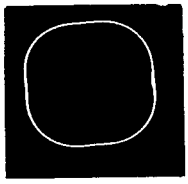

N = 5 C = 20

#5

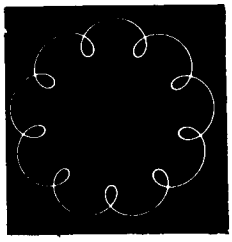

N = 10 C = 5

#6

N = 10 C = 10

#7

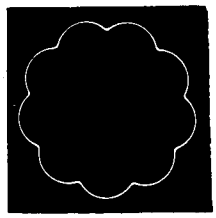

N = 10 C = 15

#8

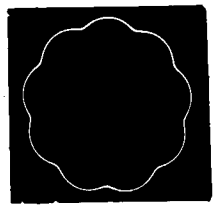

N = 10 C = 20

#9

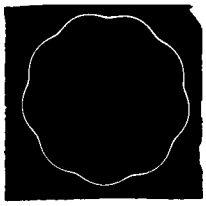

N = 10 C = 25

#10

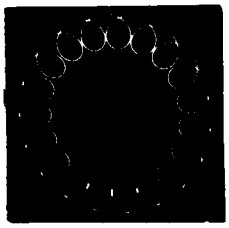

N = 20 C = 5

#11

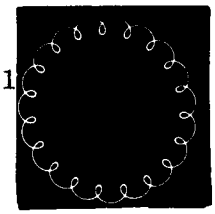

N = 20 C = 10

Fig. 1

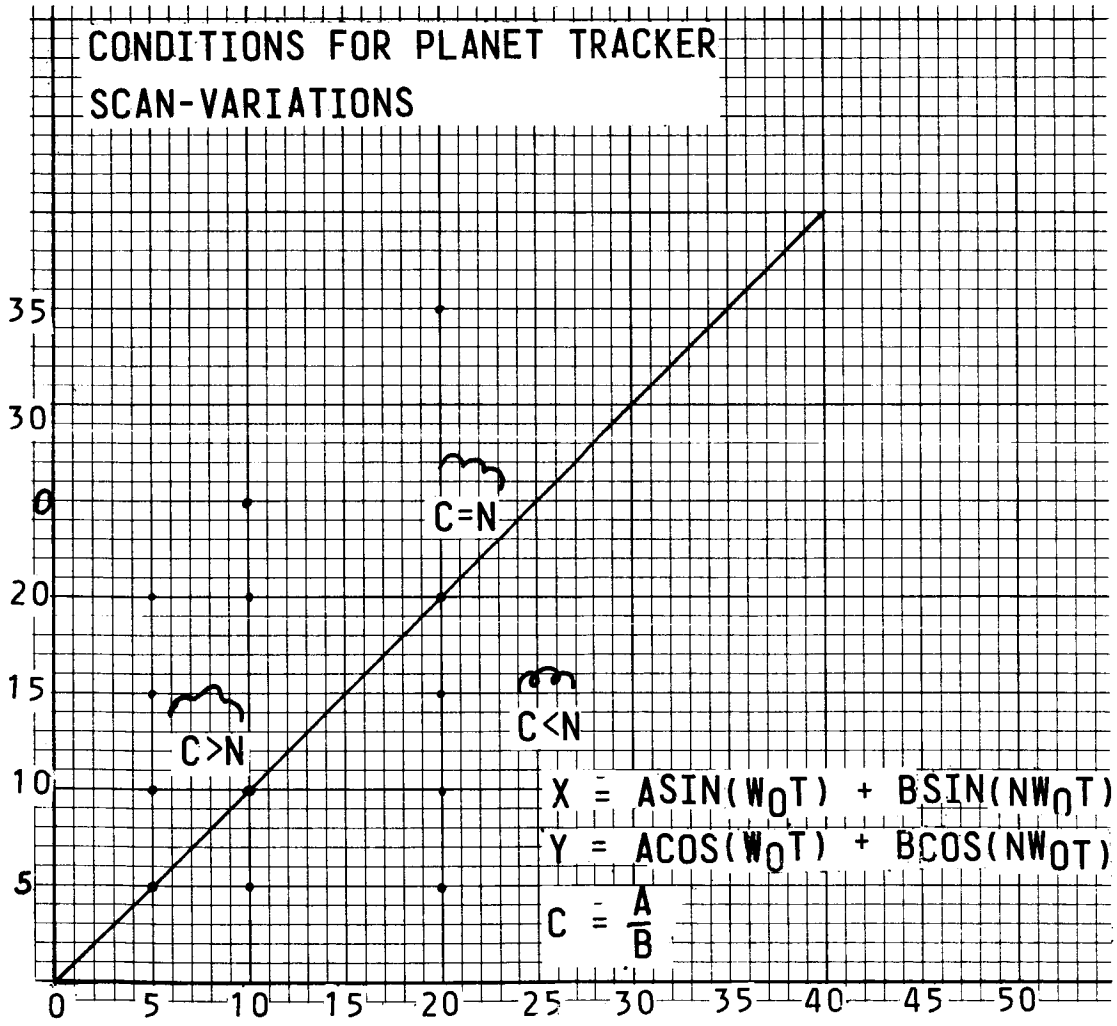
CONDITIONS FOR PLANET TRACKER
SCAN-VARIATIONS
35
30
20
15
10
5
0
5
10
15
20
25
30
35
40
45
50
C=N
C>N
C<N
X = ASIN(W0T) + BSIN(NW0T)
Y = ACOS(W0T) + BCOS(NW0T)
C = A/B

FIG 4.3

4-10A

$x = A \sin \omega_o t + B \sin N \omega_o t \quad y = A \cos \omega_o t + B \cos N \omega_o t \quad \omega_o = 2\pi\ 100 \quad C = A/B$

#12

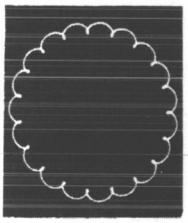

N = 20 C = 15

#13

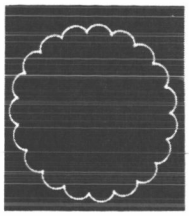

N = 20 C = 20

#14

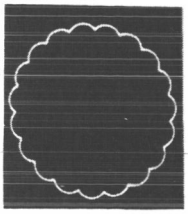

N = 20 C = 25

#15

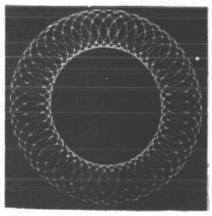

N = 50 C = 5

#16

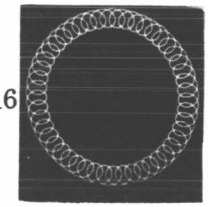

N = 50 C = 10

#17

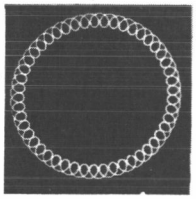

N = 50 C = 15

#18

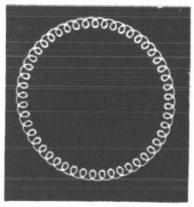

N = 50 C = 20

#19

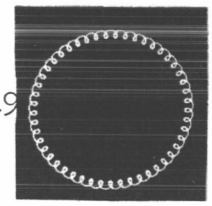

N = 50 C = 25

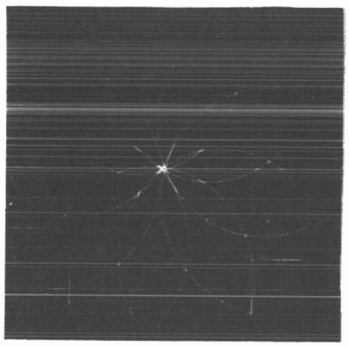

#20

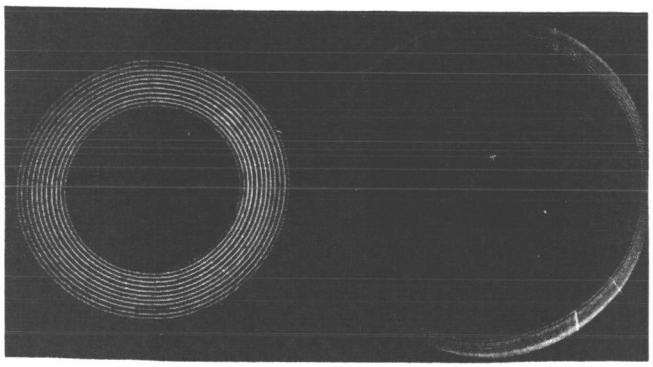

#21

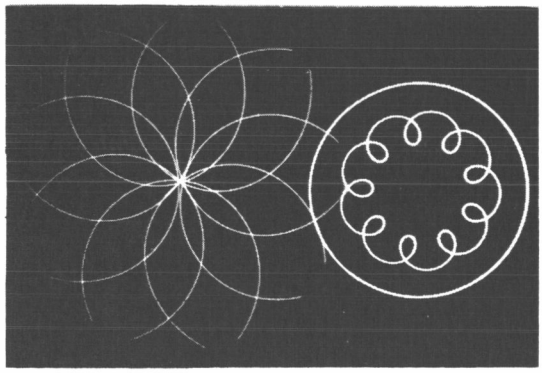

#22 N = 10

FIG 4.5

in a given time interval, and (2) the time interval in terms of required information rate. These limitations are considered to be fundamental. A secondary limitation concerns the size and shape of the field of view versus two different scanning schemes; one employing photometric balance and the other relying on scanning a known geometry. The contract states that the information bandwidth is for all practical purposes 10 c/s. This determines how rapidly one must extract position information from the photons in the planet image. From Jupiter, for the conditions described in more detail in other sections of this report, there are 10^5 photons per second available at the detector. Assuming the detector has a quantum efficiency of .1 and that the time interval is .1 sec, there are 10^3 photonelectrons leaving the photocathode in .1 sec. This implies that the signal to noise ratio is approximately 30 to 1 due to photon noise alone. If it is required to obtain position information more rapidly than at a 10 c/s rate, the signal to noise will decrease. A constant signal to noise ratio requires that more photons must be made available during the given time period.

The secondary and less fundamental limitation concerns the nature of the field of view and type of scan, that is, a photometric balance scheme or a geometric center determination scheme. To determine the geometric center, one must operate on the planet's edge. Photons coming from the center of the planet yield no information concerning the location of the edge. It follows, that since the only meaningful photons are those near the edge of the planet, the size of the field of view must be on the same order as the accuracy with which the planet's edge is to be located. There is little point in scanning the center of the image if information is to be derived from the edge crossings. Various present day earth sensors exhibit severe limitations because the scanning scheme causes the field of view to move across the earth's disc. The photometric balance scheme cannot track the geometric center and therefore can use photons coming from the entire planet disc. The S/N ratio is inherently better, but the planet's geometric center cannot be tracked. The planet tracking scheme proposed and being investigated is severely constrained by the worst case-worst case considerations for the planet Jupiter.

Various choices are available to improve the S/N ratio. These are briefly discussed in the following paragraphs. Careful consideration must be given to the need for solving the absolutely worst case, especially if its solution lessens the performance of the tracker on more usual planet situations.

The following ways for performance enhancement are considered:

1. Use the entire aperture of the I.R.O.A.O. for tracking.
2. Enlarge the instantaneous field of view of the planet tracker for Jupiter.
3. Invent a more efficient coding scheme for edge information.

Considering the fundamental limitations described previously, one of the ways to enhance performance is to provide more photons to the detector. This can

be done simply if the O.A.O. is operating in the infrared spectrum by employing a beam splitter diverting visible energy to the planet tracker while allowing infrared energy to pass through the beam splitter to the infrared experiment.

Enlarging the field of view for Jupiter scanning is another possibility. For the case of 10 arc seconds Mars image, a field of view of 1 second using our scanning scheme yields a noise equivalent angle of .2 arc seconds. Jupiter's image is approximately 30 arc seconds suggesting that it may be possible to achieve better performance by enlarging the field of view by a factor of 3 and capturing about 10 times more photons. The present roulette scanning pattern requiring a bandwidth on the order of 3000 cycles to encode planet image position information is somewhat inefficient in terms of encoding efficiency relative to the output bandwidth of 10 cycles. Although the coding scheme allows a very sophisticated determination of the planet's geometric center, it may be possible to invent a coding scheme which reduces the bandwidth to the actual information bandwidth. In general, this is very difficult to do in optical scanners, and in fact, getting the actual predetection bandwidth within a factor of 2 or 3 of the information bandwidth is difficult.

4.7 INVESTIGATION OF THE POSSIBLE USE OF VIDICONS AS A VISIBLE EDGE TRACKER

Preliminary calculations have been made to determine the feasibility of using a vidicon for the planet tracker. For this purpose, the responsivity of two vidicons, namely, the 7062A and 7038, have been selected because they were considered to have spectral responses typical of all RCA vidicons.

Sensitivity calculations have been completed for these two vidicons. The spectral response for these two tubes is shown in Figure 4.6. Two curves are shown for each tube. Both of these come from RCA sources. For the case calculated, the poorest responsivity was used. The highest responsivity would provide signal to noise ratios about twice those listed below.

Planet	S/N
Jupiter	0.018
Venus	0.636
Mars	0.051

This data was calculated with the following assumptions:

1. 3.5 inch aperture
2. 33% optical transmission
3. Bandwidth 10 cps
4. Load resistor 10 megohms

Since signal current is so low, the limiting noise level of the system is the Nyquist noise generated by the input load resistor. The large load resistor selected for the calculation was picked because it tends to maximize the signal to noise ratio. This arises because the signal voltage is proportional to the resistance while the noise is proportional to the square root of the

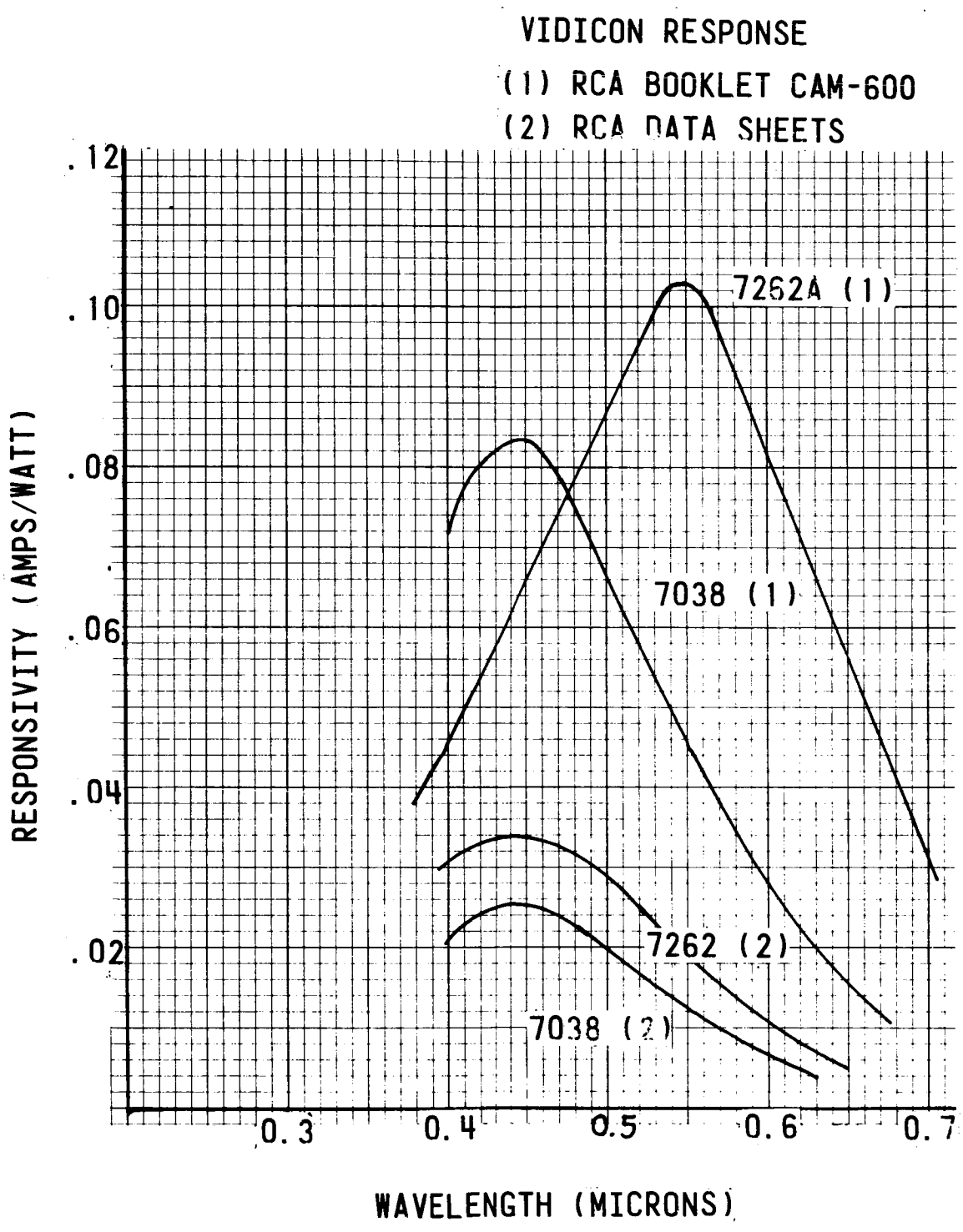
VIDICON RESPONSE
(1) RCA BOOKLET CAM-600
(2) RCA DATA SHEETS
RESPONSIVITY (AMPS/WATT)
.12
.10
.08
.06
.04
.02
7262A (1)
7038 (1)
7262 (2)
7038 (2)
0.3
0.4
0.5
0.6
0.7
WAVELENGTH (MICRONS)

FIG 4.6

resistance. Larger loads than that selected could possibly be used, but circuit time constants and interference problems are considered to offset the possible gains.

Although only two tubes were studied in detail, the responsivities of many tubes were checked and all fall within a factor of 2 or 3 of those used for the calculations. This factor is not sufficient to make the use of a vidicon possible for this system.

Slow scan vidicons could possibly provide slightly improved signal to noise ratio; however, the limit achievable is restricted by the required system bandwidth. Within this limitation, the use of a vidicon would still not be feasible.

An additional problem associated with the possible use of the vidicon is that the target must be discharged approximately once every frame time to avoid underscanning the image. The vidicons are designed to have each part of the target discharged every frame. However, if this is not done, charge builds up on those parts of the target which are not discharged by the scanning beam. This charge build-up and the need to increase the beam current to discharge the highlights degrades the performance of the vidicon considerably, particularly in the area of low signal to noise ratio. The application of vidicons to non-TV type scan modes must be done carefully. Therefore, for the reason of sensitivity and application problems, the use of vidicons is considered not feasible.

4.8 CONCLUSIONS

1. Infrared radiometric balance techniques do not appear to be feasible primarily because of signal to noise ratio problems which would require significantly larger apertures than the ground rules allow. In addition, infrared planetary radiation characteristics are not well known; some evidence indicates that there are several asymmetric gradients against the planets which may provide fundamental difficulties for infrared trackers.
2. Infrared edge tracking techniques are not feasible because the amount of energy available is even less than for the radiometric balance approach.
3. Visible photometric balance approaches are not feasible because the wide variation of the illumination centroid relative to the geometric center. Several scans have been proposed to circumvent these difficulties. These scans are more complex than edge tracking schemes.
4. The most feasible technique is to employ the visible spectrum and use an edge tracking approach. The technique originally proposed in Ref. 1.1 appears to be basically sound and was used as the basis for detailed design evaluation.

Section 5

GENERAL TRACKER DESIGN CONSIDERATIONS

5.1 INTRODUCTION AND SUMMARY

Preceding sections of this report discussed planetary radiation characteristics, traded off various tracking approaches, and concluded that a visible edge tracking scheme was most appropriate. This section proceeds from that point with a discussion of the specific edge tracking approach initially considered, and describes the evolution through the final design concept. The final design concept leads directly to the detailed design, fabrication, and test of the breadboard tracker.

The analyses described herein are based on three independent but complementary approaches:

1. Mathematical analysis where appropriate equations are written and closed form solutions are attempted.
2. Analog simulation where a cathode ray tube and photomultiplier are used with appropriate planet masks to generate actual error signals.
3. Digital computer where signal analysis programs are written for evaluation on a large digital computer.

These three techniques are used interchangeably and significant benefits were derived from checking the results of one against the other. The analog simulation was particularly useful because it was used to develop actual planet tracker circuits which were then used in the operation of the simulator.

5.2 GENERAL EXPLANATION OF EDGE TRACKING TECHNIQUES

Section 4.5 discussed the use of roulette patterns to facilitate an edge tracking scheme. This section describes, in relative simple mathematical terms, the signal coming from the Reconotron as a result of the roulette scanning pattern.

Signal Analysis: Significance of Various Harmonics

The edge tracking method chosen for the Planet Tracker is based on electronically generating a roulette scan pattern in a vidicon or image dissector tube. The particular patterns used are shown in Figure 4.2. These pictures were generated on a cathode ray tube by driving the deflection plates with the following signals:

$$X = A \sin w_o t + B \sin n w_o t \qquad 5\text{-}1$$

$$Y = A \cos w_o t + B \cos n w_o t$$

Switching from Cartesian to polar coordinates results in a radius vector

$$r = \left[A^2 + B^2 + 2AB \cos (n-1) w_o t\right]^{1/2} \qquad 5\text{-}2$$

The scan pattern formed moves in and out of a circle with a radius of $\left[A^2 + B^2\right]^{1/2}$ at the rate of $\frac{(n-1)w_o}{2}$ cycles per second. If this scan pattern is applied to the deflection plates of an image dissector having a uniform circular planet image radius $\left[A^2 + B^2\right]^{1/2}$ focused on its photocathode, the resulting output signal will be a perfect square wave (Figure 5.1) of frequency $\frac{(n-1)w_o}{2}$ when the center of the scan pattern coincides with the center of the planet image. If the center of the scan pattern and the center of the planet image do not coincide, a different pattern of pulses appears (Figure 5.1a) which repeats itself at a frequency of $Wo/2$. A simple harmonic analysis reveals that the signal shown in Figure 5.1a contains only frequencies of odd integer multiples of $(n-1)Wo/2\pi$ while the signal shown in Figure 5.1b contains both even and odd integer multiples of frequency $Wo/2\pi$, including the even multiples of frequency $(n-1)Wo/2\pi$. Neglecting for the moment the problem of getting the scan pattern center and the planet image center near coincidence, it is possible to achieve coincidence either by maximimizing the signal at frequency $(n-1)Wo/2\pi$ or by minimizing the signal at frequency $2(n-1)Wo/2$ or some other multiple of $Wo/2\pi$.

Signal Analysis: Fourier Composition of Reconotron Output

If we consider the pulse width modulation of the square wave signal which occurs when the scan circle is precisely the size of the planet, we have the following signal:

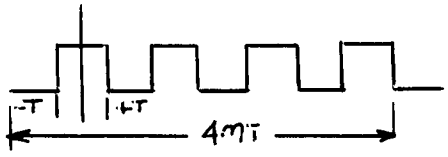

The scan frequency, $f_s = \frac{1}{4_{(n-1)}T}$ and the modulating frequency, $f_m = \frac{1}{4T}$.

$$f_m = (n-1)f_s$$

To handle the pulse width modulation, let us separately consider each of the pulses that occur in the period $4_{(n-1)}T$. The Fourier transform of a single pulse,

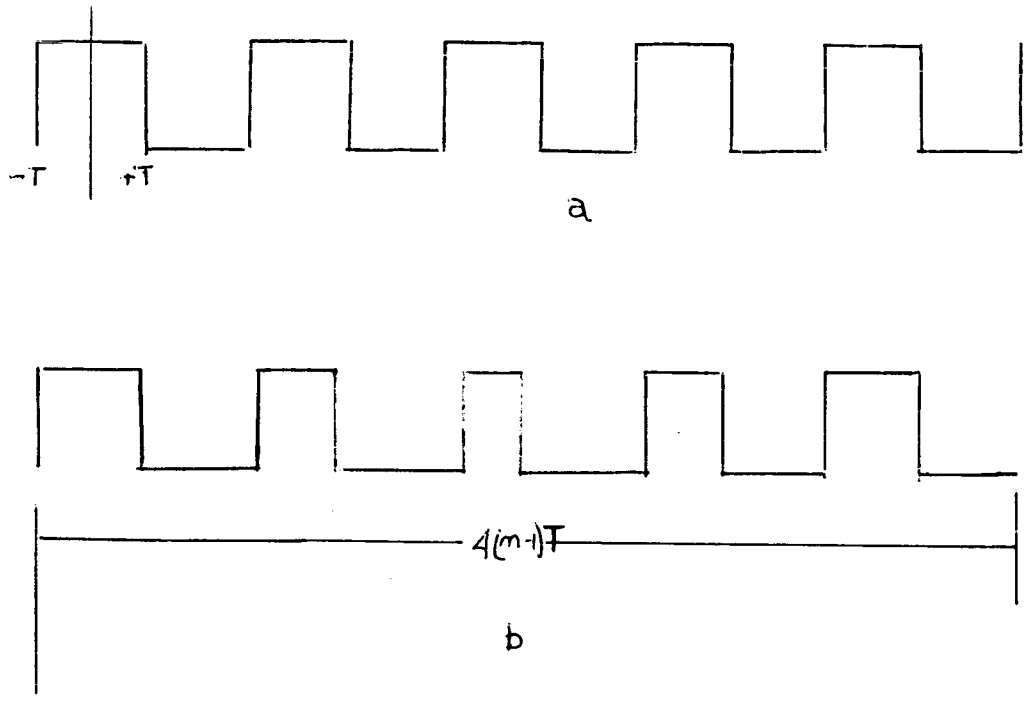

a) Signal resulting from coincidence of center of scan pattern and center of planet image (zero decentration).

b) Signal resulting from non-coincidence of center of scan pattern and center of planet image (non-zero decentration).

Fig. 5.1

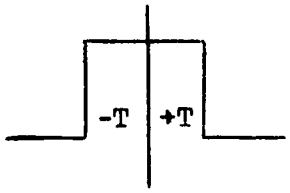

is $2T \frac{\sin 2\pi Tf}{2\pi Tf}$

For a continuous sequence of these pulses, we can obtain the time response by convolving the single square pulse with a series of Dirac delta functions. The Fourier transform of

$$\sum_m \delta(t - m\,4(n-1)T) = \frac{1}{4(n-1)T} \sum_m \delta\left(f - \frac{m}{4(n-1)T}\right)$$

Convolution in the time domain is equivalent to multiplication in the frequency domain. Thus, the Fourier transform of the pulse train is:

$$\frac{2T \sin 2\pi T f}{2\pi T f} \quad \frac{1}{4(n-1)T} \sum_m \delta\left(f - \frac{m}{(4(n-1)T}\right) =$$

$$\sum_m \frac{\sin 2\pi T \frac{m}{(n-1)4T}}{\pi m} \delta\left(f - \frac{m}{(4(n-1)T}\right) =$$

$$\sum_m \frac{\sin \left(\frac{\pi m}{(2(n-1)}\right)}{\pi m} \delta\left(f - \frac{m}{4(n-1)T}\right)$$

Up to this point only circular planet images have been considered, and these can be handled by energy balance methods. A more complete analysis of the possible image dissector signal output is needed to demonstrate the utility of this scan technique in locating the geometric center of partially illuminated planets. The complete Fourier transform, on a superposition of pulse basis, of the signal shown in Figure 5.1b is given by

$$\sum_m \sum_{p-1}^{n-1} \frac{\text{Sin } \frac{m\pi Tp}{2(n-1)T}}{\pi m} \epsilon^{\frac{-j2\pi mp}{n-1}} \delta\left(f - \frac{m}{4(n-1)T}\right)$$

5-3

where $T = \frac{2\pi}{4wo\,(n-1)}$

$2Tp$ = pulse width of the P^{th} pulse.

p = index number of the pulse. (n-1) pulses can occur in one scan of the planet, ie., every $2\pi/wo$ seconds. In the perfect square wave case, all (n-1) pulses are 2T wide.

m = index number of the harmonic of $Wo/2\pi$ being considered
m = 0, ±1, ±2, ±3 - - - -
$\delta(\ )$ = Dirac delta function

At any harmonic, m , of circle scan frequency, $Wo/2\pi$, the Fourier transform of the signal can be evaluated by taking the sum over p. For example, if the perfect square wave occurs, all the Tp's are equal to T , and for m equal to n-1 , Equation 5.3 yields a Dirac delta function of amplitude $1/\pi$ at frequency of $1/4_T$ corresponding to (n-1) $Wo/2\pi$. A similar value of $1/\pi$ occurs at m - (n-1). Since the Fourier transform of cos (n-1) Wot t is given by

$$\delta\left[f - \frac{(n-1)Wo}{2\pi}\right]\frac{1}{2} + \delta\left[f + \frac{(n-1)Wo}{2\pi}\right]\frac{1}{2} \qquad 5\text{-}4$$

the two delta functions at ± 1/4T correspond to the Fourier transform of $(2/\pi)$ cos (n-1) Wo t, the fundamental component of a square wave of unity amplitude and period 4T. Thus, by evaluating the sum over p in Equation 5-3, it is possible to compare the signal amplitude at any harmonic of $Wo/2\pi$ for any periodic series of (n-1) pulses.

The evaluation of Equation 5-3 for various conditions of planet illumination and various offsets between the planet geometric center and the scan pattern center was done using a digital computer. The computer was programmed to plot the amplitude of the m^{th} harmonic of $Wo/2\pi$ as a function of the separation between the planet geometric center and the scan pattern center. To generalize the computer output for any planet being considered, a term labeled decentration was evolved. A decentration unit corresponds to a separation between the centers equal to 10 percent of the planet radius.

Examples of the computer output are shown in the Appendix. Here, for instance, the 10th harmonic of $wo/2\pi$ is plotted against decentrations for n = 11 and a fully illuminated planet. When the planet geometric center and the scan pattern center coincide (i.e., at a decentration of zero), a maximum of the 10th or (n-1)th harmonic occurs corresponding to the perfect square wave signal. As the centers separate corresponding to an increase in decentration magnitude, the value of the 10th harmonic drops corresponding to a deviation from the perfect square wave signal.

To determine which harmonic of $Wo/2\pi$ would be best suited to provide tracking information, the first 40 harmonics were plotted against decentration for six planet illumination conditions ranging from half illuminated to fully illuminated. Of these 40 harmonics only the 10, 19, 20 and 21 were applicable. These plots comprise the Appendix. It was initially thought that it would be desirable to use a harmonic which provided a minimum at zero decentration such as would occur with the 20th harmonic, an even integer multiple of frequency (n-1) $Wo/2\pi$. However, Appendix 5.1 shows that the 20th harmonic also has minimums at values of decentration other than zero. Other harmonics such as the 19th and 21st had single minimum at zero decentration for fully illuminated planets. The

harmonic providing the most unambiguous indication of coincidence between the planet geometric center and the scan pattern center for all conditions of planet illumination proved to be the 10th, which always provided a significant maximum at zero decentration.

In the preceding paragraphs, the discussion has been centered about the 10, 19, 20, 21 harmonics of the signal. It should be emphasized that these particular harmonics apply only if n = 11, which was picked arbitrarily for the computer analysis. In general, the harmonics of concern are (n-1)fo, 2(n-1)fo, and $2(n-1) \pm 1$ fo, respectively.

5.3 ANALYSIS TECHNIQUES, MATHEMATICAL, DIGITAL, ANALOG

We digress here for a discussion of the three principal analytical tools employed to determine the amount and form of the error signal generated for a given planet decentration; i.e., for a given displacement of the planet image from the tracking null center, what is the change of the electronic signal resulting from this angular displacement? These three techniques determined the final tracker design.

The mathematical techniques used are based simply on signal analysis using conventional Fourier techniques. Examples of such analyses are shown in Section 5.2. Obviously, the hand calculation of the harmonic content of numerous harmonics of the Reconotron output signal is tedious and time-consuming. For this reason, the calculations in all cases were completed on an LMSC 7094 digital computer. The computer outputs were checked in a few instances by calculating the magnitude of certain harmonics by hand and more generally by comparison with the information obtained from the analog simulator.

The computer programs for harmonic analysis are based on a geometric determination of whether the scanning spot is inside or outside the planet image. If the spot is outside the planet image, there is no output from the Reconotron. If the spot is inside the planet image, a signal results. The time sequence of the spots crossing the planet horizon generate a square wave as a function of time which can then be evaluated by computer-based Fourier analysis techniques which are well developed. The following paragraphs describe the calculation procedure in more detail.

The geometric aspects of the computer program are constructed along the following lines. The scanning circle is deviated by these X and Y voltages:

$$X = A \sin w_o t + B \sin nw_o t \qquad 5.3.1$$

$$Y = A \cos w_o t + B \cos nw_o t \qquad 5.3.2$$

The locus of the spot driven by these voltages is a roulette pattern. To compute the amount of time the scanning spot spends inside and outside of a circle or a combination semicircle and semielipse (for the gibbous case) whose diameter is equal to the diameter of the planet image, equations 5.3.1

and 5.3.2 are written in polar coordinates (ρ , θ).

The instantaneous position of the spot represented as a radius vector from the center of the planet image is compared to the planet radius. If the magnitude of the radius vector is greater than the planet radius, a "0" is written; if the magnitude is less, a "1" is written. If the instantaneous position of the scanning spot is on the planet edge, the immediately preceding symbol is written.

Since the instantaneous position of the scanning spot is a function of time, a sequence of 1's and 0's is generated where each symbol represents a given time increment. The time increment is scaled according to the frequency w_o and nw_o. The sequence of "1"'s and "0"'s is formed into a square wave which is readily able to be represented in Fourier terms using the high speed Fourier computer program, a program which has been in use at LMSC for signal analysis for several years.

Planet decentrations are readily handled by this technique by introducing appropriate translation terms, x_o and y_o. This basic analysis technique generated practically all the data in the Appendix.

The analog simulator which proved to be an equally powerful tool as the digital computer was designed and fabricated from existing LMSC components for use on this program. It actually was an adaptation of an amplitude probability distribution analyzer used in noise studies, which consists of a conventional cathode ray oscilloscope, an oscilloscope camera housing containing a photomultiplier, the photomultiplier power supplies and amplifiers, and appropriate planet masks. The planet masks are in the form of metal cutouts in the shape of a planet and are placed on the face of the cathode ray tube. Voltages are applied to the X and Y deflection amplifiers which deviate the spot on the cathode ray tube in a planet tracking mode. When the photomultiplier "sees" the scanning spot through the hole in the mask, a signal results. When the scanning spot crosses the edge of the mask, there is no signal. The photomultiplier output is therefore a square wave in time where the individual square wave pulses are pulse width modulated according to the time duration that the scanning spot spends in the mask aperture. This analog simulation assembly replaced the optics, Reconotron, radiation source, radiation source optics, and optical bench of the planet tracker and allowed the complete design and checkout of practically all the planet tracker electronics in the absence of the Reconotron (which was delivered late).

In typical operation, the X and Y voltages were generated by a series of synchronized oscillators which were eventually replaced by transistorized oszillator circuits used in the final planet tracker design. As various circuits were designed, they were tested on the simulator and configured in final form. They were then used along with the simulator to generate waveforms which were used in the design and checkout of the remaining circuits. The photographs shown in Section 4.5 were all generated by this analog simulator.

In the development of the digital computer program, two minor programming errors, which were significant only in certain extreme cases, were detected because of a discrepancy between the digital computer output and the information obtained from the analog simulator. Without the simulator, it would have been difficult to discover the problems because the program yielded satisfactory results for most of the cases examined.

The use of the simulator, however, was not without its difficulties. Problems were encountered with the long decay time of the cathode ray tube phosphor which prevented simulation of rapid signal decay times. This problem was reduced by replacing the phosphor with a faster response phosphor, but one which exhibited a "halation" effect. The halo was an inherent characteristic of the CRT and resulted from scattering of beam electrons causing a "halo" around the light spot. This problem was overcome by incorporating a threshold circuit at the output of the photomultiplier which eliminated that part of the signal associated with the slow rise and fall times caused by the halo.

Detailed evaluations of electronic circuit performance were accomplished using the simulator. This allowed optimization of the circuitry without the Reconotron and associated optics.

Tracking susceptibility to noise was tested using the analog simulator and a white noise generator. It was determined early in the program that the tracker could find and track semi-circular planets down to a signal-to-noise ratio of 10.

5.4 SIGNAL OUTPUT FOR GIBBOUS CASE

To determine the effect that a circular or gibbous planet (or a planet with radiation dropout on one side) would have on the signal output, the planet tracker computer signal analysis program was run for seven different cases. Case 1 was the full planet with a radius = $(a^2 + b^2)^{\frac{1}{2}} = (101)^{\frac{1}{2}}$ where $a = 10$ is the amplitude of the fundamental frequency and $b = 1$ is the amplitude of the dither frequency. Cases 2 - 7 were gibbous planets where the minor axis of the elliptical section was varied.

Data was calculated for gibbous planets with elliptical edges corresponding to eccentricities from 0.0 to 1.0 in steps of 0.2 (see Figure 5-2).

The harmonics calculated include the 1, 10, 11, 19, 20, and 21. These harmonics were calculated for decentrations in the x and y directions for planets having a gibbous side as shown in Figure 5.2.

The initial Planet Tracker design philosophy was based on utilizing phase information from the fundamental or circle frequency, f_o, to drive the scan toward a null at the circle frequency. When null was achieved, it was planned to switch to $2(n-1)-1$ f_o for fine tracking and proceed to null this component since it was more sensitive. This approach was based on the fact that computer analysis of the signal harmonics indicated that the $2(n-1)-1$

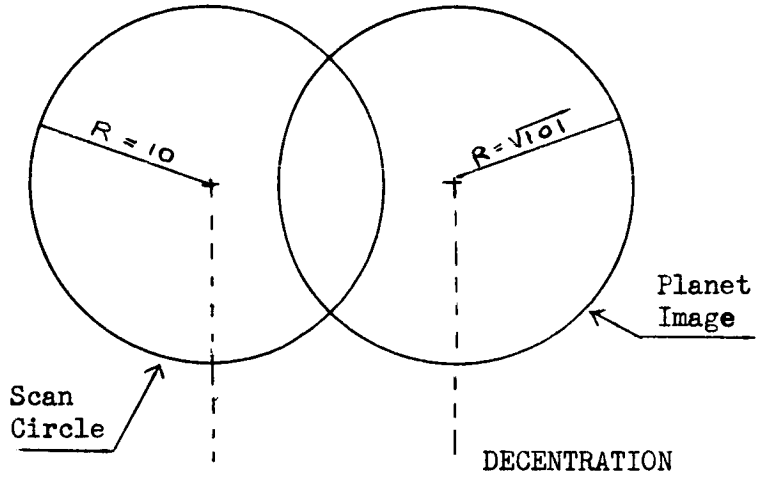

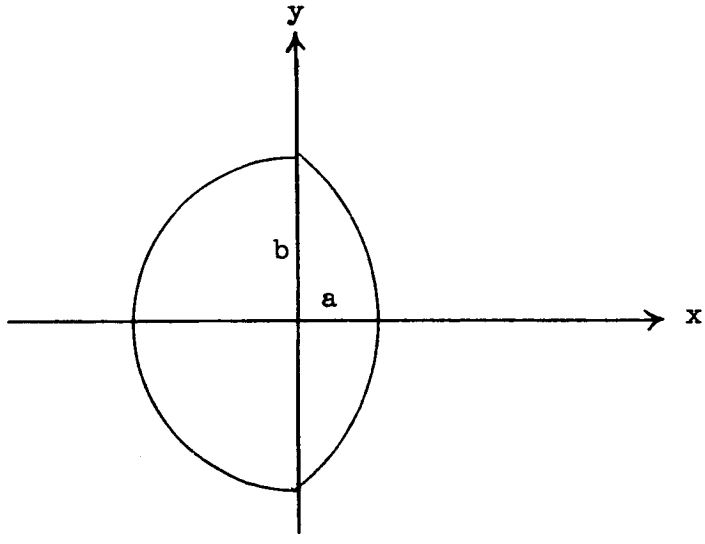

GIBBOUS PLANET
TARGET DEFINITIONS

Fig. 5.2

harmonic of the signal went to almost zero when the image and scan were aligned. As time progressed, it became evident that the computer outputs were somewhat in error, leading to the discovery of two programming errors. These errors were corrected and final harmonic data calculated. The data for the tenth harmonic is provided in the Appendix of this report.

Investigation of the refined data showed that it was difficult to proceed as originally planned. This arose as a result of the fact that within the limits set by nulling the circle frequency, more than one null occured on the 2(n-1)-1 harmonic. Techniques for selecting the correct null were investigated; however, they all seemed difficult because of the variations involved in setting thresholds for different gibbous situations. As a result of this, it was decided to revise the basic approach.

The approach selected performs initial acquisition as originally planned with final fine tracking achieved by peaking (n-1) f_o. The reason for this selection is evident from reviewing the computer data. For example, motion in the Y direction produces a peak signal on axis in all gibbous situations. Motion along the X axis produces good peaks in all cases; however, in some cases the peak is about one decentration from the center line.

For the corresponding worst target situation, Venus has a radius of about 5.5 seconds when A/B = .8. This will result in an error of one tenth of 5.5, or 0.55 second error. In the case of Mars, when A/B = 0.8, the planet radius is almost 4.8 seconds, so an error of .48 second is possible. Jupiter is always almost round (A/B = .98) and thus presents no problems.

The nominal 0.55 second error encountered in the case above is considerably less than the 1.6 second specification and only exceeds the goal by .05 second.

Comparison of the digital computer data and the analog computer data for approximately the same decentrations indicates the results may be better than those calculated from the digital data. This arises because the digital data was "rounded off" for each decentration unit.

These paragraphs described the final results of the rather extensive digital computer and analog simulator analyses and briefly reviewed the evolution of the planet tracker signal processing design.

5.4.1 Mathematical Analysis

A suggestion made by M. Hansen of NASA/Ames Research Center concerning scanning pattern generation involves the use of amplitude modulation of the following form:

$$x = A \sin w_o t + B \sin n w_o t \sin w_o t$$
$$y = A \cos w_o t + B \cos n w_o t \cos w_o t$$

Investigation showed that this scan pattern generation technique is not as satisfactory as the previously described technique because: 1) it is difficult to implement; 2) it provides no fundamental advantage in sensing image position errors; 3) it generates peculiar periodic waveforms which spread signal energy into several harmonics rather than tending to concentrate signal energy in a few harmonics. It is also not obvious that this technique does not introduce considerable ambiguity in the location of harmonic nulls.

5.5 TRACKER CONCEPT DETAILS

Section 5.4 described the evolution of the signal processing techniques for the design of the planet tracker. The discussion was primarily based on analytical considerations. The activities described in Section 5.5 involves the implementation of the analyses in a tracker configuration and parallels the activities discussed in Section 5.4.

The basic acquisition and scan circuitry in the block diagram (Fig. 5.2A) is almost identical to that originally proposed. However, to incorporate the peak seeking circuitry, it has been necessary to include a third component in the scan. The details of this scan motion and the subsequent signal processing ard discussed in the following sections.

The scan consists of a rosette type pattern which slowly moves around in a circular manner. In order to generate a scan of this type, it is necessary to generate three different frequencies which are synchronized. The three frequencies are called, respectively, the circle, dither, and slither frequencies. These three frequencies in addition to components, shifted 90°, are respectively summed and applied to the deflection circuits of the Reconotron.

In the block diagram (Fig. 5.2A) the three frequencies are developed from the dither frequency clock (nf_o = 1200 cps) which is counted down by $\frac{1}{n}$, (n = 12), to develop the circle frequency which is in turn counted down by 1/P (P = 5) to develop the slither. Since the outputs of the countdowns are square waves, the individual frequencies are filtered to develop sinusoids with less than 1% harmonic distortion.

In order to accomplish initial target location, it is necessary to cycle the amplitude of the circle diameter. This is accomplished by sawtooth amplitude modulation of the circle frequency amplitude during the search mode. The sawtooth is generated in a ramp generator.

In the search mode, the slither frequency input to the scan summer is turned off and the scan circle changes in amplitude. Upon intersection of the scan with a target of sufficient amplitude, the signal threshold is exceeded and a

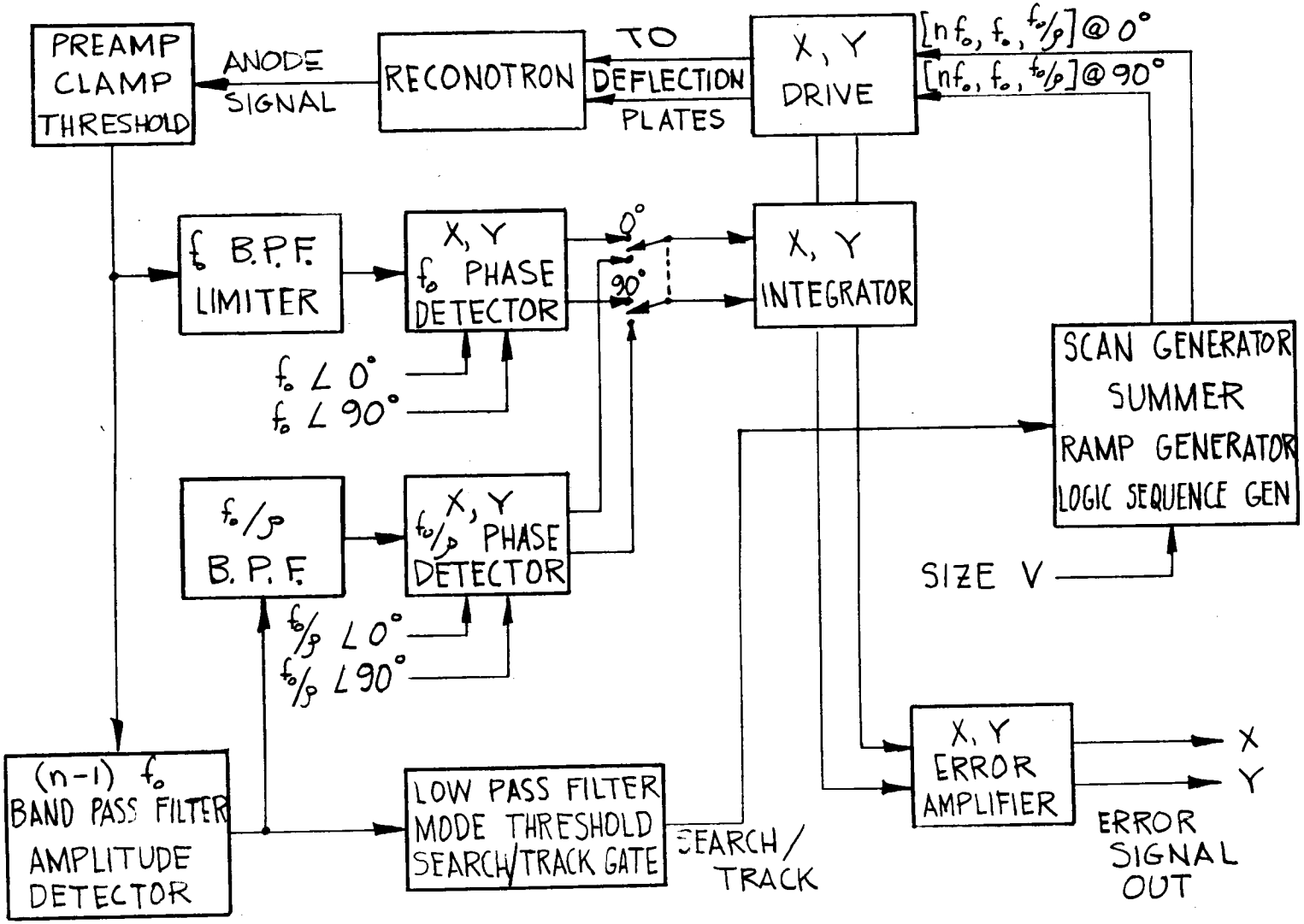

Figure 5.2A

SIMPLIFIED BLOCK DIAGRAM

narrow pulse (about 2.0 ms) is generated. This pulse occurs at a rate equal to the circle frequency, f_o, and is thus passed through a f_o bandpass filter and subsequent limiter to normalize signal amplitudes.

The location of the target intersection is determined by phase detection of the resulting f_o signal with the f_o scan components. The output of the two (X and Y axes) phase detectors is smoothed and used as an input for the X and Y Reconotron drive amplifiers. Thus, the center of the scan circle moves toward the center of the planet image.

As the scan and image become aligned, a component at (n-1) f_o is generated as a result of the fact that more dither loops intersect the target. This component is filtered, limited, and integrated in a diode detector low pass filter circuit. When the output of the low pass filter exceeds the mode threshold, it provides one of two outputs to an AND gate which flips the search track switches. The second input to the AND gate is provided when the scan circle diameter is equal to the known target diameter. This information is generated by comparing the scan circle diameter or the ramp generator output to the target size input.

As the AND gate is energized, all the search track switches are energized to the track mode. At this time the ramp is turned off and the target size is fed directly to the scan amplitude control, thus fixing the scan diameter. Also, the 1/P countdown starts slither motion. The output of the (n-1) f_o amplitude is at f_o/P and this frequency is filtered and passed through X and Y phase detectors and subsequently to the X and Y drive, with such a polarity to drive the signal toward a maximum. The resulting error signal is scaled from the X and Y drive signals.

The block diagram shown in Figure 5.6 was further modified from the original concept by the addition of the slither circuits. The revision was necessary because analysis of the computer data indicated it would be more advantageous to peak the signal on the (n-1) f_o signal harmonic than on the 2(n-1) 1 f_o harmonic. More specifically, use of the (n-1)f_o harmonic eliminated several double null conditions that could exist when gibbous planets were being tracked.

The slither circuits were added to the overall diagram because the (n-1)f_o signal harmonic must be driven to a peak rather than a null as had been the case with the (2n-1)-1 f_o harmonic. Thus, in effect, the slither circuits differentiate the f_o harmonic.

5.6 CHOOSING THE VALUES OF n, A, AND B

The relationship between n and A/B which determines the shape of the roulette pattern has been discussed in Section 4. Also, it has previously been established that the reltaionship between the planet radius R and the value of A and B must be

$$R = \left(A^2 + B^2\right)^{1/2}$$

to provide a square wave output when the scan pattern circle is coincident with the geometric center of the planet image.

It was originally decided to fix the value of B and let only A vary to accommodate the various planet sizes. The value of B was to be set at ten percent of the radius of the smallest planet. This would insure that the scan pattern would penetrate far enough into the smallest planet image to provide a suitable signal and yet not allow a loop of the pattern to extend through a gibbous planet and disrupt the signal logic. If these conditions were met for the smallest planet, they would certainly be met for all larger planets. When the value of B was fixed at ten percent of the radius of the smallest planet, it was less than two percent of the radius of the largest planet. Due to the nonlinearities inherent in the deflection circuit of the image dissector, it was impossible to maintain a perfect scan circle when the scan pattern covered a large portion of the image dissector photocathode. Thus, when the dither amplitude, B , was less than two percent of the scan circle amplitude, A , a change in the signal output large enough to cause an unacceptable error occurred. By fixing the ration of A/B at 10, a suitable signal was obtained for all planet sizes.

The determination of the value of n was based on the premise that it is desirable to have as many loops in the roulette pattern as possible to obtain the maximum sampling of the planet edge. However, there are two basic limitations on how large n can become. The first is the desired information bandwidth of 10 Hz placed on the tracking output signal. The second is the maximum preamp bandwidth that can be used and still maintain a signal to noise ratio of at least 10 at the preamp output for the lowest planet radiance.

The information bandwidth requirement of 10 Hz requires that the circle frequency be at least 10 Hz. However, large electronic components must be used to make an oscillator of such a low frequency, making a larger frequency more desirable. In order to avoid any interference with the laboratory 60 Hz power, a scan circle frequency of 100 Hz was chosen. It was then determined that the maximum preamp bandwidth that would still allow a signal to noise ratio of 10 had its 3 db point at approximately 3000 Hz and rolls off at 6 db per octave. The maximum fundamental component of the signal square wave that could be accommodated under these conditions was found to be 1100 Hz. Since the circle frequency was set at 100 Hz and since (n-1)100 - 1100, the maximum value of n is 12.

This discussion has indicated that the determination of the values of n , A , and B were made purely on a practical engineering basis. At the time the electronic circuitry was being designed, no optimization calculations had been performed. Volume II of this report shows how the exact values of n, A, and B should be determined for the optimum scan pattern.

5.7 SIGNAL TO NOISE REQUIREMENTS

The electronic system developed to track the geometric center of Mars, Jupiter, and Venus, and described in Section 6, requires an input signal to noise ratio of at least 10 in order to work effectively. To fully specify this signal to noise ratio, the measurement conditions must be stated. The final electronic configuration has a 100 Hz circle frequency, a 1200 Hz dither frequency resulting in an 1100 Hz signal output, and a 20 Hz slither frequency. This combination of frequencies allows the required output information bandwidth of 10 Hz to be met and results in a preamp noise equivalent bandwidth of 3000 Hz. The signal to noise ratio that is under consideration is therefore the peak signal at the image dissector output obtained from a scan of the planet image divided by the "noise in signal" contained in a 3000 Hz bandwidth.

The signal to noise ratio that will result when a planet is imaged on the photocathode of the image dissector through a 5-inch diameter optical system is determined in the following manner. The signal current referred to the photocathode surface is given by:

$$I_s = A_o \Omega T \int_0^\infty N(\lambda)\, \sigma(\lambda)\, d\lambda \qquad -1$$

where

I_s = signal output in amperes
A_o = collecting area of the optics = 125 cm^2
Ω = field of view determined by the image dissector aperture and the optical focal length = 0.84 arc sec^2
T = efficiency of the optical system = 0.50
$N(\lambda)$ = planet radiance in watts/cm^2 - arc sec^2 - micron
= responsivity of the image dissector in amperes/watt
$d\lambda$ = wavelength in microns

The value of the integral has been determined for all three planets using a 7094 digital computer (see Sections 3 and 4). The smallest value of the integral occurs in the case of Jupiter and results in a value of 2.02×10^{-16} amps/cm^2 - arc sec^2. Substituting in equation -1 results in

$$I_s = 125 \times 0.84 \times 0.50 \times 2.02 \times 10^{-16} = 1.1 \times 10^{-14} \text{ amperes}$$

The "noise in signal" referred to the photocathode surface is given by

$$I_n = \left[2\, e\, \Delta f \cdot I_s\right]^{1/2} \qquad -2$$

where e = charge on an electron = 1.6×10^{-19} coulombs
f = electronic bandwidth = 3000 Hz

Substituting in equation -2

$$I_n = 2 \cdot 1.6 \times 10^{-19} \cdot 3 \times 10^{3} \cdot 1.1 \times 10^{-14} \quad o/2$$

$$= 3.24 \times 10^{-15} \text{ amperes}$$

The signal to noise ratio is then given by

$$S/N = \frac{I_s}{I_n} \qquad -3$$

$$= \frac{1.1 \times 10^{-14}}{3.24 \times 10^{-15}}$$

$$= 3.4$$

Since the electronic system requires a signal to noise ratioof at least 10, system modifications must be made to achieve effective tracking for the lowest planet radiance levels. Two basically different approaches are available: either the electronic system must be modified to work at the present signal to noise ratio, or the signal to noise ratio must be increased. The modification of the electronic system could possibly be accomplished, but not without a complete system redesign. The modifications would consist of a series of small changes to each of the present electronic subsystems. The results of the scan pattern optimization study would also be incorporated into these modifications, but at this time it is not certain that the final system could operate under the present signal to noise conditions. Only after the system has been constructed and tested can a final determination of its effectiveness be made. To increase the present signal to noise ratio by a factor of three, it is necessary to increase the radiation power falling on the photocathode by a factor of nine since the signal to noise ration is proportional to the square root of the signal current. Assuming the present quantum efficiency of image dissectors will not be significantly increased in the near future, the optical collecting area must be increased by a factor of nine to obtain the desired signal to noise ratio. The resulting 15-inch optical system is very undesirable and certainly not within the planet tracker specifications. However, the signal to noise ratio could be increased by the desired amount if the bandwidth of the preamp were reduced by a factor of nine. The result on the entire system would be that the output information bandwidth would be reduced from 10 Hz to 1.11 Hz. Considering that large astronomical telescopes are to be positioned, and based on design consideration evolving from LMSC's Apollo Applications Program studies, a 1 Hz information bandwidth might be entirely acceptable and possibly more reasonable than a 10 Hz bandwidth. Changing the operating frequencies of the electronic system would not require a complete redesign, but merely scaling changes to the present system where effective planet tracking capabilities with an input signal to noise ratio of 10 have already been demonstrated.

5.8 OPTICAL DESIGN CONSIDERATIONS AND CONSTRAINTS

The general requirements for the planet tracker optical system are to collect enough energy (energy equivalent to what would be collected for planet tracking from the IROAO), place an image of appropriate size and angular resolution on the photocathode of the Reconotron, and to achieve these requirements within a package diameter of 7" x 12" long.

The specific requirements, i.e., those which were required to be met by the optical design, are:

Angular Resolution	= 1 arc sec
Diameter of Airy Disk	= .002 inch
F.O.V. (square)	= 4.5 x 4.5 arc min
Max. dimensions of whole package	= 7" diameter x 12" long
Sensor: Type CL-1147 Electrostatic Reconotron	

Several designs were considered initially and a Zoomar objective and a Luminar field lens were finally selected. The combination provided an f/80, 5" diameter, f = 400" system.

The design approach emphasized using commercially-available telescopes, because of their on-the-shelf availability and low cost.

Because the optics selected were diffraction limited, it was necessary to determine the contribution of the Airy disk to system response. For the purpose of this analysis the planet can be considered an extended source, the edges of which display an intensity gradient caused by diffraction. The electron beam of the Reconotron sweeps across the diffraction pattern at the edge of the planet. The resulting waveform is then an S-shaped ramp rather than a step function. The shape of the waveform results from the convolution of the edge intensity gradient and the beam sensitivity gradient.

The intensity gradient of the planet edge can be represented as the normalized diffraction pattern of an edge type extended incoherent source which has been defined as

$$\frac{I}{I_o} = \frac{1}{2\pi}\left(2\mathrm{Si}(2K \alpha D) + \pi - \frac{2\sin^2(K \alpha D)}{K \alpha D}\right)$$

where $K = \frac{2\pi}{\lambda}$ = .5 microns

and D = aperture diameter

by R. C. Redden et al (Ref. 5.1). A plot of the normalized curve is provided in Figure 5.3.

For an assumed focal length of 250 inches (actually 400 inches were used in the completed tracker), the width of the diffraction pattern is

$$\frac{250}{6} \times .5 \times 10^{-6}\alpha = 2.08 \times 10^{-5} \text{ m}$$

If it is assumed that the scan beam intensity distribution is given by the following general Gaussian equation,

$$Y = \frac{h}{\sqrt{\pi}} e^{-h^2(X)^2}$$

where: y = relative beam intensity

$h = \frac{1}{2\sigma}$

x = the distance from the peak of the intensity curve
= the point on the x axis where the integral from 0 to x is 0.34

h must equal $\sqrt{\pi}$ to normalize the equation.

Thus $Y = e^{-\pi x^2}$

$Y =$

when y = 0.2 $X = \sqrt{1/\pi \, Ln \, 5}$

X, however, must be related to the beam dimensions, therefore let X = kr and we know that r = 0.001 when y = 0.20 from the CBS data sheet.

Thus $X = kr = x = kr = \sqrt{1/\pi \, Ln \, 5} = 10^{-3}K$

$K = 716 \text{ in.}^{-1}$

Thus $Y = e^{-\pi(716)^2 r^2}$

the standard distribution of which is

$$\sigma = \frac{1}{hK\sqrt{2}} = \frac{1}{716\sqrt{2\pi}} = 5.57 \times 10^{-4} \text{ in.}$$

The convolution integral can be evaluated incrementally to a good approximation. If one superimposes the beam spot area on the diffraction pattern distribution and moves the beam spot by 1σ while evaluating the superimposed area for each 1σ increment, the total response can be evaluated. The results of such a technique are given in Figure 5-4.

The resulting slope in the waveform edge as illustrated in Figure 5-4 shows a 10 to 90% rise time of the equivalent of 2.5 arc seconds. An increase in focal length will increase the linear dimensions of the diffraction pattern while the scan beam remains the same. Since the overall image size increases at the same rate as the edge, an increase in focal length would tend to steepen the waveform.

Comparison between the longer and shorter focal length systems, on the basis of the requirements, is listed below:

Normalized Single Slit Diffraction Pattern Intensity Distributions Due to the Edge of an Extended Source

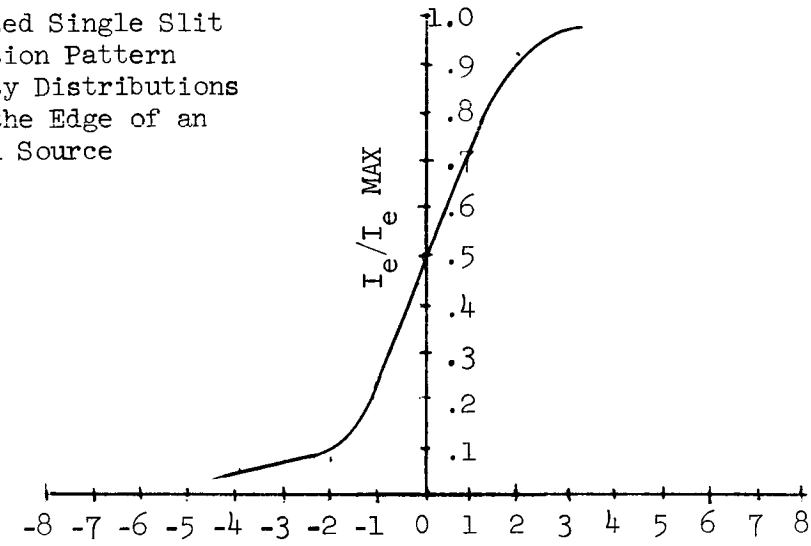

Figure 5.3

Convolution of Single Slit Diffraction Pattern (Fig. 5-3) and Gaussian Scan Beam

$\lambda = 0.5\mu$

$f_L = 250"$

$\alpha = 0.00082"$

D = 6 in.

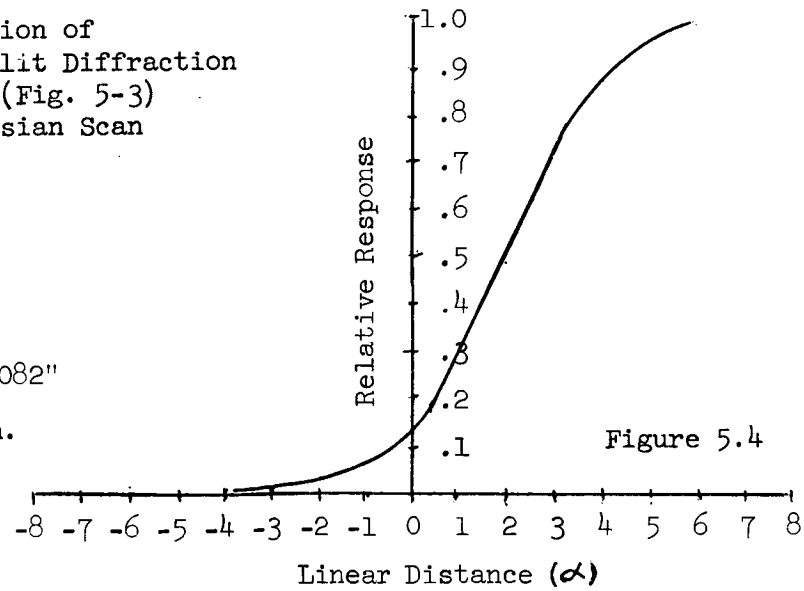

Figure 5.4

	384" System	210" System
S/N	Best in Track Mode	Best in Search Mode
Linearity		Best, utilizes minimum sensitive surface
Drive Electronics	Same	Same
Size	Somewhat larger than spec.	About equal to spec.

The longer focal length system is chosen because it will provide better tracking capability.

The final optical system configuration is shown in Figure 5-5 and consists of a Zoomar Reflectar of 40" focal length, effective aperture f/8, and 5" diameter, used with a Luminar of 16 millimeter focal length. The object distance is 17.6 millimeters and the image distance is 176 millimeters, giving a magnification of 10 times. (Note: The "object distance" (or short conjugate) is between the "object-sided nodal point" of the Luminar and the primary image ("the object") of the Zoomer Reflectar. The Image Distance" (or long conjugate) is between the "image-sided nodal point" of the Luminar and the image on the Reconotron (10 x magnified).)

The final configuration has an effective focal length of 400" and an effective aperture of f/80, and a 5" diameter.

5.9 CONCLUDING COMMENTS

The information reported in this chapter represents a considerable part of the entire Planet Tracker activity. The analyses are the result of extensive cross-checking and re-evaluation. The final designs are the distillation of trade-off analyses which continued for several months. The apparent logical sequence of section headings and technical descriptions belies the intensive scrutiny, re-appraisals, and re-evaluations in obtaining agreement between the various analytical techniques used and in configuring block diagram approaches to implement the schemes analyzed.

As a result of this activity, we conclude:

1. The original design concept as proposed is basically sound, although significant modifications are needed so that the tracker can operate reliably under all conditions of illumination and planet size.
2. The basic technique is a visible edge tracking technique which makes use of the harmonic content of the various error signals generated by a roulette scan of the circular part of the planet image. The (n-1)fo, harmonic provides reliable and unambiguous indications of decentration direction and magnitude for all planetary cases considered.
3. The analytical evaluation resulted in the configuration of block diagrams which allow technologically feasible and realistic hardware implementation.

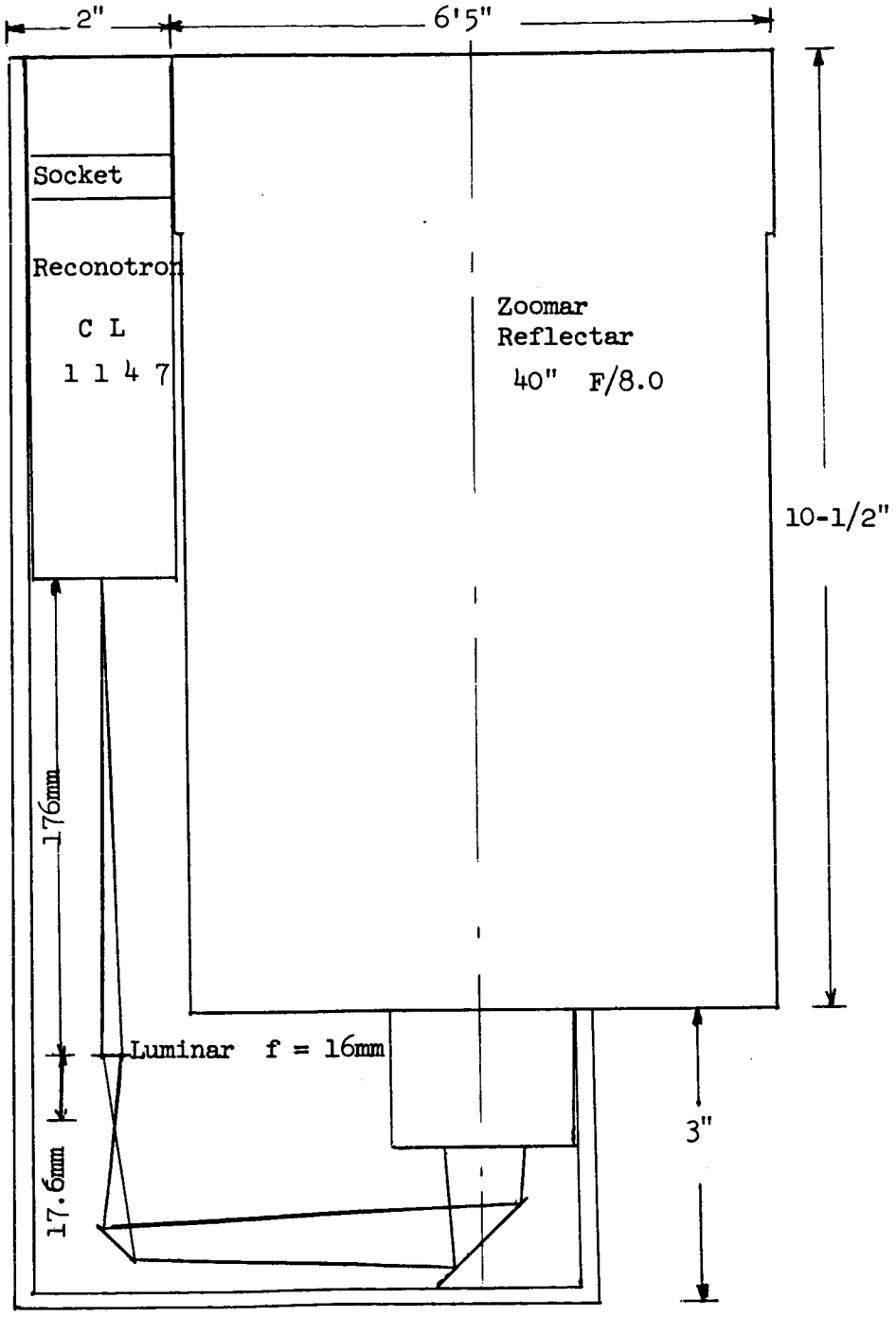

Figure 5.5 Folded Optical System for Planet Tracker

Section 6

INSTRUMENT DESIGN

6.1 INTRODUCTION AND SUMMARY

Preceding sections have described the trade-offs among various design approaches. Section 4 concluded that an edge tracking system operating in the visible region of the spectrum was the best approach. Section 5 treated visible edge tracking systems in detail and came up with a final design approach and recommended implementation to satisfy the requirements. This section, Instrument Design, discusses the actual breadboard hardware. Section 6.2 contains the major information, i.e., the theory of operation. Section 6.3 describes the system operations, and Section 6.4 is a short section summarizing optical and mechanical characteristics of the breadboard hardware.

6.2 THEORY OF OPERATION

The operation of the planet tracker is discussed thoroughly in Section 5. Briefly reviewing, the basic scan is a roulette pattern having 11 loops. The planet is initially found in the search mode utilizing a spiral scan. The planet tracker then switches from "search" to "track". In the track mode, a f_o/p slither modulation is used to allow tracking on the true center of the planet rather than the center of the illuminated area. These scans are illustrated in the photographs of Figures 6.1 through 6.5. Waveforms at various circuit points corresponding to these scans are shown in Figures 6.6 through 6.12.

The planet tracker operation was determined on the basis of computer analysis which provided the output amplitude of the f_o and $(n-1)f_o$ harmonics as a function of decentration in the x and y axes. The case of the planet with $a/b = 0.6$ on the f_o harmonic has been replotted in Figure 6.17 to include phase information and the outputs of synchronous 0 degree and 90 degree phase detectors. The familiar S-shaped response results. A null occurs at $y = 0$, $x = 1.5$ du (decentration unit; refer to definition in Section 1; 1 du = 0.1 planet radius) for $a/b = 0$. The worst case would be for $z/b = 0$, where $y = 0$, $x = -2.5$ du. The largest resulting error for the worst case planets of Appendix 5.4 is for $a/b = 0.2$, radius ' 9.6", $y = 0$, $x = 2$ du $= -2$". This exceeds the spec value of $\pm$ 1.6".

Therefore, to achieve the desired accuracy, a f_o/p slither modulation is added to the scan. This results in modulation of the $(n-1)f_o$ harmonic amplitude (see Figures 6.9 - 6.12). The peak of the $(n-1)f_o$ amplitude vs. decentration curve can be found electronically by using an amplitude detector followed by f_o/p phase detectors at 0 and 90 degrees for x and y. This circuit will allow tracking on a null or secondary peak, as well as the

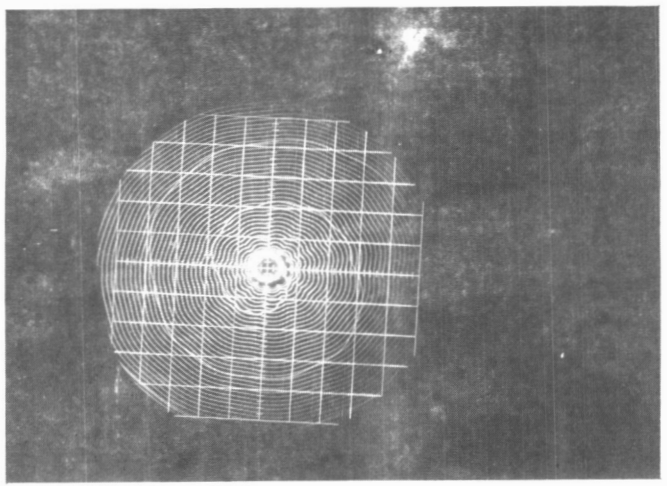

Figure 6.1 Search Mode

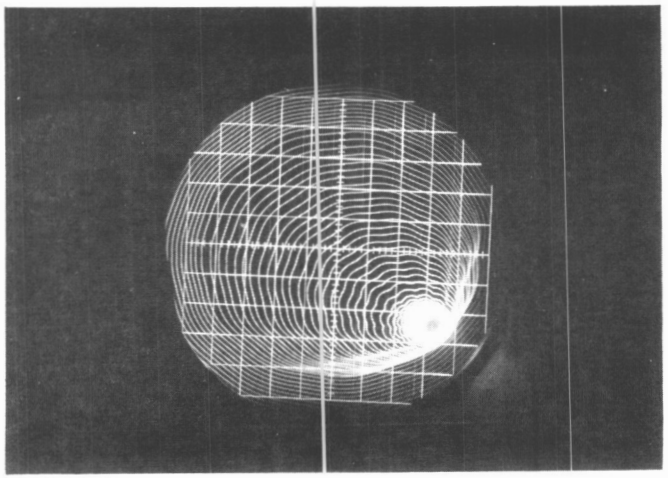

Figure 6.2 Search & Find

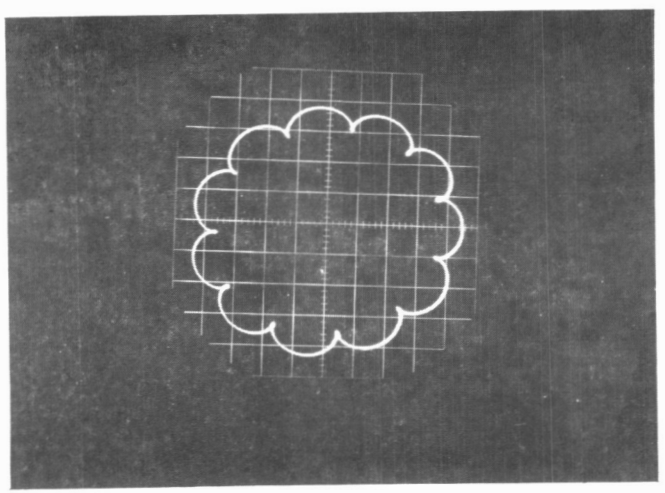

Figure 6.3 Track on f_o

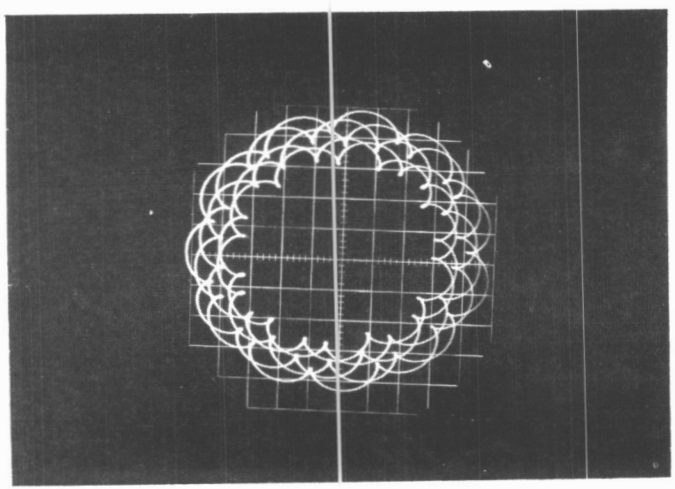

Figure 6.4 Track on Coarse Slither

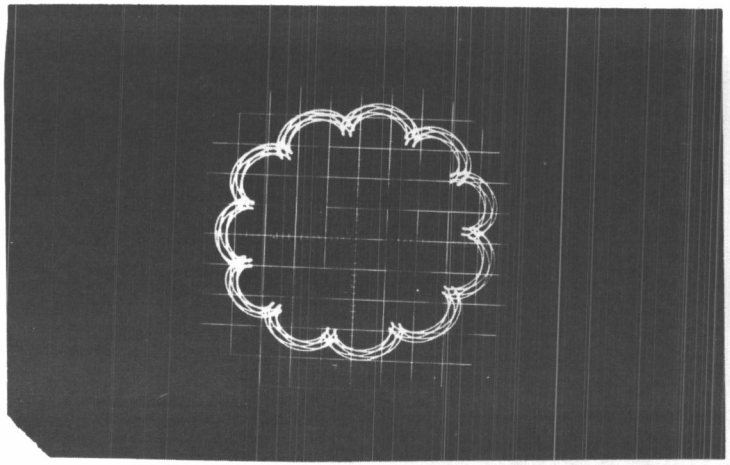

Figure 6.5 Track on Fine Slither

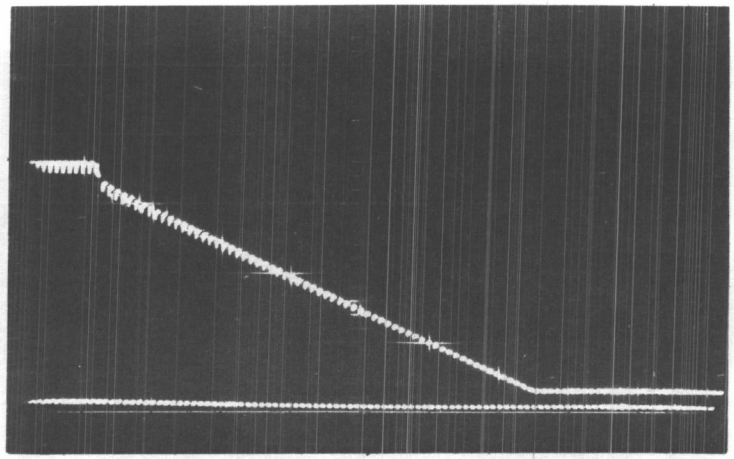

Figure 6.6 Chopped Ramp
.4 V 100 ms (Bd. 10, p.12)

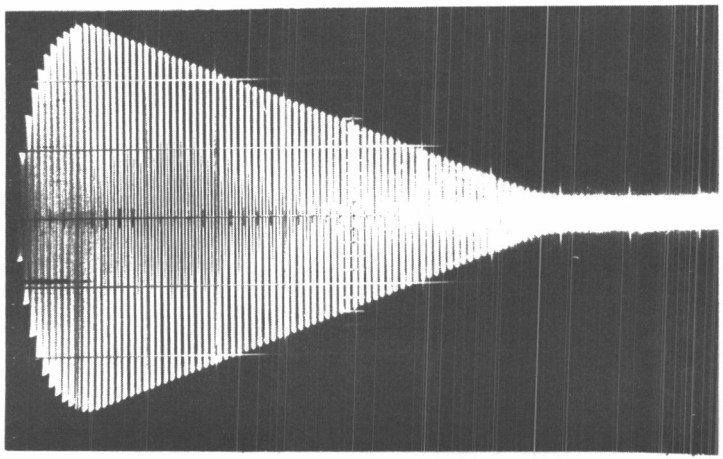

Figure 6.7 Modulated f_o (Bd. 10,p.11)
1 V 100 ms

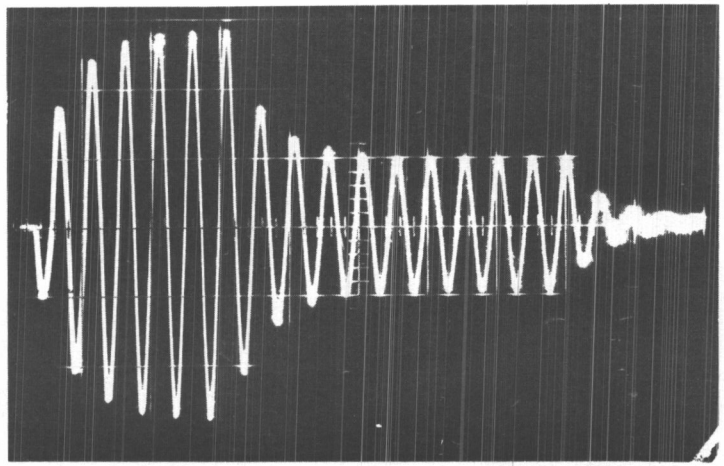

Figure 6.8 Slither Modulation f_o/p
.1 V 100 ms (Bd. 11, p.9)

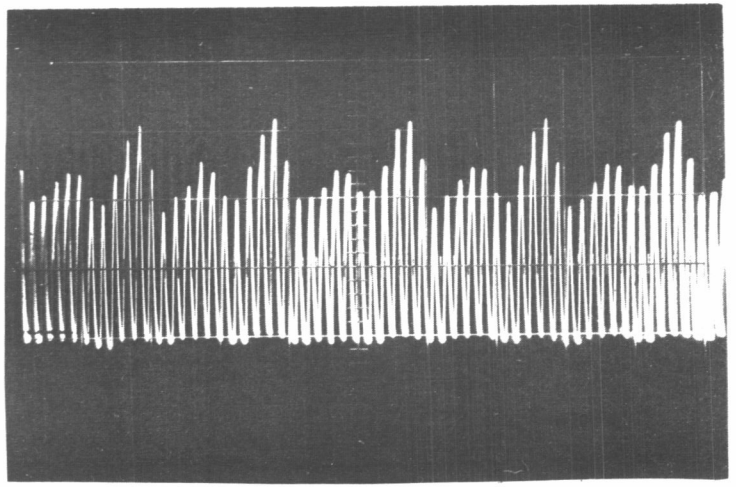

Figure 6.9 Preamp Out with 90° Planet Track on f_o
1 v/cm, 5 ms/cm

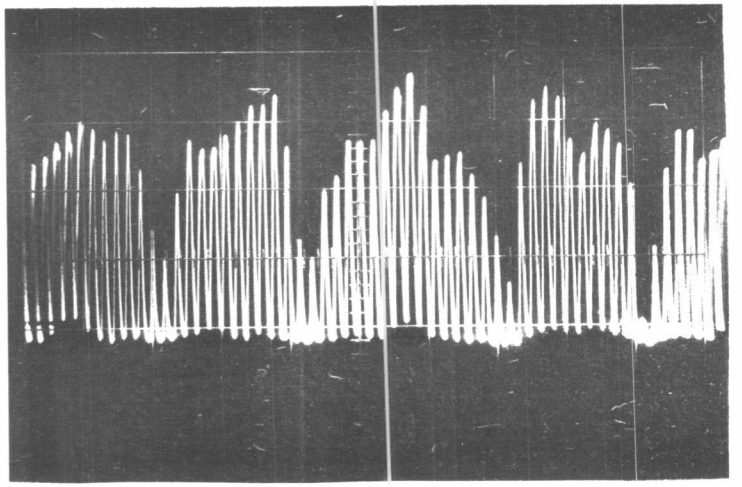

Figure 6.10 Preamp Out with 90° Planet Track on f_o/p
1 v/cm, 5 ms/cm

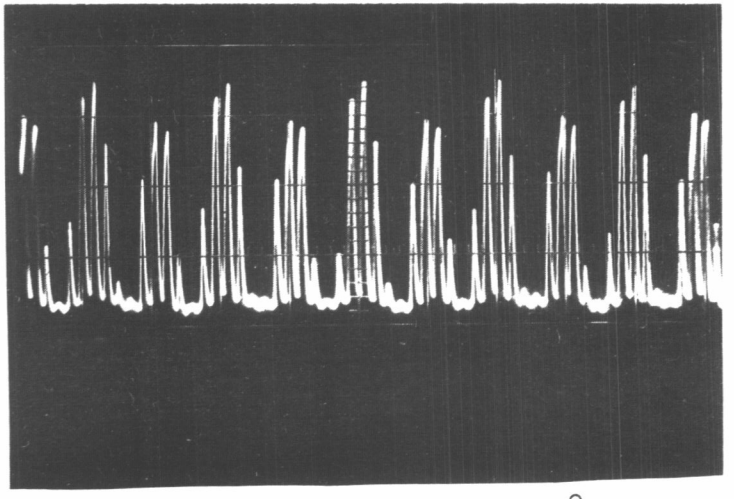

Figure 6.11 Preamp Out with 55° Planet Track on f_o
1 v/cm, 5 ms/cm

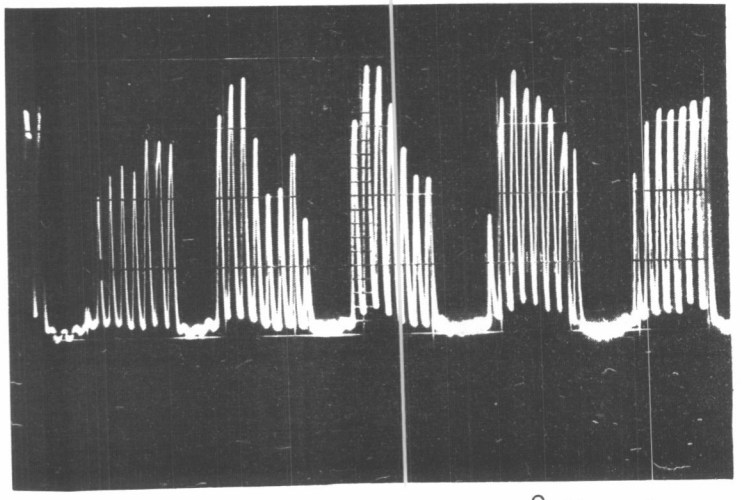

Figure 6.12 Preamp Out with 55° Planet Track on f_o/p
1 v/cm, 5 ms/cm

primary peak. Therefore, a further condition is imposed on the track mode that the $(n-1)f_o$ amplitude must be greater than .13 amplitude units.

Accuracy of the slither mode of operation can be estimated by referring to Figure 6.16 and the $(n-1)f_o$ computer curves. The planet tracker will track on that point of a peak where $\pm$ .5 du produces equal excursions of $(n-1)f_o$ amplitude. This criterion is only an estimate because, (a) crosstalk effects when using x and y slither modulation simultaneously were not evaluated; and (b) the 20 c/s slither modulation changes the circular 100 c/s modulation into a roulette having 4 loops. Using this criterion, the worst case is for a/b = .8 where y = 0, x = -.8 du. The largest resulting error for the worst case planets is for a/b = 0.8, radius = 5.6", y = 0, x = .75 du = -.42". This is well within the spec value of $\pm$ 1.6".

6.3 SYSTEM OPERATION

6.3.1 Block Diagram Explanation

The scan patterns of Figures 6.1 through 6.5 are produced by applying appropriately modulated sine and cosine waveforms to the x and y deflection plates of the Reconotron. The minimum circle size or f_o amplitude is set equal to the planet size by means of the external size voltages or the size pot. The Reconotron output is amplified, the bottom or "dark" part is clamped, and the upper or "light" part is thresholded to eliminate effects due to variation of planet illumination. This also greatly reduces the effect of Reconotron quantum efficiency variations across the photo cathode.

For the "search" and "track on f_o" modes, the thresholded preamp signal passes through an f_o band pass filter (BPF), limiter, and x, y phase detectors. The x and y phase detected signals then go through x, y integrators, which act as long time constant low pass filters. The x, y integrator outputs are applied to the x, y drive amplifiers and thence to the Reconotron deflection plates, and also the x, y error amplifier to furnish the x, y output error signals. In the "track on f_o/p" mode, the thresholded preamp signal goes through a $(n-1)f_o$ BPF, amplitude detector, and x, y phase detectors. The phase detected outputs then pass through the integrators, drive amplifiers, and error amplifiers as for the f_o case.

6.3.2 Detail System Operation

The detailed block diagram appears in Figure 6.16. See also the waveforms of Figures 6.1 through 6.12, plus circuit specifications, selection of salient circuit characteristics, circuit diagrams and wiring diagram, and Reconotron data sheets and specifications.

6.3.2.1 Scan Generators

The 1200 c/s dither signal is produced by a 19.2 KC crystal oscillator followed by a 16:1 countdown circuit. The fundamental sine wave is selected with a BPF for the x deflection and a 90° phase shift circuit is used for

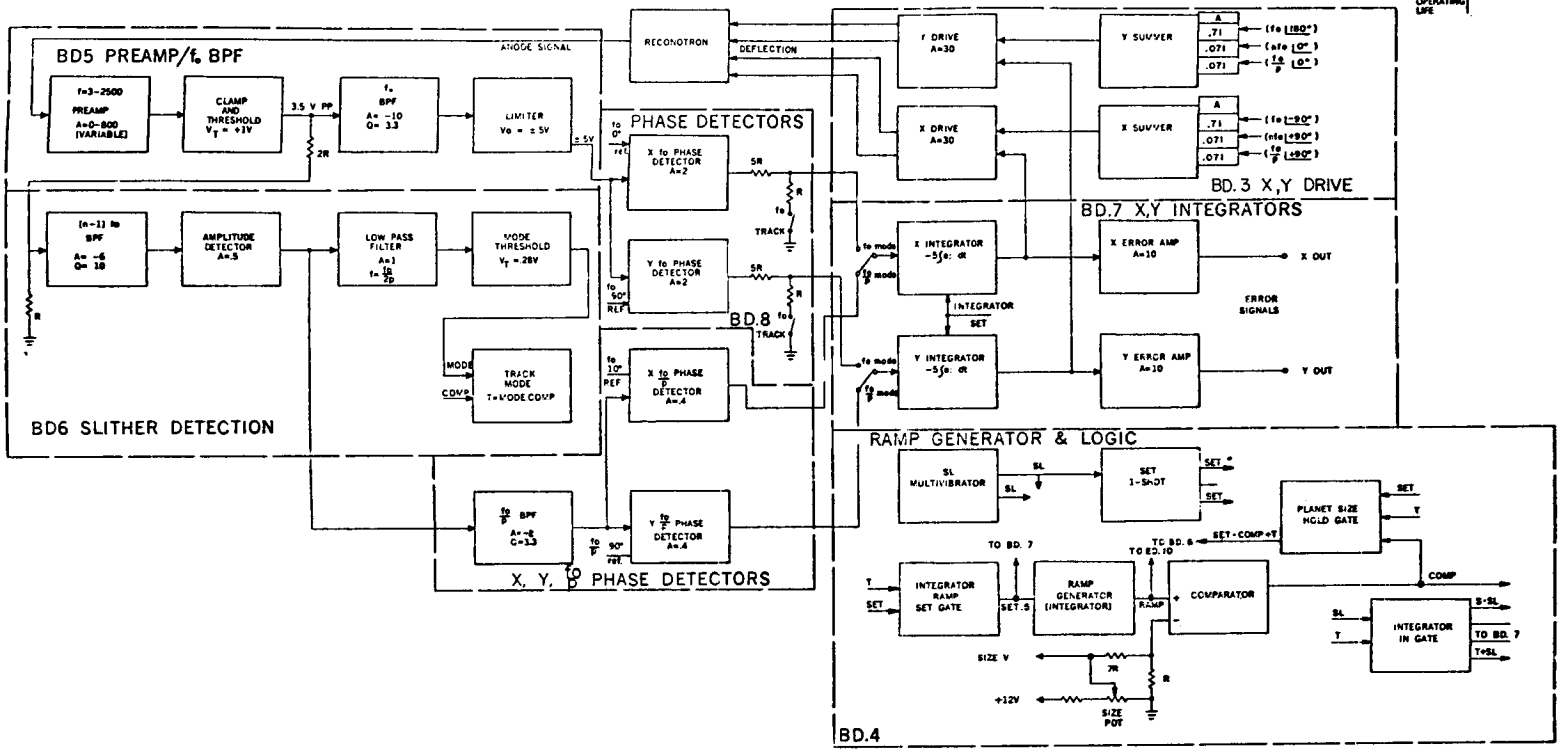

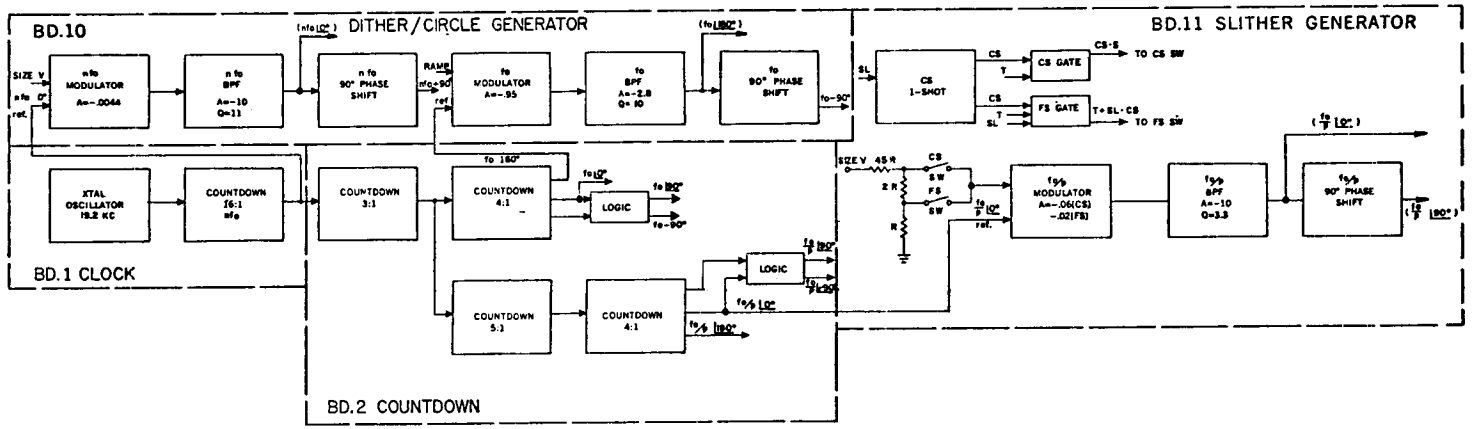

3. (BD 10,7) DURING TRACK, PREAMP, V= 1/8 SIZE V.
2. BPF = BAND PASS FILTER, CS = COARSE SLITHER, FS = FINE SLITHER, SL = SLITHER.
1. SYMBOLS IN PARENTHESIS ARE SINE WAVES OTHERS ARE SQUARE WAVES.

NOTES

QTY REQD	CODE IDENT	PART OR IDENTIFYING NO.	NOMENCLATURE OR DESCRIPTION	MATERIAL DESCRIPTION OR NOTE	MATERIAL SPECIFICATION	ZONE	ITEM NO.

PARTS LIST

INTERPRET DWG PER

UNLESS OTHERWISE SPECIFIED DIM ARE IN INCHES. TOLERANCES ON: FRACTIONS = ± 1/16 DECIMALS: .X = ± .1 .XX = ± .03 .XXX = ± .010 ANGLES = ± 2 DEG

DATE 8/24/67
DR
APPD
APPD
ENGRG
CHK
APPD
CONTR
APPD
CCA/CB

NEXT ASSY | USED ON
APPLICATION

LOCKHEED MISSILES & SPACE COMPANY
A GROUP DIVISION OF LOCKHEED AIRCRAFT CORPORATION
SUNNYVALE, CALIFORNIA

PLANET TRACKER
BLOCK DIAGRAM
FIG. 6-13

SIZE E | CODE IDENT | DRAWING NO. | REV -
SCALE | SHEET

the y deflection. 100 c/s and 20 c/s circle and slither signals are produced with additional countdown circuits, BPF, and phase shift circuits.

The amplitudes of the dither, circle, and slither signals are controlled by modulating the height of the square waves applied to the BPF's. The spiral circle scan is generated by applying a ramp to the f_o modulator (see Figures 6.6 and 6.7). The dither amplitude is slaved to produce 10% of the minimum circle amplitude and the slither amplitude is slaved to produce 15% during coarse slither and 5% during fine slither.

The timing signals are produced by a 2s multivibrator, two 1-shots, and logic. The ramp is generated with an integrator.

6.3.2.2 Preamp, Clamp, Threshold

A wideband preamp having a maximum gain of 800 is used. The input is differentially coupled across the anode load resistor to minimize pickup from the +1200 V power supply. The output, consisting of a series of pulses, is clamped by a diode to ground and thresholded at +1 V.

6.3.2.3 f_o Band Pass Filter (BPF), Limiter

The thresholded preamp signal is filtered by a f_o BPF and limited at $\pm$.5V. The limiter is required as an AGC on the f_o amplitude. The f_o signal is small when the planet is located at the outer extremities of the field of view, and much larger in the track mode.

6.3.2.4 x, y f_o Phase Detectors

The f_o phase detectors produce x and y error voltages which are used for driving the center of the scan to the center of the planet during the "search" sequence. The reference voltage is a square wave and the input voltage is a square wave when the signal is large enough to operate the preceding limiter. The transfer function, Vout/ϕ in, is linear for square waves. A 6:1 attenuator switch operates during the "track on f_o" mode (t_2 to t_3 of Figure 6.14) to reduce system gain and prevent "jitter." The higher gain is necessary during the "spiral scan," (t_1 to t_2), especially for the case of a small planet located at the outer extremities of the field of view, where the duty cycle of the pulses at the f_o frequency can be as low as 7.5%. During the "track on f_o" mode, the duty cycle of the pulses increases to 50%.

6.3.2.5 x, y Integrators

The input to the integrators is switched to either the f_o phase detectors or the f_o/p phase detectors by means of FET switches, depending on the mode of operation. The 0.1 uf integrating capacitor is connected as the feedback element of an operational amplifier resulting in an effective time constant greater than 10 s. The capacitor is initially set to 0 with an FET switch connected in shunt. The output signals are amplified by d.c. amplifiers to produce the output error signals having slopes of 180 mv/arc second.

6.3.2.6 x, y Drive

The drive amplifiers are dc-coupled differential amplifiers having double-ended inputs and outputs. The dither, circle, and slither voltages are summed at one input and the error voltage is connected to the other input. The outputs drive the deflection plates of the Reconotron in push-pull. +120 V regulators are included to power this board.

6.3.2.7 $(n-1)f_o$ BPF, Amplitude Detector, Low Pass Filter, Mode Threshold

The clamped and thresholded preamp signal is filtered by the $(n-1)f_o$ BPF. This carrier is full wave rectified by the amplitude detector and filtered by the $f_o/2p$ low pass filter to eliminate the slither modulation. The resultant signal is applied to the mode threshold which decides whether a planet has been found, and switches from search to track. The track gate allows the track mode to exist only when the scan size equals the target size.

6.3.2.8 f_o/p BPF; x, y f_o/p Phase Detectors

The amplitude detected $(n-1)f_o$ carrier is filtered by the F_o/p BPF to improve the signal to noise of the slither. The slither is phase detected with a circuit similar to that of Bd. 8, and the resultant signals drive the x, y integrators during the track mode.

6.3.2.9 Sequential Details of Planet Tracker Operation

The following information, including Figure 6.14, provides a detailed explanation of the sequential aspects of the planet tracker operation:

Clock nf_o = 1200 (was 1100) c/s

Dither $(n-1)f_o$ = 1100 (was 1000) c/s

Circle f_o = 100 c/s

Slither f_o/p = 20 c/s

Search Repetition Period = 2 seconds

Deflection Voltages

$x(t) = A(t) \sin 2\pi f_o t + B \sin 2\pi n f_o t + C \sin 2\pi f_o/pt$

$y(t) = A(t) \cos 2\pi f_o t + B \cos 2\pi n f_o t + C \cos 2\pi f_o/pt$

See Figure 6.14 for A(t)t

$B = 0.1\ V_s$

V_s = size voltage

$C = 0.15\ V_s$ coarse slither

$C = 0.05\ V_s$ fine slither

C = 0 during (a), (b), (c)

I. Search Mode

(a) $t_0 - t_1$ x and y integrators are zeroed.

(b) $t_1 - t_2$ Circular scan spirals in to minimum target size making a maximum of 50 turns. If target is acquired, the center of circle is moved in the correct direction using f_o resulting in a scan-like Figure 6.15b.

(c) $t_2 - t_3$ Center of circle continues to be driven to center of target on f_o signal.

(d) $t_3 - t_4$ Coarse slither at ± 1.5 decentration units* is enabled at the f_o/p rate driving center of circle to center of target on $(n-1)f_o$ carrier frequency.

(e) $t_4 - t_5$ Fine slither at $\pm .5$ dec. u* is enabled at f_o/p frequency. If $(n-1)f_o$ amplitude searches 0.13 amplitude units, the AND gate is actuated and results in switching to the track mode. If not, the search sequence repeats.

II. Track Mode

Fine slither at $\pm .5$ dec. u* is used to position center of circle.

$A(t) = V_s$

$B = 0.1\ V_s$

$C = 0.05\ V_s$

6.4 RECONOTRON

Section 4 described the evaluations leading to the choice of an image dissector, specifically, a CBS Laboratories Reconotron, as the photosensor for the planet tracker. This section describes the Reconotron and its characteristics as they relate to the performance of the planet tracker. The Reconotron, which is the name that CBS Laboratories applies to their image dissectors, is an all-electrostatic image dissector, whose light weight, small size, and extreme ruggedness and stability commend it for use in aerospace applications. Tubes can be supplied with concave-convex or fibre optic faceplates, with any of the conventional photocathodes, and with any size or shape of aperture required by the system application. The Reconotron consists of a metal and glass envelope containing an image section in which are mounted a photocathode, an electrostatic deflection system, and a dissecting aperture followed by a twelve stage, linear focused electron multiplier.

6.4.1 Description of Operation

An optical image is focused on the photocathode, releasing photoelectrons which are accelerated and focused on the image section electrodes into the

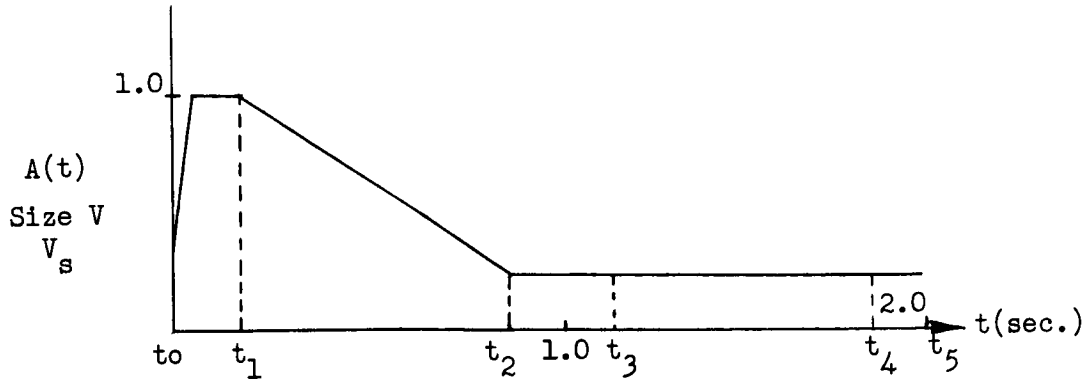

Fig. 6-14 Ramp A(t) vs. t

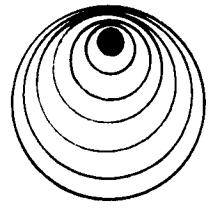

Target

Fig. 6-15 Search Mode Scan During Target Acquisition

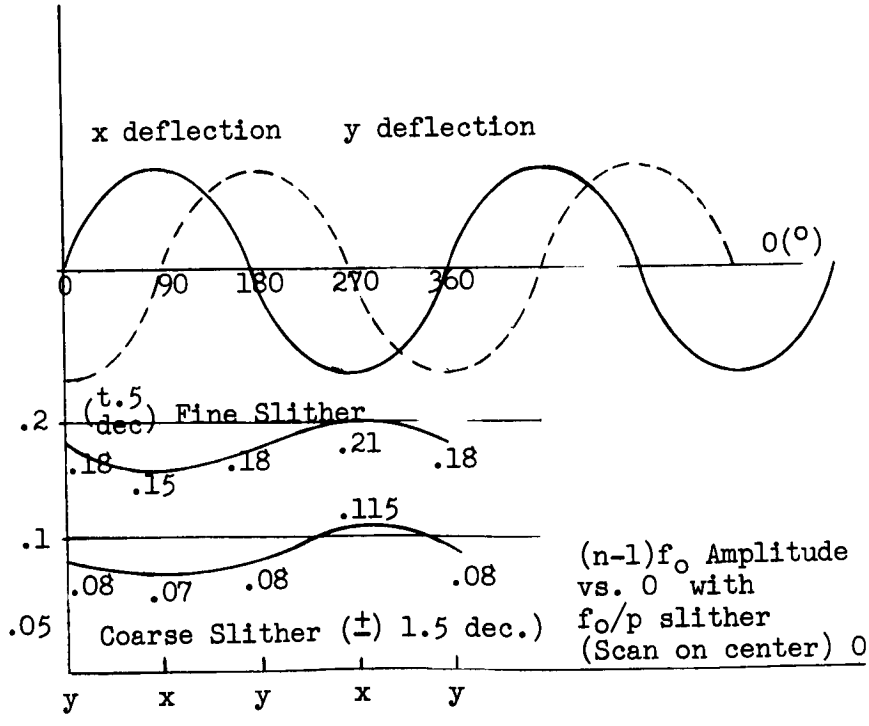

Fig. 6-16 (n-1)f_o Amplitude Detector Output with Slither a/b = 0.6

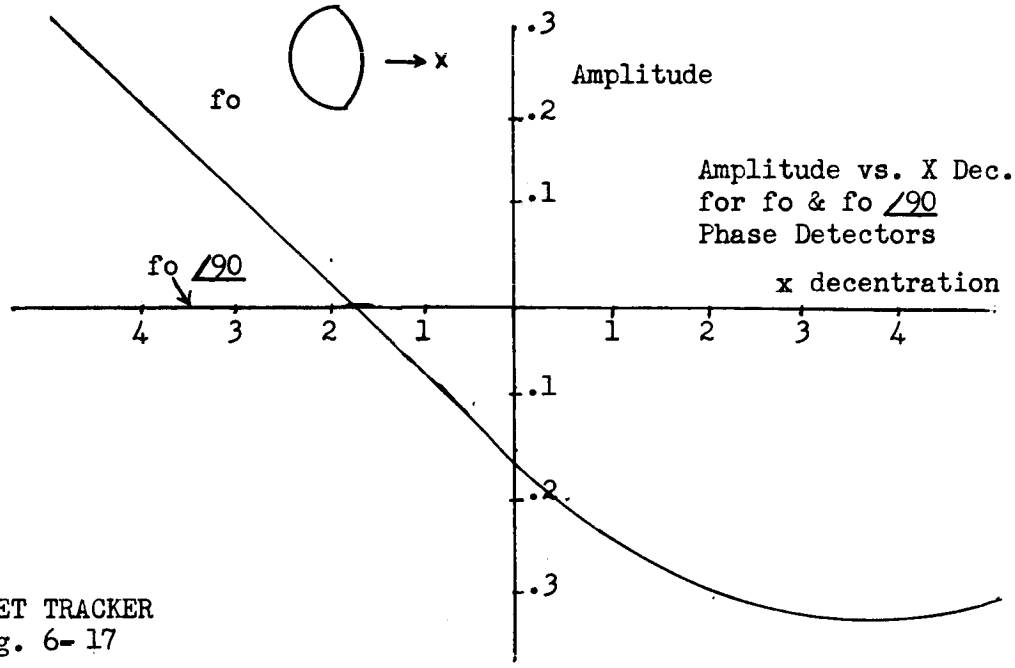

PLANET TRACKER
Fig. 6-17

fo & fo ∠90 Amplitude vs.
x & y decentration for a/b=0.6

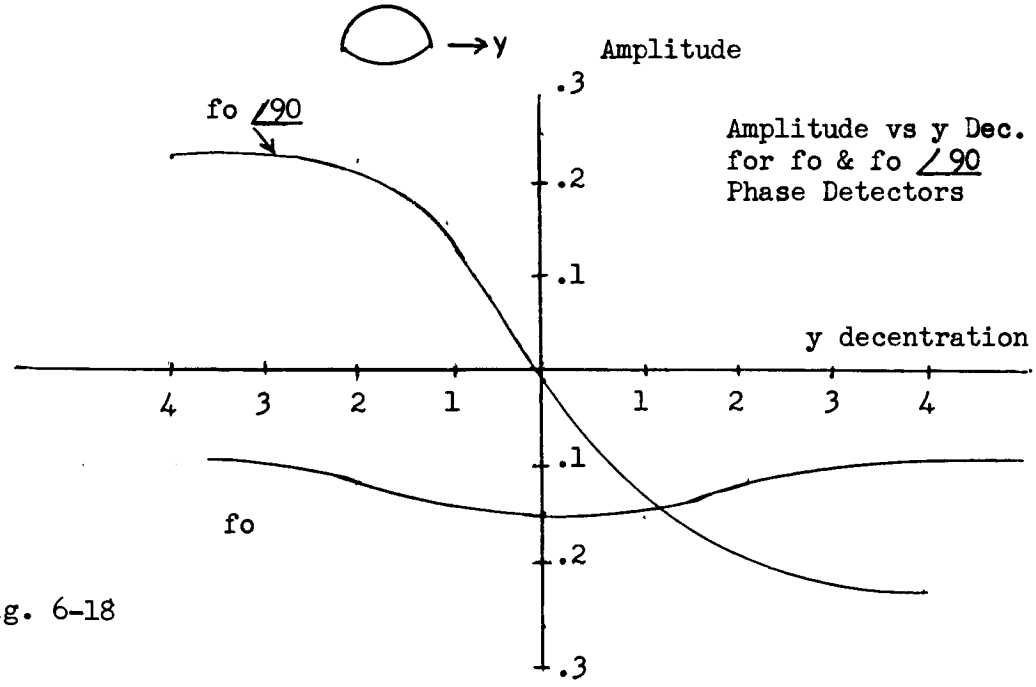

Fig. 6-18

plane of the dissecting aperture. Only those electrons landing in the aperture pass through to the multiplier section, where the signal is amplified and collected at the anode output lead.

In order to measure the signal from each point on the photocathode, the electrostatic deflection system deflects the electronic image across the aperture so that the photocurrent from each element of the photocahode may be sampled or dissected in sequence. The size of each resolution element depends on the size of the dissecting aperture.

While the data set characteristics of the Reconotron appear to be suitable for use of this tube in a planet tracking operation, interactions with CBS Laboratories technical personnel prior to purchase of the tube raised basic questions concerning the tube's linearity. The linearity data presented in the data sheet is somewhat ambiguous. The data quoted, nominally 1% linearity, is generated only for a line through the center of the tube. For lines not through the tube's center, up to 10% linearity errors are possible, with the result that considerable pincushion distortion can occur in some cases. This type of distortion would be very detrimental to tracker performance since linearity over the entire tube surface is a requirement.

At our request, CBS obtained additional data. This particular data was taken on a tube with a .0035" aperture. After reviewing the data, it became apparent that the tube's linearity would be satisfactory except possibly for some targets in the corner of the field of view.

Concurrent with the CBS discussions, discussions were held with Jet Propulsion Laboratories (JPL) and International Telephone and Telegraph (ITT). JPL has only recently become concerned about the Reconotron linearity problem because of a new tube application. The problem is fundamental to the type of deflection plates used, and arises because finite space must be left between the horizontal and vertical plates for electrical isolation. It can and has beencompensated for in a cathode ray tube by adding small tabs to the front of the deflection cone. We believe that JPL will issue a contract to CBS to improve Reconotron linearity.

Discussions with ITT indicate that their image dissector does not have measurable pincushion distortion (less than 1%) because tighter control of the beam can be obtained with magnetic deflection. It is also to be noted that the ITT tube has considerably better resolution, a flat field, and lower noise. The major disadvantages of the tube are weight and power requirements arising from the magnetic scan. For these reasons, the Reconotron appears to be a better choice than the ITT image dissector, particularly since the linearity problems appear to be solvable.

The following specification was submitted to CBS Laboratories in April 1966. A previous specification had been rejected by CBS because we had asked for 1% linearity (the linearity figure quoted on their data sheet). As a

result of several technical discussions, CBS made linearity measurements on four image dissectors according to our specification. The worst case results indicated that linearities on the order of 3.5% might result. CBS said that they would quote to that linearity, although they privately expected that the linearity would be considerably better. On this basis, an order was placed according to the following specification.

If poorer than expected linearity were obtained, planet tracking errors may result ior planet images far off axis. If such were the case, we were prepared to incorporate analog non-linear correction circuits to the deflection drive amplifiers to compensate for the distortion. This proved not to be necessary.

CBS LABORATORIES SPECIFICATION
RECONOTRON CL-1147

1. The spectral response will be S-20. Minimum response shall be 110 micro amps per lumen.
2. The photocathode will be of the end-window type.
3. The window diameter shall be 0.9" minimum.
4. The window index of refraction shall be approximately 1.55.
5. The window of the tube may be either concave, convex, or plano-concave according to the wish of the customer, although the latter is strongly recommended by CBS Laboratories. The window thickness shall be 0.40" $\pm$ 0.005" at the thinnest point (concave window), and be uniformly maintained throughout the extent of the concave-convex window, should that be chosen.
6. The radius of curvature of the concave photocathode shall be 1.25".
7. The useful photocathode diameter shall be 0.75".
8. The aperture diameter shall be 0.002".
9. The deflection characteristics shall be no worse than the numbers represented in circles on the attached Lockheed drawing. Parenthetically, it may be noted that the measurements on a few tubes to date indicate a better performance than this, but the data is inadequate to be certain that such figures can be regularly maintained.

   The conditions of the test are essentially those described in Section 9 of the Lockheed proposed specifications.
10. Resolution of 50% contrast shall be 400 TV lines per inch in the center and 250 TV lines per inch at a point 0.2" from the electrical center.
11. The multiple gain at 125 volts per stage shall be greater than 10^6.
12. The anode dark current shall be no greater than 0.03 micro amps when the tube is operated in such a way as to have an overall response as to have 100 u ampers per lumen.

13. The environment for the above measurements shall be that obtained in laboratory conditions.

14. If Lockheed finds that a resistor network of 1.5 megohms per stage is adequate, the overall dimensions of the shield shall be a nominal 6-7/8" long by 1-7/8" diameter. If, however, resistance values other than 1.5 megohms per stage are chosen, the overall length shall be increased to a nominal 7-1/2".

The Reconotron was delivered in late September 1966, and subsequent measurements indicated that the tube was satisfactory.

The dark current from the image tube anode, as measured with the identical type of equipment as used by CBS, is two or three-tenths of a nanoamp. This is approximately an order of magnitude below the dark current measured by CBS. This decrease in dark current is attributed to the fact that many photoemissive types of tubes, particularly those with S-20 response, tend to "clean up" with time due to the action of the getter.

With the low dark currents measured, only several noise pulses exist every second. These noise pulses are individual electron events. Because the pulses are so far apart, the conventional signal to noise calculation becomes difficult to utilize in defining the noise equivalent angle of the system.

6.5 OPTICAL MECHANICAL DESIGN

Detailed optical design was described in Section 5.6 as part of the optical trade-off discussion. That optical design was incorporated into a mechanical assembly 36" long, 8" wide, and 15" high. This assembly was configured as a laboratory breadboard which allowed sufficient mechanical, electronic, and optical flexibility to optimize tracker performance. A sketch of the breadboard planet tracker is shown in Figure 6.19.

The basic Zoomar lens system is shown on the left in Figure 6.19. The field lens and the Reconotron are located in the housing to the right. Both the field lens and the Reconotron are mounted on x,y slides so that optical positioning is easily facilitated in keeping with the research breadboard character of the tracker. The mechanical assembly was designed to be fixed on an optical rail which is part of the 40" collimator used in the checkout of the planet tracker. The actual assembly proved to be very effective in allowing optimization of not only the optical and mechanical parameters of the tracker, but also in allowing the checkout trouble shooting of the electronics.

Figure 6.19

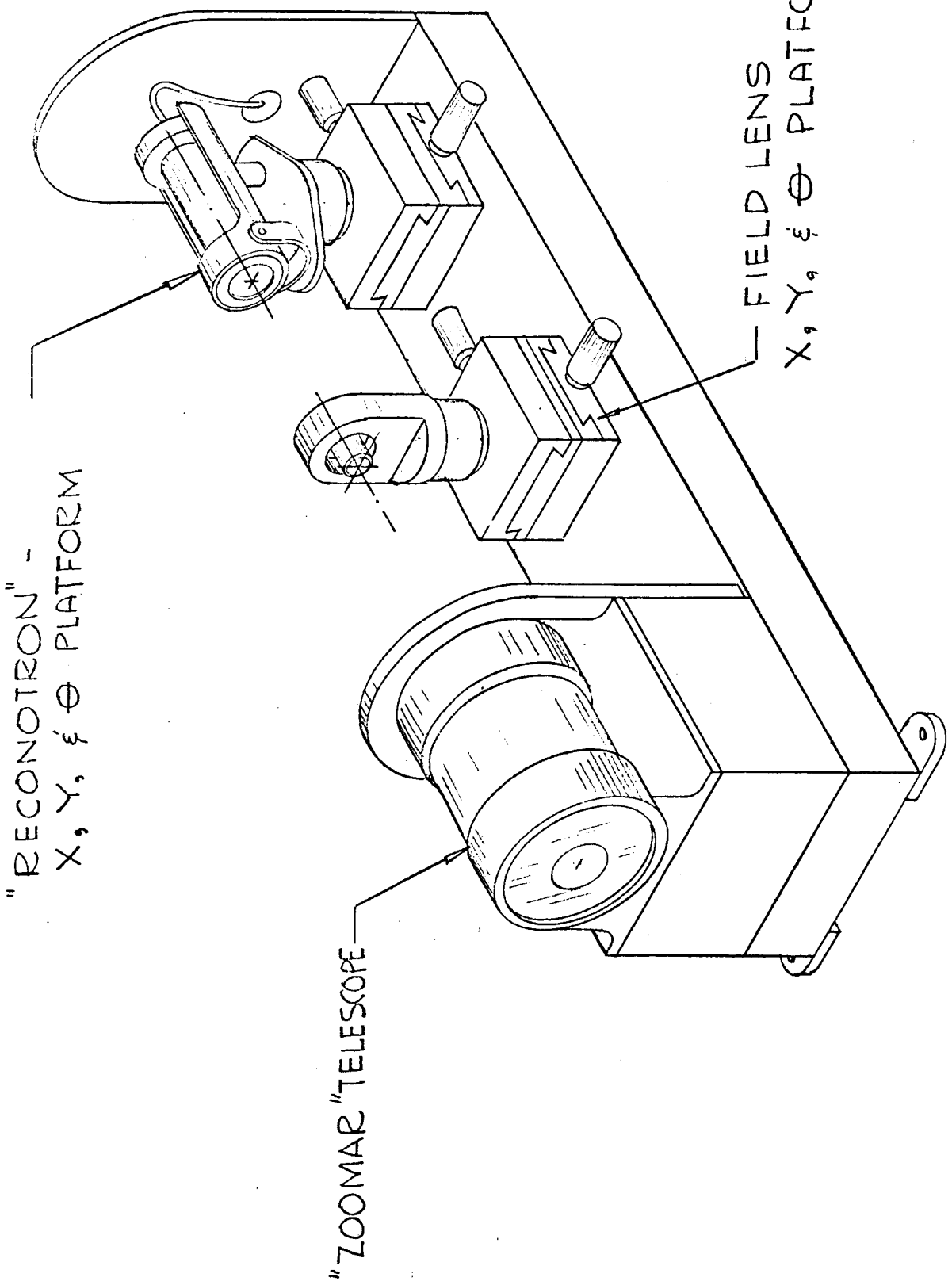
"RECONOTRON" -
X, Y, & Φ PLATFORM
FIELD LENS
X, Y, & Φ PLATFORM
"ZOOMAR" TELESCOPE
BREADBOARD-PLANET TRACKER

6.6 PLANET TRACKER WITH RADIUS SEEKER

Figure 6.18 shows the additional blocks required for a planet tracker which incorporates a planet radius seeking circuit and, therefore, relieves the necessity for a planet size voltage input. The improved planet tracker would work in the following manner:

(1) The scan spirals down toward the planet size while tracking on f_o. This is the same step used in the existing planet tracker.

(2) When the $(n-1)f_o$ amplitude reaches a preset level, a switch closes to stop the radius from shrinking further. The scan is now approximately equal to the planet size. The planet tracker continues to track on f_o.

(3) The radius is now modulated larger and smaller at an f_o/pq frequency, which is lower than the slither frequency. The resulting $(n-1)f_o$ component of the output signal is synchronously demodulated, filtered in an integrator, and used to correct the radius amplitude. Tracking on f_o continues.

(4) After a short interval, the planet is tested to determine if it is circular or noncircular. This is accomplished by checking the amplitude of the 2 f_o component; if greater than a preset level, the planet is noncircular.

(5) a. If the 2 f_o component is 0, the planet is circular and the radius is the correct value. The tracking then continues on f_o. The $(n-1)f_o$ amplitude is at a maximum.

b. If the 2 f_o component is above the preset level indicating a noncircular planet, the radius continues to be modulated, but now the f_o component of the output signal is synchronously demodulated, filtered, and used to correct the radius amplitude. The tracking is now on f_o/p (slither). The radius reaches the correct value when the f_o component is a maximum for the noncircular case.

6.7

On the basis of detailed electronic, optical, and mechanical design, and of the various subassembly tests performed, the following comments are appropriate:

(1) The optical and mechanical design is fairly straightforward and will meet the design requirements.

(2) The completed electronic design is a satisfactory solution to the requirements, although the actual design is considerably more complex

PLANET TRACKER RADIUS SEEKER

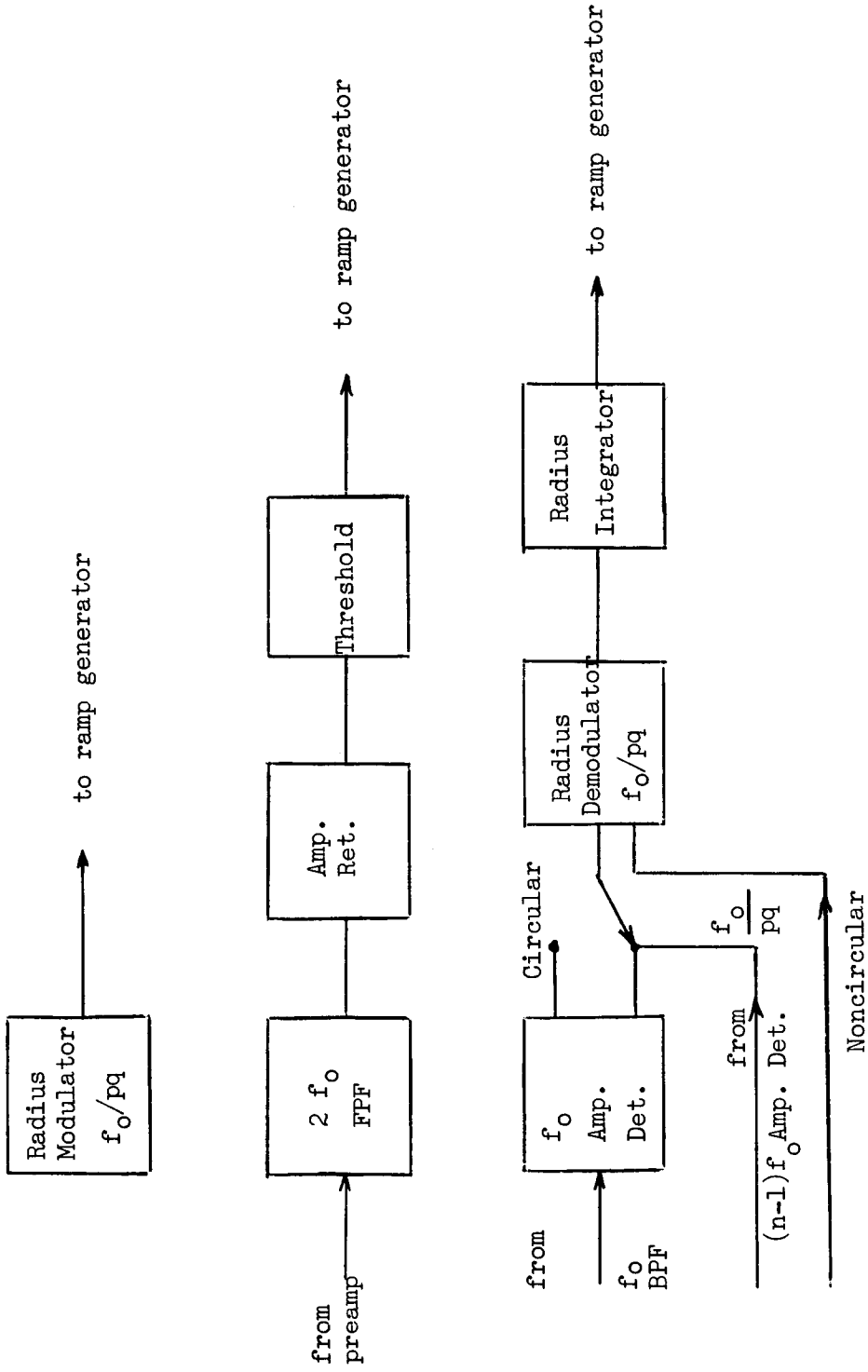

Figure 6.20

than originally anticipated, particularly with the logic associated with the several automatic search and track modes.

(3) All circuits were designed to operate over the temperature environment to be expected in space flight. The performance impact of temperature compensation was fully accounted for and does not degrade electronic performance.

(4) The electronic design was packaged as a research breadboard, although consideration was given to eventual spacecraft packaging through component selection and board assignments. The packaging design is readily adaptable to electronic changes. This adaptability, coupled with the flexibility of the design itself, allows the implementation of changes to other electronic functions, for example, measurements of planet radius, measurement of gibbosity, exact location of terminator, etc.

(5) The parts count of 530 parts is realistic for space flight considering the relatively complex function of the tracker. The estimated volume of a flight electronics package is about 80 cubic inches.

Because the design considered eventual use, it is unlikely that the parts count will grow significantly if the tracker is to be flown. In fact, it is possible that parts counts can be reduced by the use of integrated circuits which were not available at the time of the initial design.

Section 7
PERFORMANCE

7.0 INTRODUCTION

Previous sections discussed planet characteristics and basic design parameters as related to the planet shape, size and intensity. Following this, the basic system design philosophy and detailed design parameters were presented. This section discusses the actual test procedures and test results obtained from the final equipment design. The test procedures section includes both work at the circuit and final equipment levels. At the equipment level, the worst case linearity curve is plotted. Inspection will indicate the worst case individual position error, uncorrected for earth motion errors, was 2.3 seconds.

7.1 GENERAL DISCUSSION

Testing was performed at three levels: the electronic board level to the specifications of Section 6, the subsystem level, and the system level. Testing of the electronics was aided by use of the analog simulator previously described. Testing at the system level was accomplished using the 40-foot collimator and a movable aperture and source. The collimator was aligned with the planet tracker and various planet masks were placed in the focal plane of the collimator to simulate typical planet dimensions in the focal plane of the tracker. The simulated sizes were selected from the data in Section 3. Exact sizes of the planets selected are tabulated. To simulate planet motion across the image plane of the tracker, the masks were moved in the focal plane of the collimator where approximately 0.002 inches motion corresponds to one arc second motion. System measurements were hindered by earth motion of collimator and failure of the 1900°K black body source. Motion of the collimator corresponded to about one arc second of error. Measurements were made on the round, gibbous, and crescent planets. Only the worst case results are presented.

7.2 TEST PROCEDURES

7.2.1 Optical Alignment

A collimator with a forty foot focal length was used as the basic test equipment. Motion of planet masks in the collimator focal plane was used to simulate planet motion. The alignment of the forty foot collimator is necessary

to obtain a collimated bundle of light prior to installing the planet tracker on the rails. For accuracy and calibration tests, the following method is used for alignment.

Initially a diagonal mirror is positioned on the center line of the 18" collimator mirror. An illuminated pinhole is next placed just out of the 18" bundle at the approximate focal point which has been folded. Following this, a good quality, first surface mirror is placed in the 18" bundle to direct the collimated energy back to the diagonal and pinhole. If the return image is larger or smaller than the pinhole, the relationship between the pinhole and focal length of the 18" mirror is incorrect. By moving the pinhole in or out, it is possible to make the pinhole and the return beam the same size, and the instrument is collimated.

The base plate, which holds the planet tracker, can now be placed on the rail in such a way that the energy from the collimator is passed through the Zoomar lens, to a Luminar lens and finally focused onto the face plate of the Reconotron tube.

A Luminar lens is used in the planet tracker to pick up the image of the Zoomar lens and magnify it ten times on the face plate of the Reconotron tube. The lens is mounted in a cell which in turn is mounted to a spherical ball. The nodal point of the lens must be placed at the exact center of the inner ball. The nodal point can be located by shining collimated light in from one end of the lens and observing the image at the other end of the lens, with a microscope. The lens is then moved in the ball so that it is possible to move the ball in any direction and see no apparent motion of the image.

One end of the lens cell is threaded and is screwed to a plate which is mounted to the inside ball and held in place by four screws. With collimated light coming in at the BFL of lens and using a microscope to look at the image at the working distance of lens, shims are added between the plate and ball until all motion is removed when the ball is moved. Once this is obtained, the nodal point of the lens is placed at the center of the spherical ball.

The next step is to locate the Luminar magnifier with respect to the Zoomar. This is done using knowledge of the Zoomar focal length (measured accurately by the vendor). The Luminar lens is placed at the nominal positions with respect to the faceplate of the Reconotron and the spherical ball. The final adjustments of the ball and tube are made with the planet tracker operating. The position of the Luminar magnifier is adjusted to give maximum signal.

7.2.2 Signal to Noise Ratio Measurements

The signal to noise is defined as peak signal voltage divided by rms noise voltage at the preamp output. The peak signal is measured on an oscilloscope (about 4 V) while the tracker is operating in the scan mode. The rms noise can be measured in the scan mode by measuring the narrow band noise at 500 c/s with a narrow band wave analyzer, and correcting for the noise equivalent band width (NEB) of the preamp. Alternatively, the noise can be measured by

stopping the scan and directing the scan beam onto the planet while measuring the broadband noise voltage with a Ballantine 320 rms voltmeter.

7.2.3 Linearity Measurements

The linearity is checked by causing the planet image to move across the Reconotron photocathode. This is implemented by moving the planet mask in the focal plane of the 40-foot collimator along the following paths. The exact position of the mask is determined from dial indicators located on a reference surface. The linear motion is then converted to equivalent angular motion since .0023 inches on the collimator corresponds to one arc second of motion. Tests were performed for the following cases:

(a) $y = 0$, $x = -135''$ to $+135''$
(b) $x = 0$, $y = -135''$ to $+135''$ (" = arc seconds)
(c) $x = -100''$, $y = -100''$ to $+100''$

The x and y output voltages corresponding to planet position, are read on the digital voltmeter.

7.2.4 Null Accuracy Measurements

The null accuracy is measured as a function of planet size and amount of gibbosity. A circular planet corresponding to a planet 47 arc seconds in diameter is used as the reference. The turret containing the masks is rotated to the next planet in line and the incremental shift in the x and y output voltages is recorded and converted to the equivalent angle.

7.2.5 Noise Equivalent Angle

The noise equivalent angle was determined by measuring the rms a.c. output voltages (x and y) and converting to the equivalent angle.

7.2.6 Tracking Rate Measurements

The tracking rate is measured by determining how fast a planet can move in arc seconds per second with the tracker remaining in the track mode. To implement this measurement, the planet mask in the focal plane of the collimator was manually moved by turning a lead screw over a measured distance at various rates.

7.3 TEST RESULTS

7.3.1 Electronics Performance Using Analog Simulator

The performance of the electronics was tested in a closed loop system by using the analog simulator previously described. The dynamic response of the system is illustrated in Figures 7.1 - 7.7. The ordinate is amplitude of the

Figure 7.1

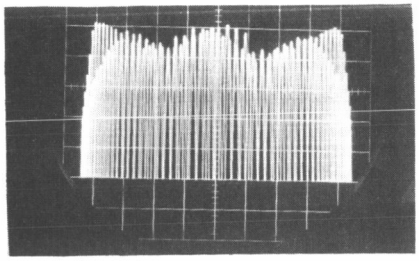

Circular Planet
Scan corresponds to $\pm$
1.5 d.u. in X direction

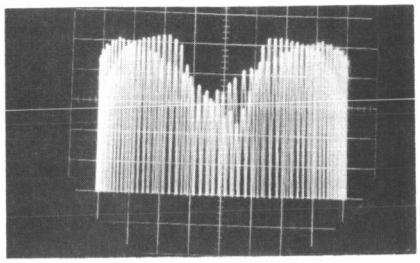

Circular Planet
Scan corresponds to $\pm$
.5 d.u. in X direction

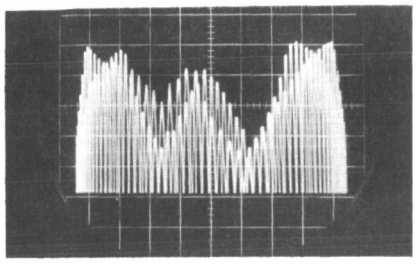

Gibbous Planet $\frac{a}{b} = .8$
Scan corresponds to $\pm$
1.5 d.u. in X direction

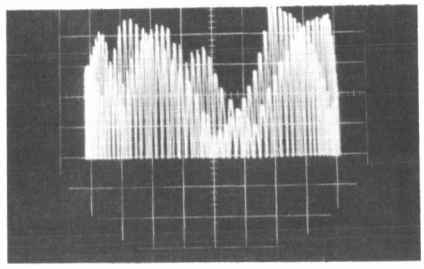

Gibbous Planet $\frac{a}{b} = .8$
Scan corresponds to $\pm$
.5 d.u. in X direction

Figure 7.4

Figure 7.5

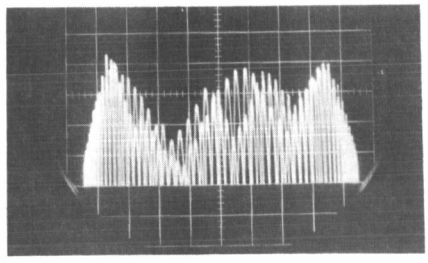

Gibbous Planet $\frac{a}{b} = .66$
Scan corresponds to $\pm$
1.5 d.u. in Y direction

Figure 7.6

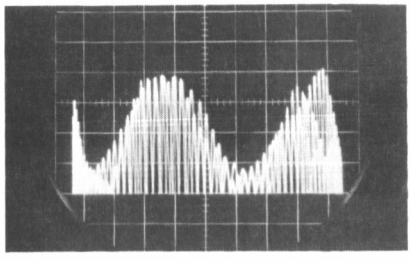

Gibbous Planet $\frac{a}{b} = .66$
Scan corresponds to $\pm$
1.5 d.u. in X direction

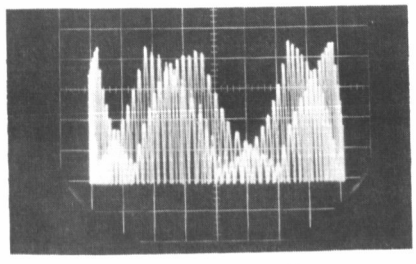

Gibbous Planet $\frac{a}{b} = .66$
Scan corresponds to $\pm$
.5 d.u. in X direction

Figure 7.7

detector output and the abscissa is 20 c/s sweep. The 20 c/s sinusoidal sweep was derived from the dither frequency. These curves correspond to the computer curves modified by system response to the 20 c/s sweep. For the purpose of obtaining these photographs, the dither amplitude in the axis noted was adjusted to correspond to ± 1.5 decentration units. The dither on the other axis was set to zero.

7.3.1.1 Signal to Noise

The minimum tolerable S/N was measured by injecting white Gaussian noise into the preamp input. It should be noted that this noise does not exactly simulate the actual Reconotron noise. The Reconotron shot noise is $In = 2e\ I\ \Delta f$; therefore, the noise on top of the signal (illuminated) is greater than the noise on the bottom of the signal (dark). Using a 0.66 gibbous mask and a signal of 3.5 V pk, the electronics continued to operate properly with 0.38 V rms, or a S/N of 10.

7.3.1.2 Null Accuracy

The relative null accuracy was observed by using a 0.66 gibbous mask and observing the shift caused by switching from "track on f_o" to "track on f_o/p". A shift of 1.5 decentration units was observed as compared to the shift predicted from the computer curves of 2 decentration units.

7.3.1.3 Noise Equivalent Angle (NEA)

The NEA was measured at a S/N of 10. The x and y output voltages were 30 mv peak to peak. Using the conversion of 180 mv/ arc second, this corresponds to a NEA of 0.17 arc seconds peak to peak.

7.3.1.4 Tracking Rate

The maximum tracking rate was measured by simulating planet movement using the oscilloscope positioning controls. Actually, this results in motion of the scan pattern rather than the planet mask, but the net effect is the same. This resulted in a measurement of 15 arc seconds/second for a circle and 7 arc seconds/second for a 15° gibbous case.

7.3.1.5 Reconotron Responsivity and Gain

The responsivity and gain of the Reconotron were measured and calculated without using the tracker optics (see accompanying data). For this test, the Reconotron was flooded with radiation from a 1000° C black body which was 5 inches from the photocathode. Initially, the Reconotron linearity was verified by grounding the deflection plates and measuring the anode current as a function of the black body aperture size. The measured anode current was later found to be 52% of the calculated value indicating either low responsivity, low gain, or a combination. The gain was then calculated from noise considerations and found to be 23% low.

7.3.2 Final Equipment Tests

On completion of the analog simulator tests, a series of tests on the complete tracker were performed. These tests are discussed in the following sections.

7.3.2.1 Noise Level Measurements

Tracker noise can occur from numerous sources. A complete understanding of tracker performance requires a determination of the magnitude of each noise producing source, with a subsequent evaluation to determine if the noise magnitude is close to its theoretical value.

Ideally the system noise level is determined by the Reconotron dark current shot noise. The preamp output noise due to the shot effect can be calculated as follows:

$$= (2\ e\ I_k\ \Delta f)^{\frac{1}{2}} = (3.2 \times 10^{-19} \times 2 \times 10^{-10} \times 3 \times 10^{3})^{\frac{1}{2}} = 4.4 \times 10^{-13} A\ .$$

The preamp output noise level is then

$$= 4.4 \times 10^{-13} \times .7 \times 10^{6} \times .5 \times 10^{6} \times 800$$

$$= 123 \text{ Microvolts.}$$

For comparison, the Johnson noise out of the preamp is

$$= (4KTR_L\ \Delta f)^{\frac{1}{2}}\ Av$$

$$= 1.6 \times 10^{-20} \times .5 \times 10^{6} \times 3 \times 10^{3} \times 800 = 4 \text{ mv.}$$

Thus, in the dark if no other noise sources exist, Johnson noise would dominate.

The measured preamp broadband output noise level was 10 mv, compared to the 4 mv calculated value. The difference arises largely from ripple on the high voltage power supply. In practice the preamp output is set to 4 volts, thus the signal to preamp noise ratio is 400 and does not effect operation. In actual operation the noise level is specified from the shot noise in the signal, not the preamp noise.

The output of the preamp as seen on an oscilloscope showed pulses with rise times of about 20 microseconds and fall times of 50 to 100 microseconds. The pulse height was a function of the total photomultiplier dynode voltage. The estimated pulse heights and time intervals are given below.

Dynode Voltage	E Peak Average	Time Between Pulses
1500 volts	1.0 volts	10 sec.
1200 volts	.15 volts	100 sec.

The basic source of these pulses appears to be leakage current. Since the occurrence of the pulses was low, with the 1200 volt operating condition, they did not affect system operation.

The signal to noise ratio was measured using a 1000°C black body source and the 40-foot collimator. The anode current, I_a, was measured to be 2.7 nanoamperes (nA) with the source aperture open and .04 nA closed, for a net signal current of 2.3 nA. The output noise, e_{no}, was measured to be 450 mv rms. This corresponds to an input current of:

$$i_{ni} = \frac{e_{no}}{-Av\ R} = \frac{450\ mV}{(800)(.4)10^6} = 1.125\ 10^{-9}$$

Therefore, the S/N, $I_a/i_{nA} = \frac{2.3\ nA}{1.125\ nA} = 2.05.$

The S/N calculated from the shot noise of the cathode current is:

$$S/N = \frac{I_k}{2e(I_k + I_d)\ \Delta f^{\frac{1}{2}}} = \frac{Ia/u}{\frac{(2e\ I_k + I_d\ \Delta f)^{\frac{1}{2}}}{u}}$$

$$= \frac{2.3 \times 10^{-9}}{\frac{.7 \times 10^6}{(3.2\ 10^{-19}\ \frac{2.7\ 10^{-9}}{.7\ 10^6}\ 3 \times 10^3)^{\frac{1}{2}}}} = \frac{3.29 \times 10^{-15}}{(37.0 \times 10^{-31})^{\frac{1}{2}}}$$

= 1.71 which is in fair agreement with the value calculated above.

The theoretical anode current is 21.9 nA versus the measured value of 2.3 nA. The theoretical S/N is 5.71 versus the measured value of 2.05. The discrepancies are partly explained by the Reconotron gain and/or responsivity being low by a factor of two. Other possible causes are the losses in the optics may have been greater than the 20% estimated. However, the largest amount of the error probably arises due to the poor Reconotron spatial resolution.

7.3.2.2 Reconotron Dark Current

The anode dark current was measured to be 2×10^{-10}A for an anode voltage of +1200 V. No change in anode current was noted at 1500 anode volts.

7.3.2.3 Noise Equivalent Angle

This parameter is best measured with the tracker tracking a planet image because the noise and, consequently, the jitter at the threshold and the preamp output is a function of planet intensity. Unfortunately, earth motion of the 40-foot collimator used in the test made the measurement impossible. It is felt that the angle measured on the simulator and discussed earlier provides a fairly accurate indication of the instrument performance.

7.3.2.4 Optical Resolution

The resolution of the tracker was checked by scanning the 2 mil Reconotron beam across two circular planets. The results indicate a 10-90% resolution of 9 arc seconds. This compares to the theoretical resolution of 3-4 arc seconds.

To understand the difference, the optical resolution of the system was checked. The check consisted of removing the Reconotron and replacing it with a Linhof camera. Using the camera, a cross hair in the focal plane of the forty foot collimator was photographed. The diameter of the cross hair was .0037 inches. The diameter of the image of the cross hair, when adjusted for the magnification of the optics involved, was .0051 inches. This diameter was measured on a microdensitometer and represents the diameter corresponding to half peak transmission of the image on the negative.

When this difference is converted to angular measure, it amounts to about one arc second compared to the 9 arc seconds measured using the Reconotron. It is therefore concluded that the poor resolution was basically a Reconotron problem.

7.3.2.5 Linearity

The linearity measurements were made for all the planet shapes listed in 7.3.2.6, and were converted to the equivalent angle. The x and y output voltages were divided by 2 before being measured by the 3-place digital voltmeter to allow accurate readings. Therefore, 100 arc seconds is equivalent to 9 V rather than 18 V.

The movement, L_s, in the collimator focal plane required to simulate 100 arc seconds motion is:

$$L_s = \frac{\tan 100}{480} = .231 \text{ in.}$$

The equivalent movement at the Reconotron is $L_d = \frac{\tan 100}{400} = .192$ in. The factor for converting source length to angle is approximated as .240 in. for 100 arc seconds, and readings were taken every .06 in.(25 arc seconds). Acquisition can be made throughout $\pm$ 136 arc seconds, and this could be extended if desired simply by increasing the spiral scan amplitude. Linearity was measured over a region of $\pm$100 arc seconds.

One of the major difficulties encountered in making this measurement was earth motion. The ends of the 40-foot collimator are supported on independent concrete blocks which are isolated from the floor. The earth motion was typically 1 arc second in a 2-minute interval and 2-3 arc seconds over a 20-minute interval. The earth motion was measured with the planet tracker and corroborated with the Hilger Watts autocollimator.

All of the round and gibbous planets were successfully tracked with the source intensity set to deliver a minimum S/N of 10 at the preamp. The few angular deviations which exceeded the 1.6 spec can be explained by the earth motion. Figures 7-8 and 7-9 are plots of the resulting worst case data.

Linearity was also satisfactory for two of the four crescent cases. Some difficulty in acquisition was noted on the crescent planets and it was necessary to manually close the track switch. The two most extreme crescent cases would not track reliably, probably due to optical blur. Further analysis of the crescent cases would best be made after running computer curves for these cases and then analyzing electronic performance with the analog simulator.

7.3.2.6 Null Accuracy

The planet null position of the various round and gibbous planets was determined by taking the average of three sets of readings to minimize the effect of earth motion. The results are tabulated below:

Planet	Angular Position (arc seconds)		Shape	
	X	Y	a/b	Radius arc seconds
Reference 6 Jupiter	0	0	1.0	23.4
Reference 7 Venus	0	+0.3	1.0	5.0
Reference 1 Mars	-0.1	-1.0	0.8	5.6
Reference 2 Venus	+1.3	-0.5	0.5	7.3
Reference 3 Venus	+0.2	-1.9	0.2	9.6
Reference 4 Jupiter	-0.4	-0.3	0.98	20.0
Reference 6 Jupiter	-0.1	--.5	1.0	23.4

The centers of the planets were positioned within + .15 arc seconds as measured on the toolmaker's microscope, so no correction was made for mask position. The worst case deviation of 1.9 arc seconds is for the most gibbous planet (0.2, 9.6 arc seconds radius, Venus.) This compares with the theoretical value of 0 arc seconds from the computer curves for this case. The second worst deviation is 1.3 arc seconds for Planet #2 (.50, 7.3 arc seconds radius, Venus), which has a theoretical deviation of about .4 d.u. or .3 arc seconds. The third worst deviation is 1.0 arc second for Planet #1 (.80, 5.6 arc seconds radius, Mars), which theoretically has the largest deviation, .75 d.u. or .24 arc seconds. The discrepancies are probably caused by poor resolution of the Reconotron.

The data taken for the crescent cases showed satisfactory null accuracy for the #1 and #2 planets with the acquisition difficulties noted in the previous section. The null for the #3 planet has a tendency to shift around and acquisition of the #3 and #4 planets was accomplished with greater difficulty. Again, lack of resolution probably caused the problems noted.

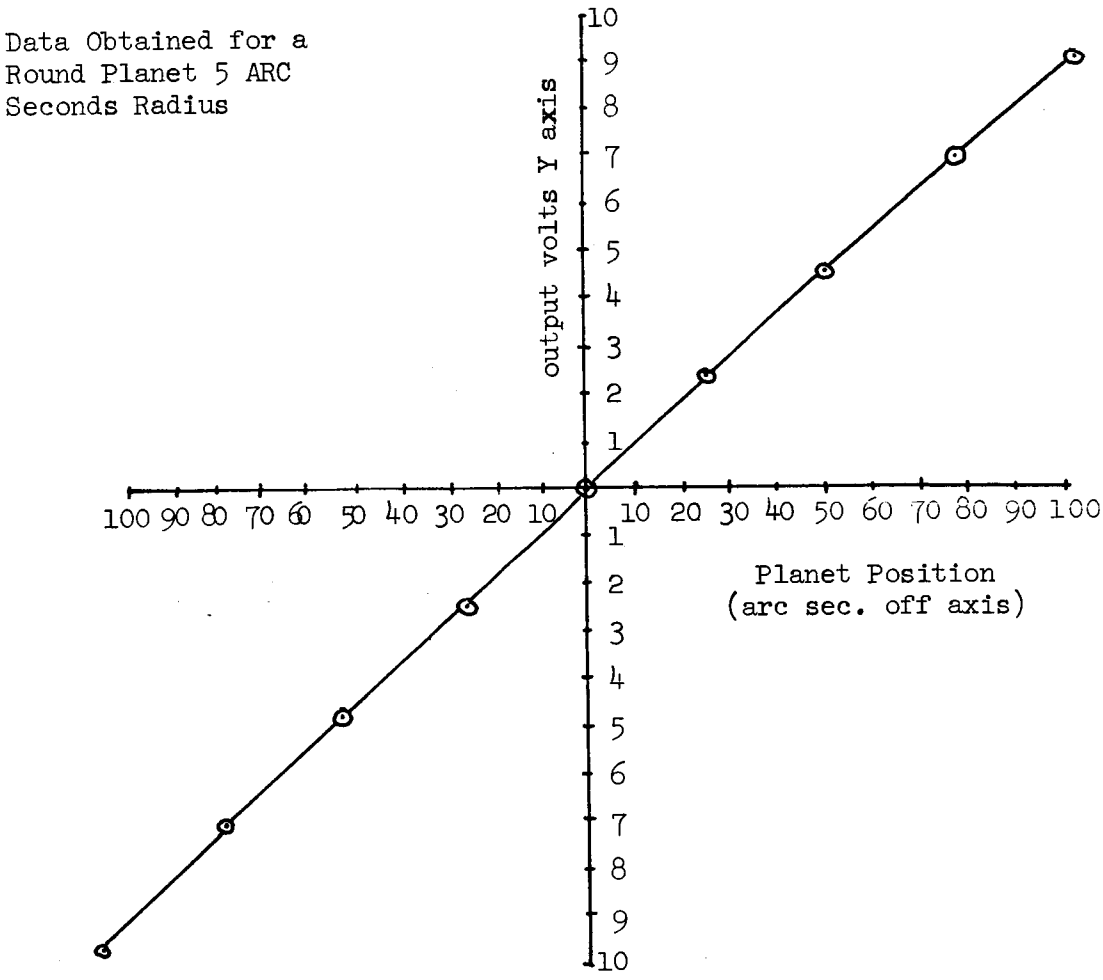

Worst Case Uncorrected Y Axis

Planet Tracker Output

Linearity

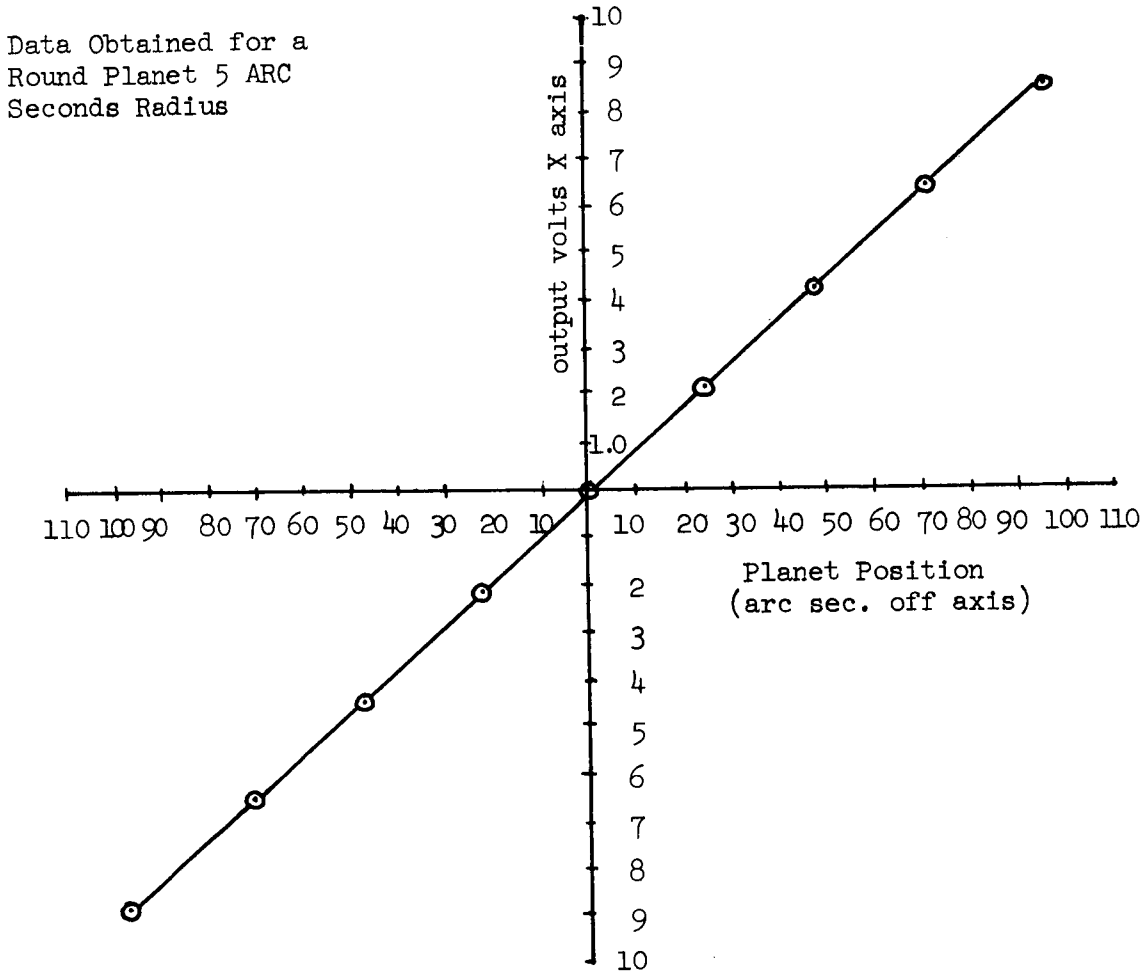

Worst Case Uncorrected X Axis

Planet Tracker Output

Linearity

Section 8

CONCLUDING DISCUSSION

8.1 INTRODUCTION

This section is the last written part of the report and is written with the perspective of having accompanied a NASA/ARC representative on a contract reporting trip and having completed all experimental activity. Section 8 briefly discusses the trip, mentions planet tracker activities at JPL and NASA/ERC, compares this planet tracker with others, discusses current application interests, comments on the performance of this geometric center tracker, and finally discusses possible areas of future work.

The previous seven sections of this report contained a logical and somewhat chronological description of the work performed on this contract. The report in Section 1 discussed the technical requirements and Section 2 summarized, in some detail, the program activity. Section 3 described planet characteristics relevant to the program and Section 4 discussed trade offs between various tracking techniques. Section 5 treated the design analysis of the visible edge tracker and Section 6 described the actual tracker design in detail. The preceding section, Section 7, dealt with the experimental results.

8.2 VISITS TO OTHER NASA FACILITIES

The follow-on contract included provisions for a trip to other NASA facilities for the purposes of reporting the results of this program, interacting with technical personnel on matters of common interest, learning about the planet tracking activities of other groups at NASA/ERC and JPL, and determining potential applications.

Facilities visited, dates, personnel contacted are listed:

6 July 1967, Jet Propulsion Laboratory
R. K. Melugin (NASA/ARC), W. H. Alff (LMSC)

10 July 1967, NASA/Langley Research Center
J. A. Dodgen, H. Kaufman; R. A. Wallner (LMSC)

11 July 1967, NASA/Goddard Space Flight Center
W. Raskin, T. Buckler, P. Scherer, R. K. Melugin (NASA/ARC),
A. R. Kraemer, R. A. Wallner (LMSC)

11 July 1967, NASA Headquarters, J. Kanter;
R. K. Melugin (NASA/ARC); A. R. Kraemer, R. A. Wallner (LMSC)

12 July 1967, NASA/ERC, M. Gorstein, S. Moskowitz, L. Kleinman, A. de Hollans; R. K. Melugin (NASA/ARC), A. R. Kraemer, R. A. Wallner, (LMSC)

The trip was very successful in that the objectives were efficiently accomplished. In fact, it is earnestly recommended that serious consideration be given to including such trips as a normal part of research development contracts.

8.3 STATE-OF-THE-ART PLANET TRACKERS

These paragraphs briefly discuss the state-of-the-art in other planet trackers so that the approaches and state of development can be reviewed. The information on the other trackers is intended to be survey information only and does not purport to be based on a critical evaluation.

8.3.1 Digital Type Planet Trackers

One of the current trackers is based on scanning a radial type pattern on an image dissector during the search mode. Rough tracking is achieved with energy balance techniques and once the image is positioned in the approximate center of the image plane, the search mode is turned off and the fine track mode is turned on. The scan in the fine track mode consists of small radial segments. The scan is achieved by scanning a line on the image tube while simultaneously moving the image mechanically in a circular manner. The error signal is then generated by digitally measuring the distance from the edge of the planet to the edge of each individual scan line. Its accuracy is 36 arc sec; this corresponds to about 1 part in one thousand over the entire field-of-view. It contains about 1400 electronic parts.

The second digital tracker operates as follows: the tracker's image dissector is programmed to search for the planet in a raster scan pattern; when the planet is located, the planet position is stored in raster coordinates and a simple digital calculation is performed to locate approximately the planet's illumination centroid. The scan pattern is changed to a track pattern which consists of radial line segments extending outward from the scan circle. The center of this scan pattern is placed on the illumination centroid and the circular spike scan is expanded to intersect the planet edge. The resulting pulses caused by the scan through the planet edge are examined for circularity in a digital computation. Elliptical terminators, if any, are rejected, and the scan centers itself on the circular planet edge, thereby locating the planet center.

8.3.2 Analog Type Planet Tracker

This tracker is described in this report and a research breadboard has been completed and tested. The tracker uses an image dissector and scans the planet edge in a roulette pattern scan. The signal arising from planet edge crossings is evaluated in terms of its harmonic content and error signals are generated to position the scan center on the planet's center. The reader is referred to other sections of this report for details.

The tracker was developed for the application of long range pointing, e.g., pointing the telescopes of an orbiting planetary observatory at a planet with high angular accuracy. Its accuracy is on the order of one arc second over a field-of-view of 2.5 arc minutes. In a flight model configuration, it is expected to weight about 20 pounds, consume about 5 watts, and occupy about 0.5 cubic feet.

8.4 APPLICATIONS FOR GEOMETRIC CENTER PLANET TRACKERS

Recent discussions, particularly those during our visits to other NASA facilities, provided this application information. Most current interest facuses on approach guidance for terminal guidance to planets. Both the JPL and NASA/ERC trackers have this objective. There is curiosity about the possibility of a visible earth horizon tracker being developed along the lines of geometric center planet trackers. This interest was expressed at NASA/LRC and NASA/GSFC. Interest remains for long range pointing, but it is certainly much less than that expressed several years ago. Some, but little, interest was indicated in the area of planet geometric center tracking for laser pointing for communication purposes.

8.5 DISCUSSION OF NASA/ARC AND LMSC PLANET TRACKER

This discussion comments on the technical performance of the NASA/ARC and LMSC planet tracker and summarizes the tracker's salient features. The discussion is expanded and concluded in section 8.6, where possible future activities are described. Section 8.5 is not intended to offer any additional comments about other planet trackers in addition to those already provided. The discussion is limited to considerations of the subject tracker.

As an initial comment, the breadboard tracker tests show that the tracker satisfactorily met nearly all of its performance requirements with the exception of output bandwidth which is on the order of one to three cycles per second rather than the ten cycles per second requested. In all other areas, the tracker performed as required. It reliably searched and tracked images of

Mars, Venus, and Jupiter under conditions of illumination corresponding to the three cycle per second output bandwidth.

Ultimate tracker performance was difficult to assess because the tracker performed better than the stability of the laboratory setup. During those periods when the laboratory collimator was stable, the tracker performance easily exceeded the requirements. The data presented in Section 7 is worst case data and is not corrected for collimator variation.

A few words are in order here about the forty foot collimator on which planet tracking testing took place. During the tests, instabilities on the order of several arc seconds were noted and were initially thought to be in the tracker. After much scrutiny it was determined that the collimator itself was unstable. Recent tests, based on August 1967 measurements and too late for inclusion in other sections of this report, yield preliminary information that the variations are probably seismic in nature and may correlate with tidal periods. Deviations of 3 arc seconds root-mean-square are often experienced, although there are also periods of several hours where the collimator instability cannot be measured. This information was not available during the testing period.

The operating characteristics of the breadboard tracker are as follows:

Field of View	4.5 x 4.5 minutes	Tracking Rate	15 arc sec/sec
Error Signal Slope	180 mv/arc sec	Offset Error	0.2 to 1.5 arc depending on illumination and planet shape
Noise Equivalent Angle	0.17 arc sec		
Linear Slope Limits	$\pm$ 2.25 arc min.		

The research breadboard was carried to a state of completion where it is possible to construct an engineering model planet tracker without difficulty. For example, optical, mechanical, and electronic designs are now available to generate the design of an engineering model. The engineering model of a flight configuration tracker could have all of the above performance characteristics; its estimated weight, power consumption, and size are 20 pounds, 5 watts, and 8.5 inches diameter x 13.5 inches long, respectively.

Even better performance is probably attainable with better spatial resolution on the Reconotron. It is likely that the resolution of the tube was a major factor in limiting the performance of the tracker to that described in Section 7. As explained previously, the other dominant factor was the collimator instability. We do not mean to imply that the Reconotron was inferior in overall performance. In fact, the vendor was quite cooperative in supplying a tube with proper linearity characteristics. More careful attention to tube selection in the area of resolution or possibly very careful adjustment of focusing potentials would have realized much better tube performance.

To summarize, the performance of the breadboard coupled with the results of the optimization study are satisfactory enough to allow the straightforward development of an engineering model planet tracker.

8.6 POSSIBLE FUTURE ACTIVITIES

As is normal at the completion of any experimental breadboard program involving significant technical challenge, there are several additional items of work which are appropriate areas for future activity. This section is not intended to be a solicitation for additional support, but rather is a listing of work which could be done to improve theperformance and applicability of the planet tracker.

- As previously mentioned, the experimental evidence indicates that the planet tracker breadboard performed well enough so that the design can readily be configured into an engineering model of space hardware. During the design, attention was paid to electronic design which would operate over the temperature range encountered in space flight. Also, board layouts were accomplished on a circuit function basis so that individual boards could be repackaged using welded modules or integrated circuits on a board-by-board basis. Optical and mechanical design was also done so that the tracker could easily be built as an engineering model. It, therefore, appears to be quite reasonable to consider rebuilding the breadboard tracker as an engineering model.

- The laboratory tests indicate that further work needs to be done on the CBS Laboratories' Reconotron, particularly in the area of spatial resolution. It would be appropriate to interact more extensively with CBS and possibly Electro-Mechanical Research regarding electrostatic image dissectors for applications of this type. Emphasis is also needed on the question of scan linearity, and the effect of nonlinearities on tracker performance. It is possible that careful measurements could be made on the existing tube and various tube voltages varied in an effort to improve resolution. It is likely that the most significant performance improvements on the breadboard tracker would come from improved Reconotron resolution.

- The results of the optimization studies conducted under the follow-on contract showed that the current tracker design has been partially optimized. It is possible to apply more stringently the results of the optimization study to the current tracker and experimentally verify that performance predicted by the optimization study could be obtained. It would further be of interest to change the bandwidth parameters to values which are more realistic in terms of probable application.

- If sufficient interest exists, it is feasible to make performance tests on the current breadboard, but with a different optical system, to simulate operation under earth or moon horizon scanning situations. Interest in this possibility was shown at NASA/LRC and NASA/GSFC.

- Similarly, the design of the tracker is flexible enough so that it can be adapted to an approach guidance application without too much dificulty. It should be easy to reconfigure the tracker for approach

guidance missions and to determine experimentally its performance for that application.

Our ability to make long term precision measurements on the tracker was hampered by lack of Reconotron resolution and by instability on the collimator. The collimator instability is being investigated under LMSC funds and the collimator will be redesigned and rebuilt. If better Reconotron spatial resolution can be obtained out of the current tube, it would be desirable to make more extensive and more accurate measurements on performance of the tracker against gibbous, oblate (Jupiter), and crescent targets.

Section 8 is intended to collect all salient information and to report it in the perspective of having completed the program. Information contained in a report like this, no matter how detailed, is only a small part of the actual information available. Significant amounts of experimental evidence, only summarized in Section 7, are available for inspection and discussion.

REFERENCES

1.1 LMSC Proposal #893537, Study and Development for a Planet Tracker, dated 29 June 1964

1.2 Contract NAS 2-2485

1.3 Contract NAS 2-2485 F/O

3.1 C. W. Allen, Astrophysical Qualities, 2nd Edition

3.2 P. C. Keenan, "Basic Astronomical Data," Stars and Stellar Systems, Vol. III

3.3 L. Larmore, "A Note on Infrared Stellar Magnitudes," October 1954 Publication of Rand Corporation.

3.4 Vol. III, Planets and Satellites, C. P. Kuiper

4.1 A. E. Anderson, R. W. Decker, Thermicon Tube Performance, Proceedings of IRIS, Vol. 5-1, January 1960, P. 435 - 440

4.2 Laser, M. Cholet, P., H. Emmons, Electronic Scanning System for Infrared Images, I.R.E., December 1959, p. 2069-2075.

4.3 Space/Aeronautics, November 1961, p. 105-123

4.4 NASA Request for Proposal, A-8516, dated May 15, 1964

4.5 Servo Corporation of America Thermistor Data Sheet for Model GI 13227575, 1962

4.6 R. W. Engstrom, "Absolute Spectral Response Characteristics of Photosensitive Devices," RCA Review, June 1960, Vol. XXI, No. 2

5.1 "Infrared Diffraction Pattern Scanning Study, Final Report", R. P. Day, R. G. Clow, R. C. Redden, LMSC 2-03-62-2, October 1962, AD #447641

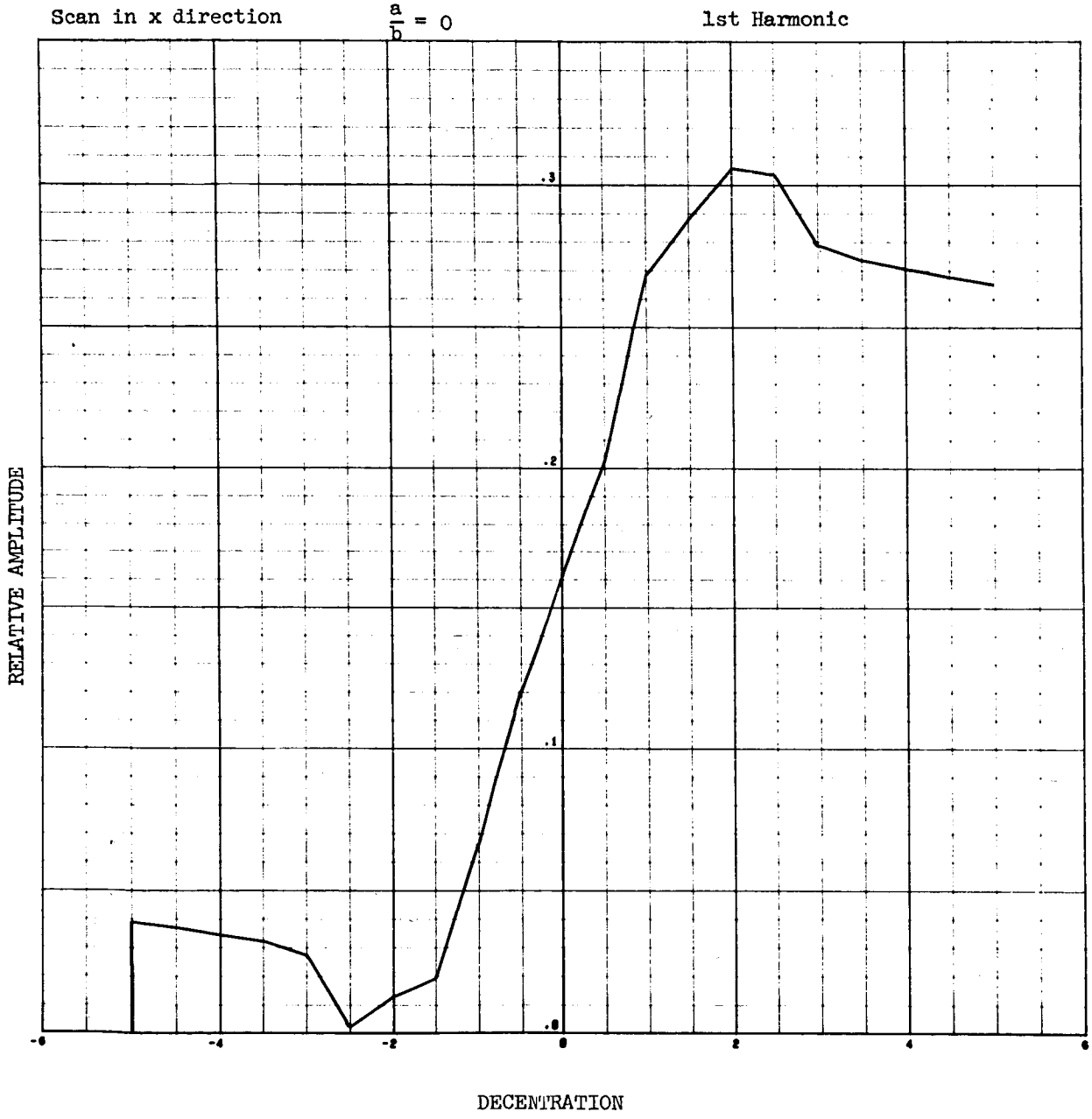
Scan in x direction
a/b = 0
1st Harmonic
RELATIVE AMPLITUDE
.3
.2
.1
0
-6
-4
-2
0
2
4
6
DECENTRATION

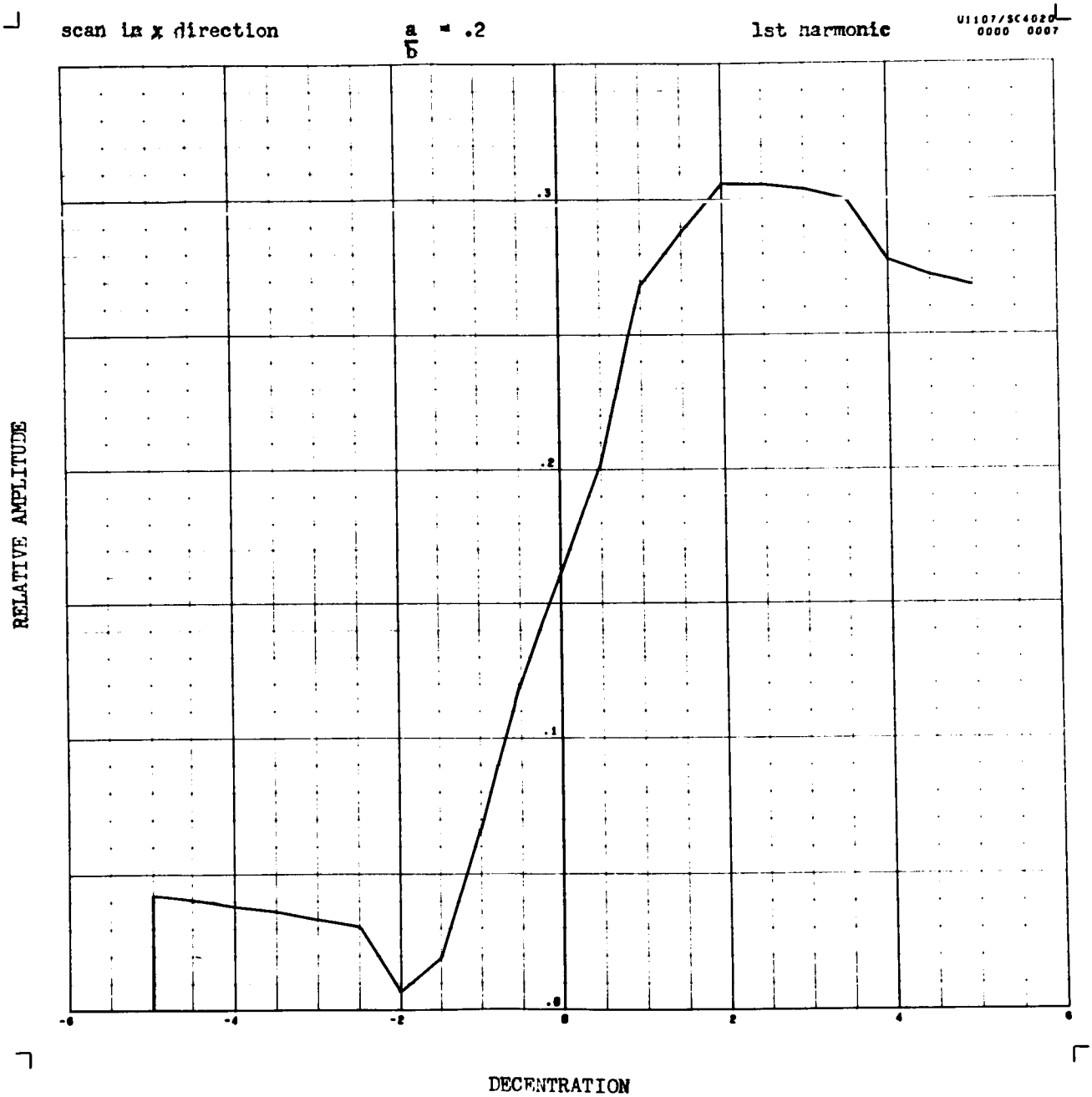
scan in x direction
a/b = .2
1st harmonic
U1107/SC4020
0000 0007
RELATIVE AMPLITUDE
.3
.2
.1
.0
-6
-4
-2
0
2
4
6
DECENTRATION

Appendix
-2-

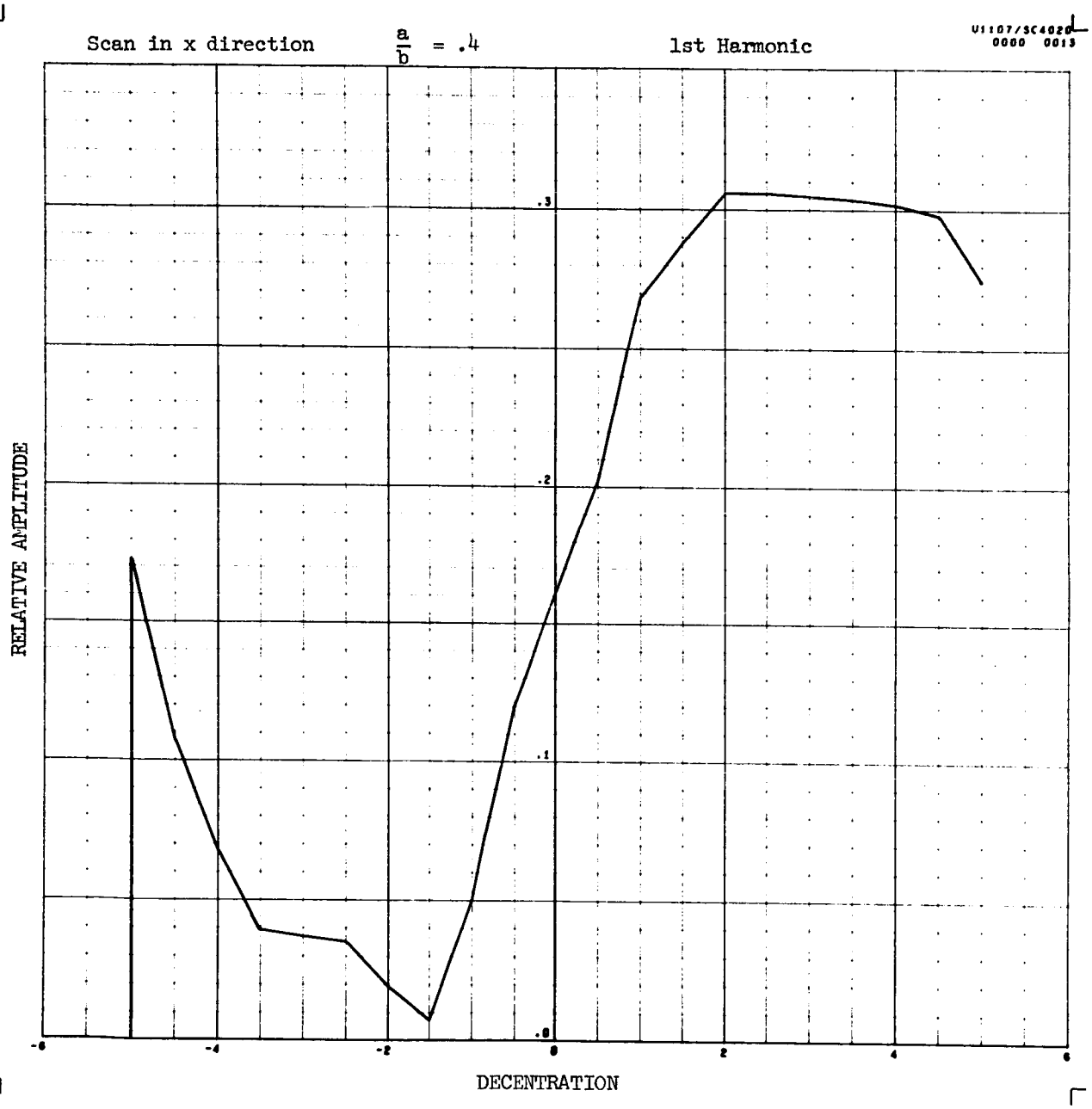
Scan in x direction
a/b = .4
1st Harmonic
V1107/SC4020
0000 0013
RELATIVE AMPLITUDE
.3
.2
.1
.0
-6
-4
-2
0
2
4
6
DECENTRATION

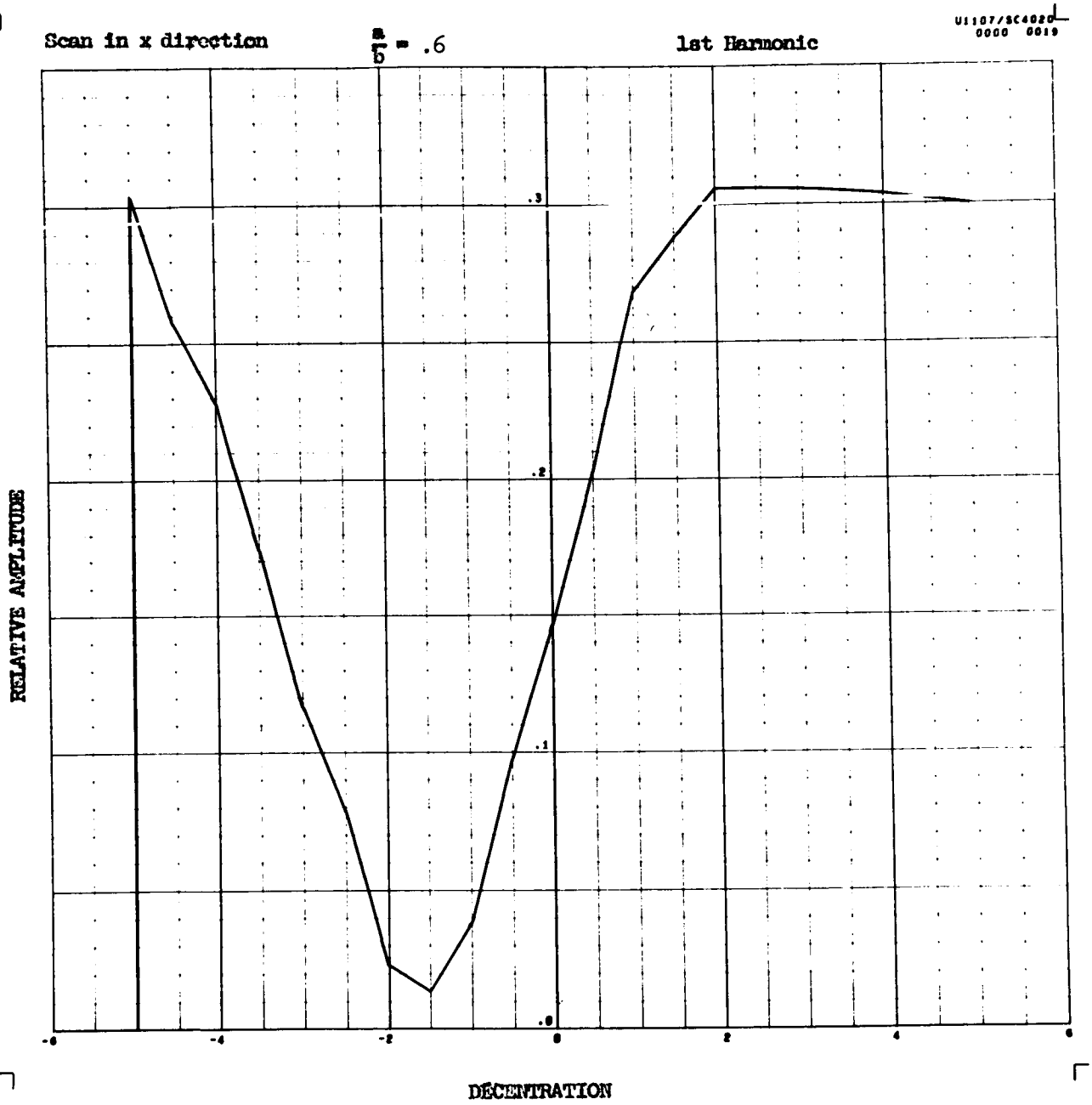
Scan in x direction
a/b = .6
1st Harmonic
U1107/SC4020
0000 0019
RELATIVE AMPLITUDE
.3
.2
.1
.0
-6
-4
-2
0
2
4
6
DECENTRATION

Appendix

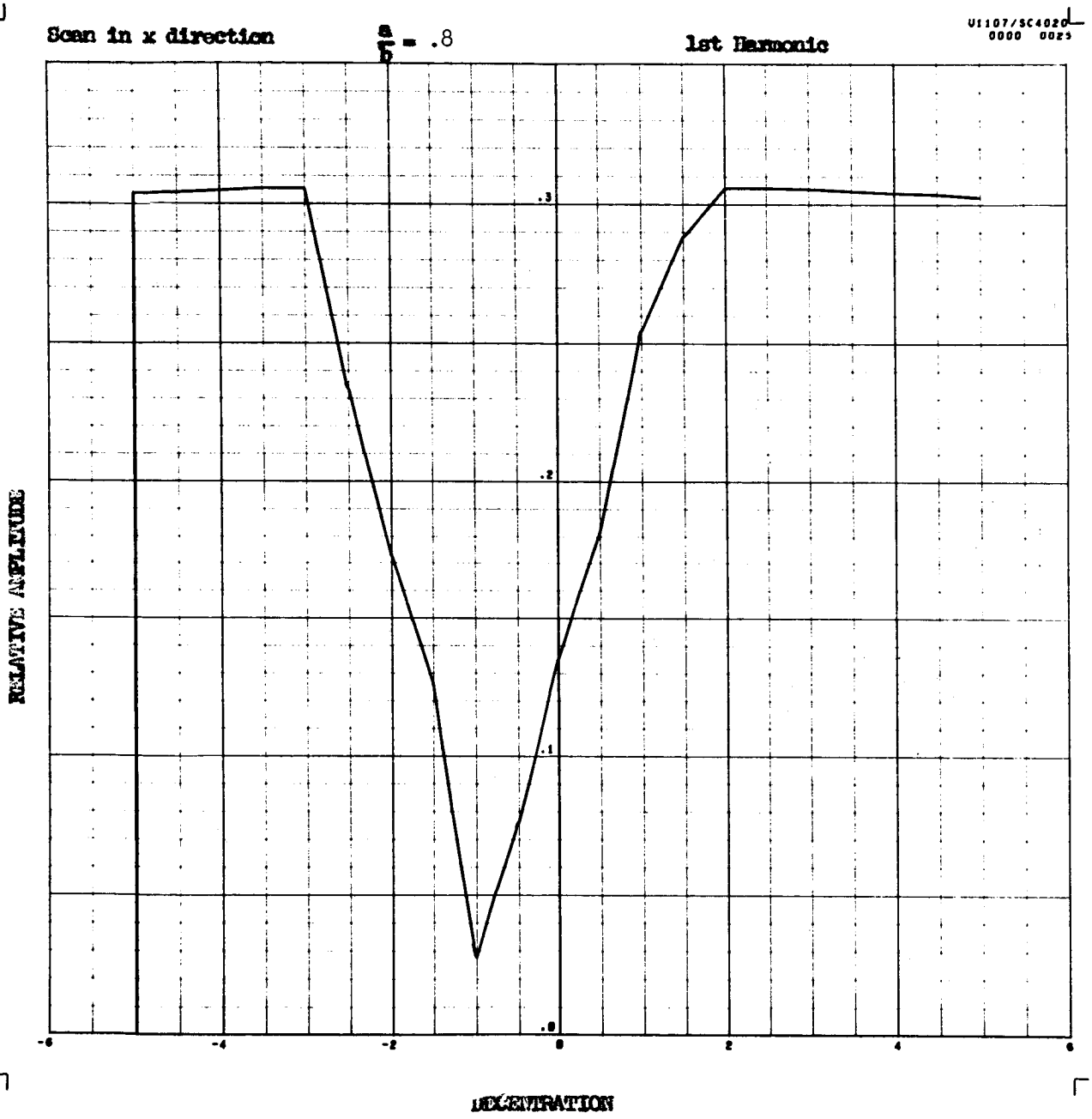
Scan in x direction
a/b = .8
1st Harmonic
UI107/SC4020
0000 0025
RELATIVE AMPLITUDE
.3
.2
.1
.0
-6
-4
-2
0
2
4
6
DECENTRATION

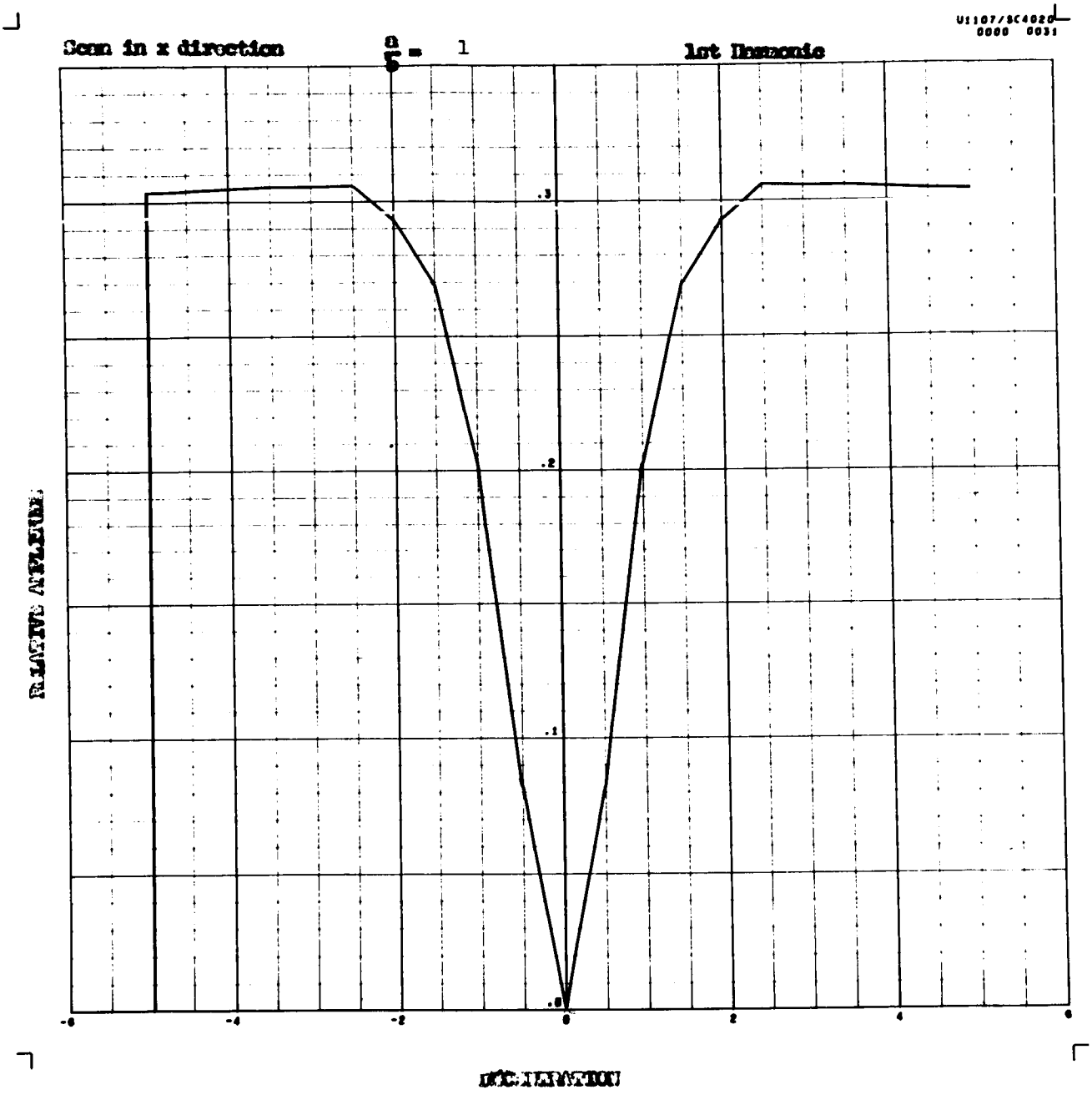

Appendix
-6-

Scan in y direction $\frac{a}{b} = 0$ 1st Harmonic

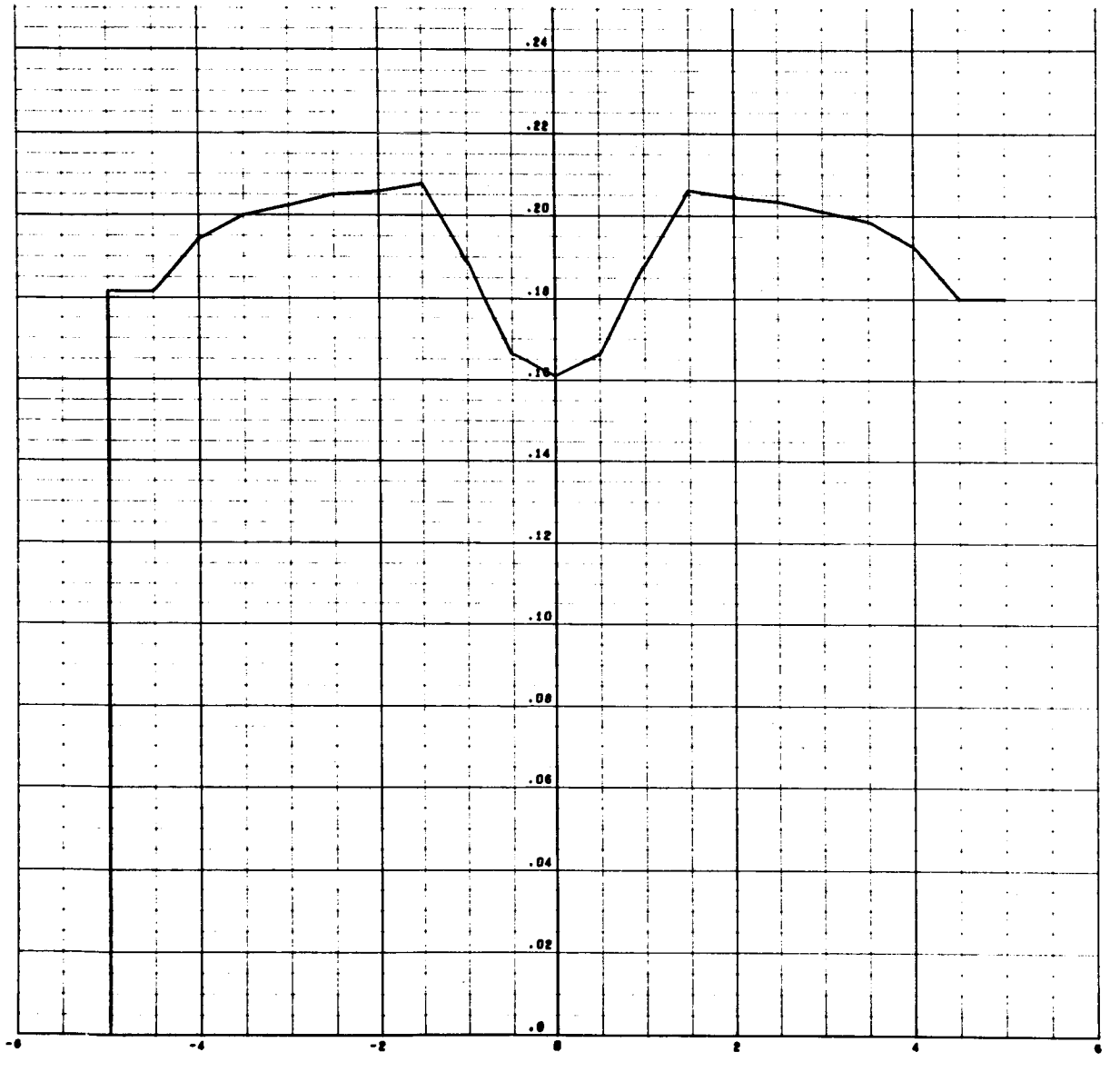

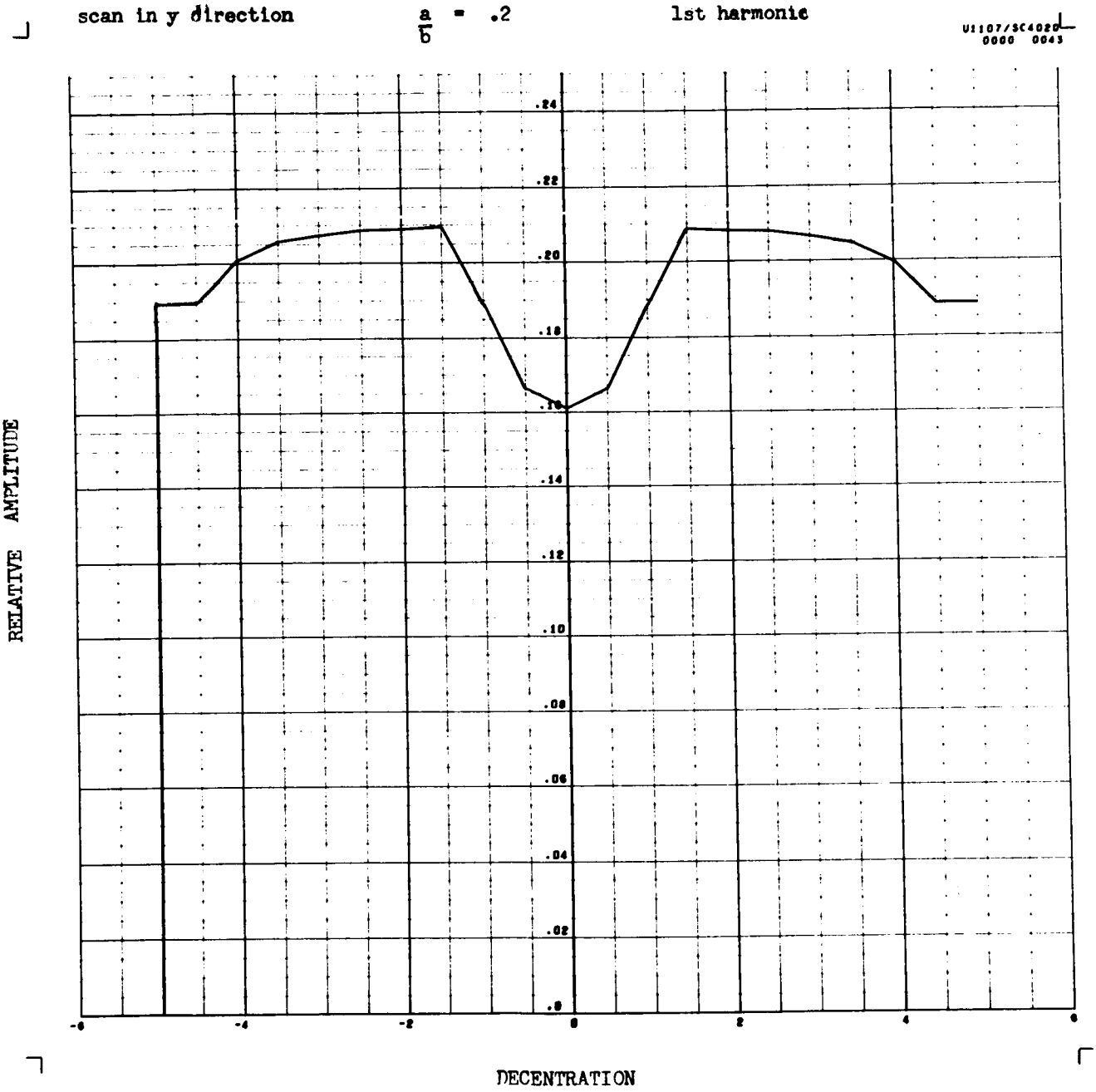
scan in y direction
a/b = .2
1st harmonic
U1107/SC4020
0000 0043
RELATIVE AMPLITUDE
.24
.22
.20
.18
.16
.14
.12
.10
.08
.06
.04
.02
.0
-6
-4
-2
0
2
4
6
DECENTRATION

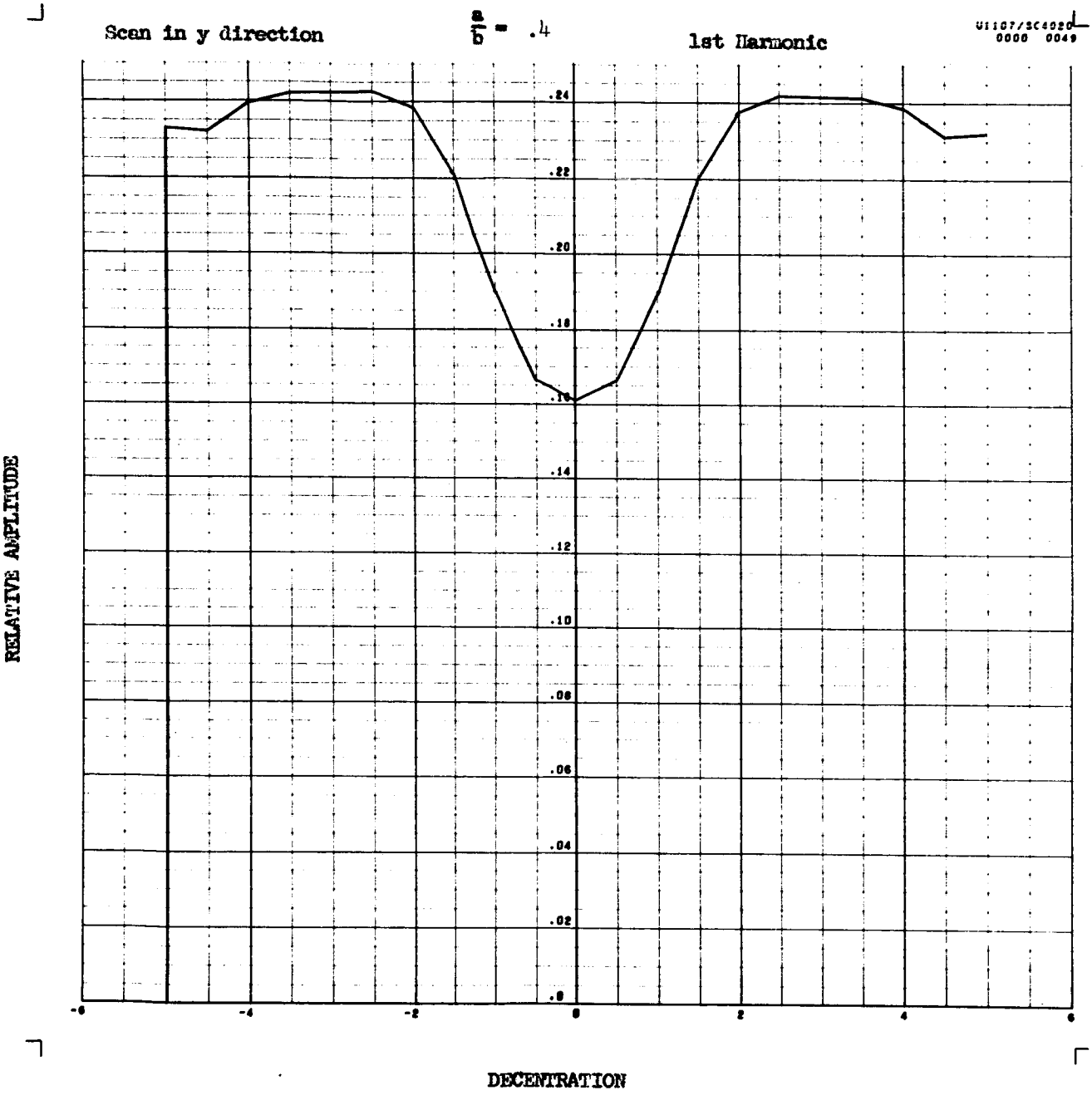
Scan in y direction
a/b = .4
1st Harmonic
U1107/SC4020
0000 0049
.24
.22
.20
.18
.16
.14
.12
.10
.08
.06
.04
.02
.0
-6
-4
-2
0
2
4
6
RELATIVE AMPLITUDE
DECENTRATION

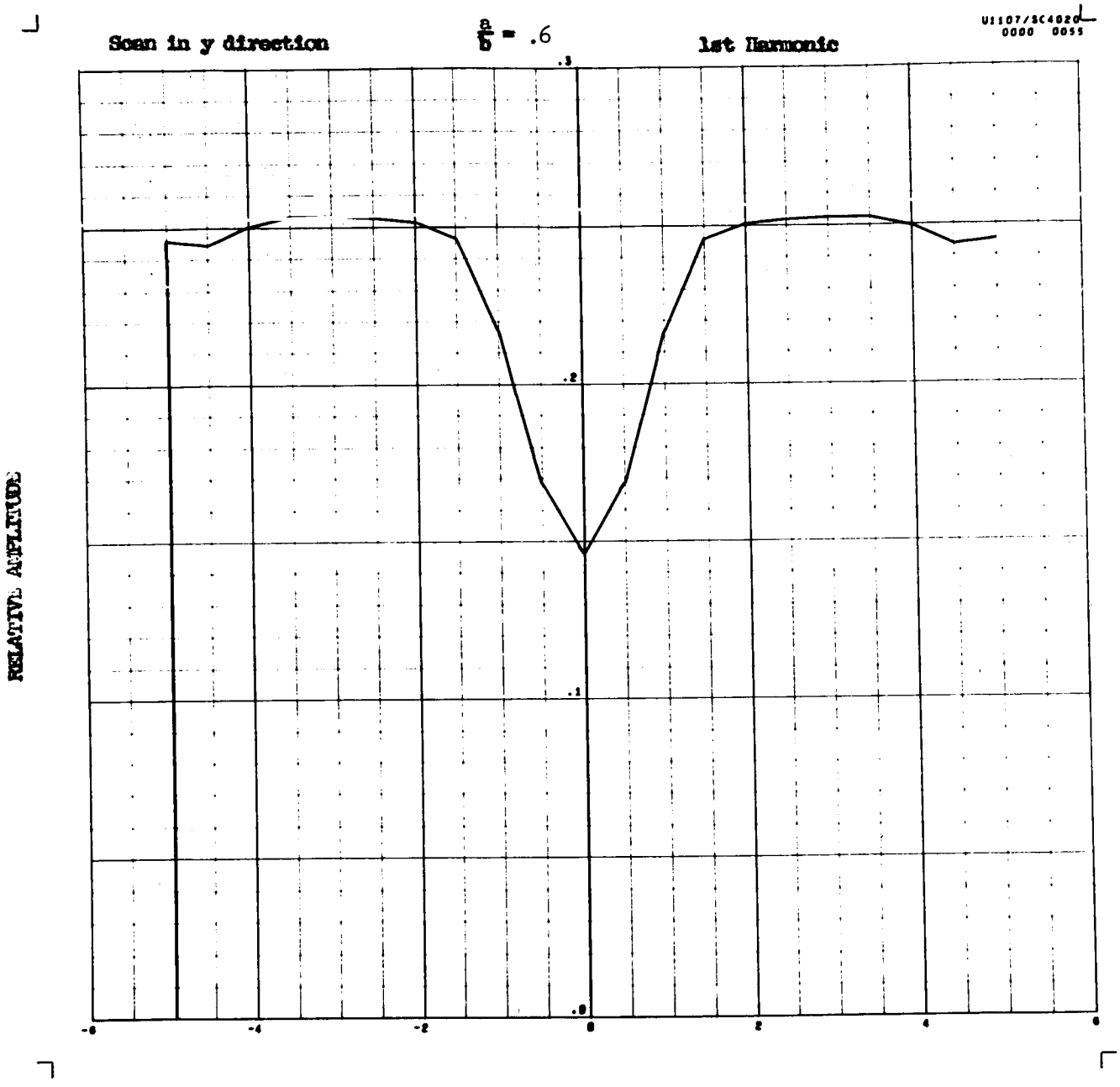
Scan in y direction
a/b = .6
1st Harmonic
U1107/SC4020
0000 0055
RELATIVE AMPLITUDE
.3
.2
.1
.0
-6
-4
-2
0
2
4
6
DISCRIMINATION

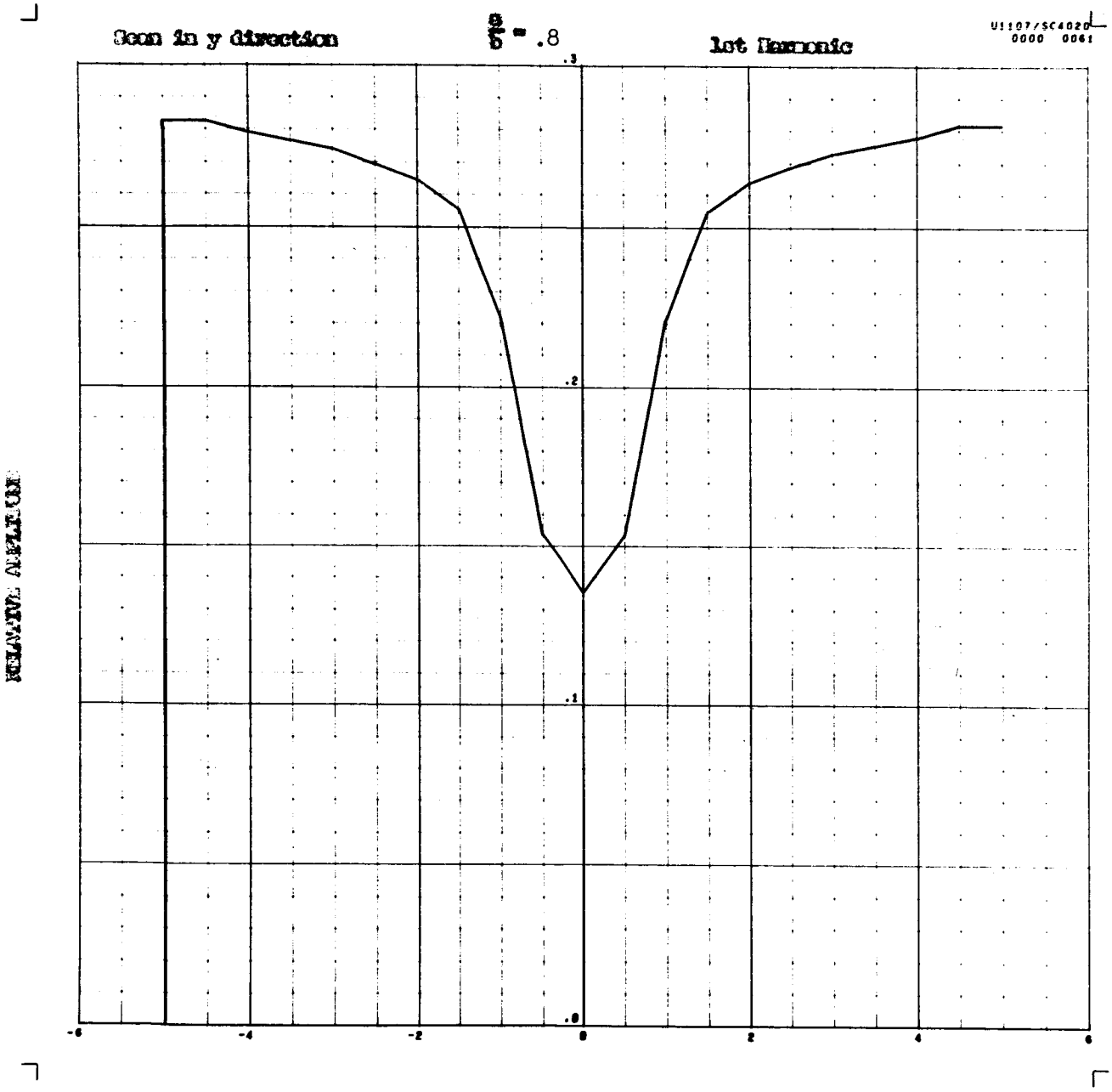
Scan in y direction
a/b = .8
1st Harmonic
U1107/SC4020
0000 0061
.3
.2
.1
.0
-6
-4
-2
0
2
4
6

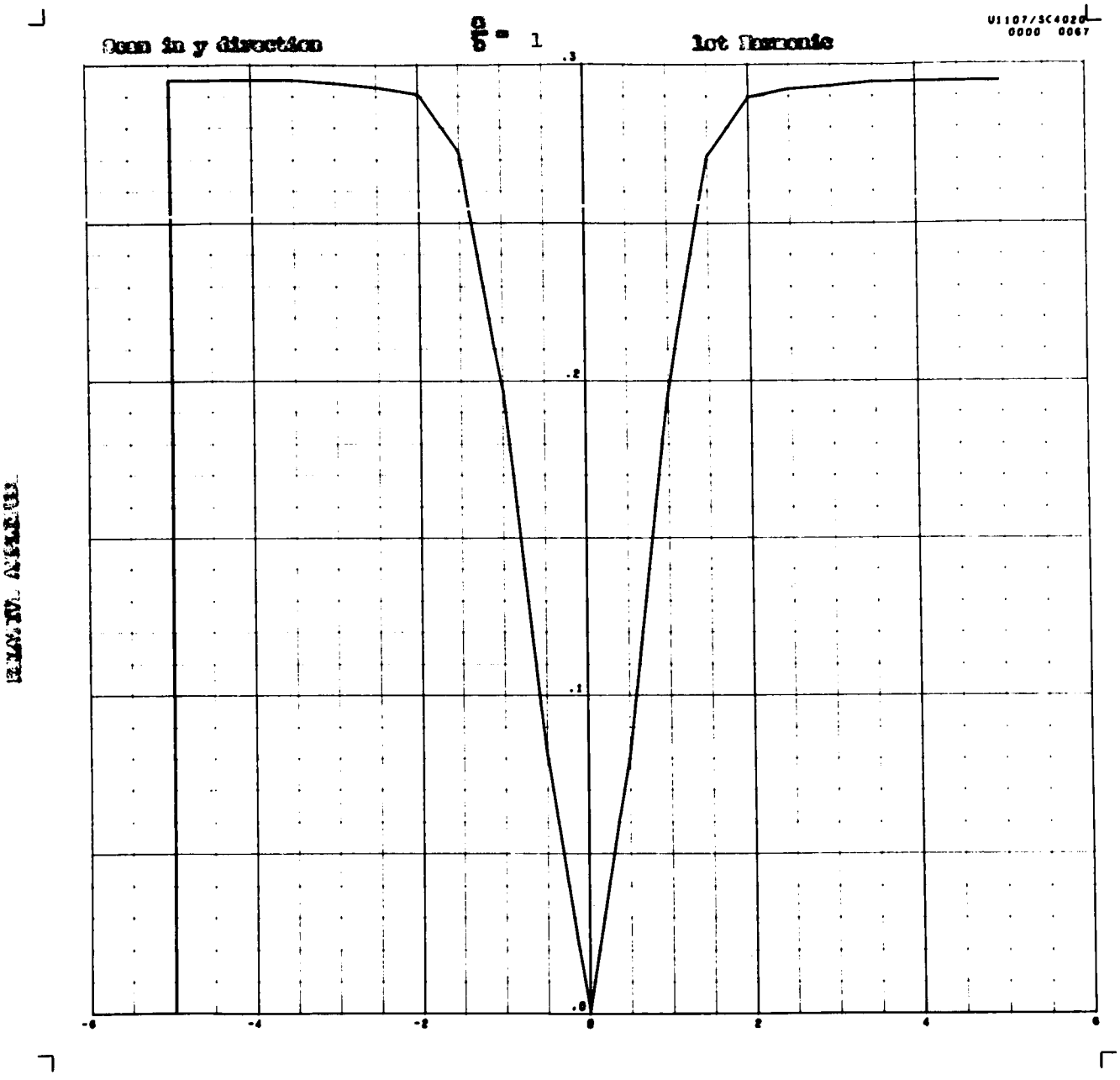
Scan in y direction
n/n0 = 1
lot Harmonic
U1107/SC4020
0000 0067
.3
.2
.1
.0
-6
-4
-2
0
2
4
6

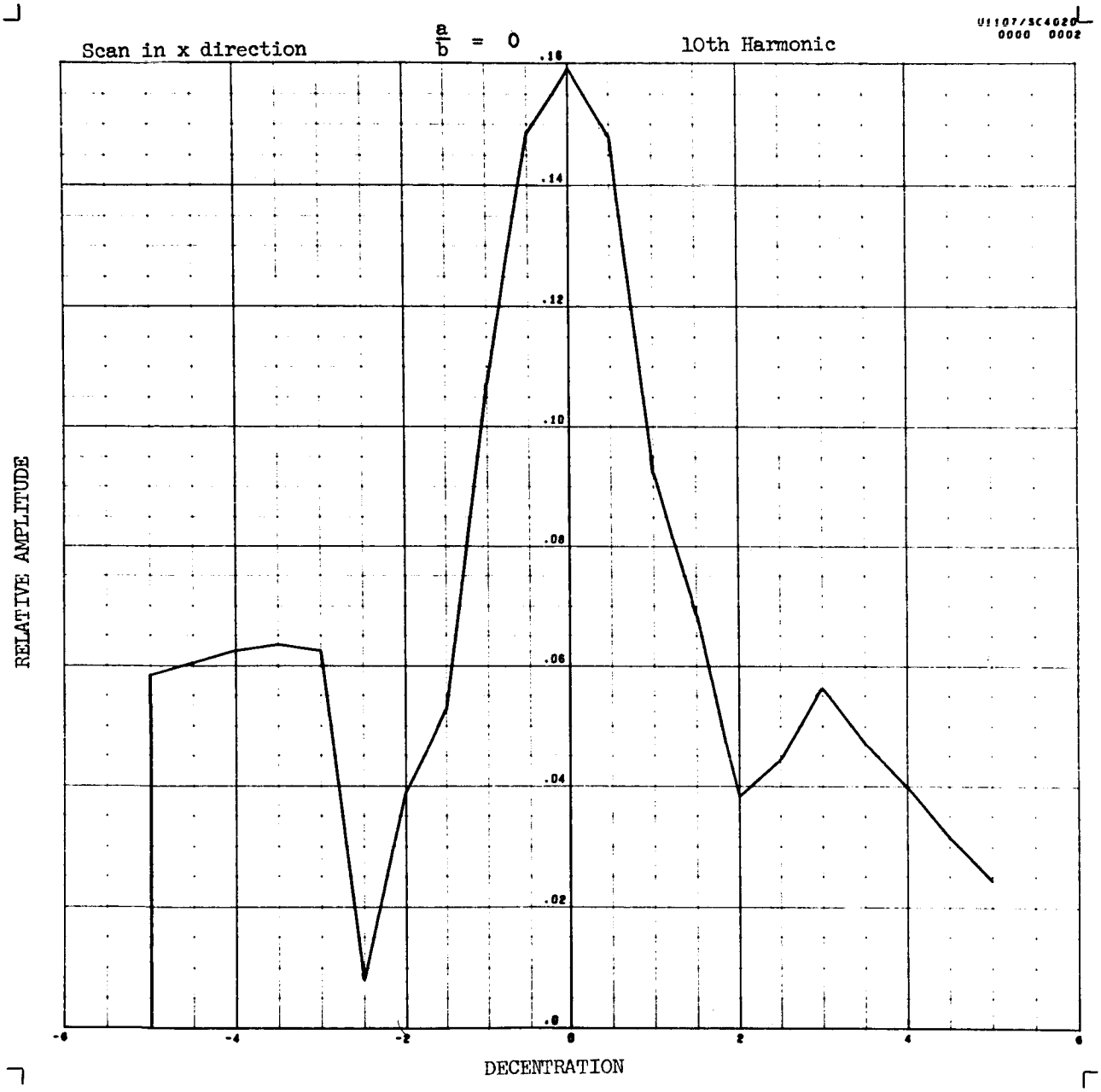
Scan in x direction
a/b = 0
10th Harmonic
U1107/SC4020
0000 0002
.16
.14
.12
.10
.08
.06
.04
.02
.0
-6
-4
-2
0
2
4
6
RELATIVE AMPLITUDE
DECENTRATION

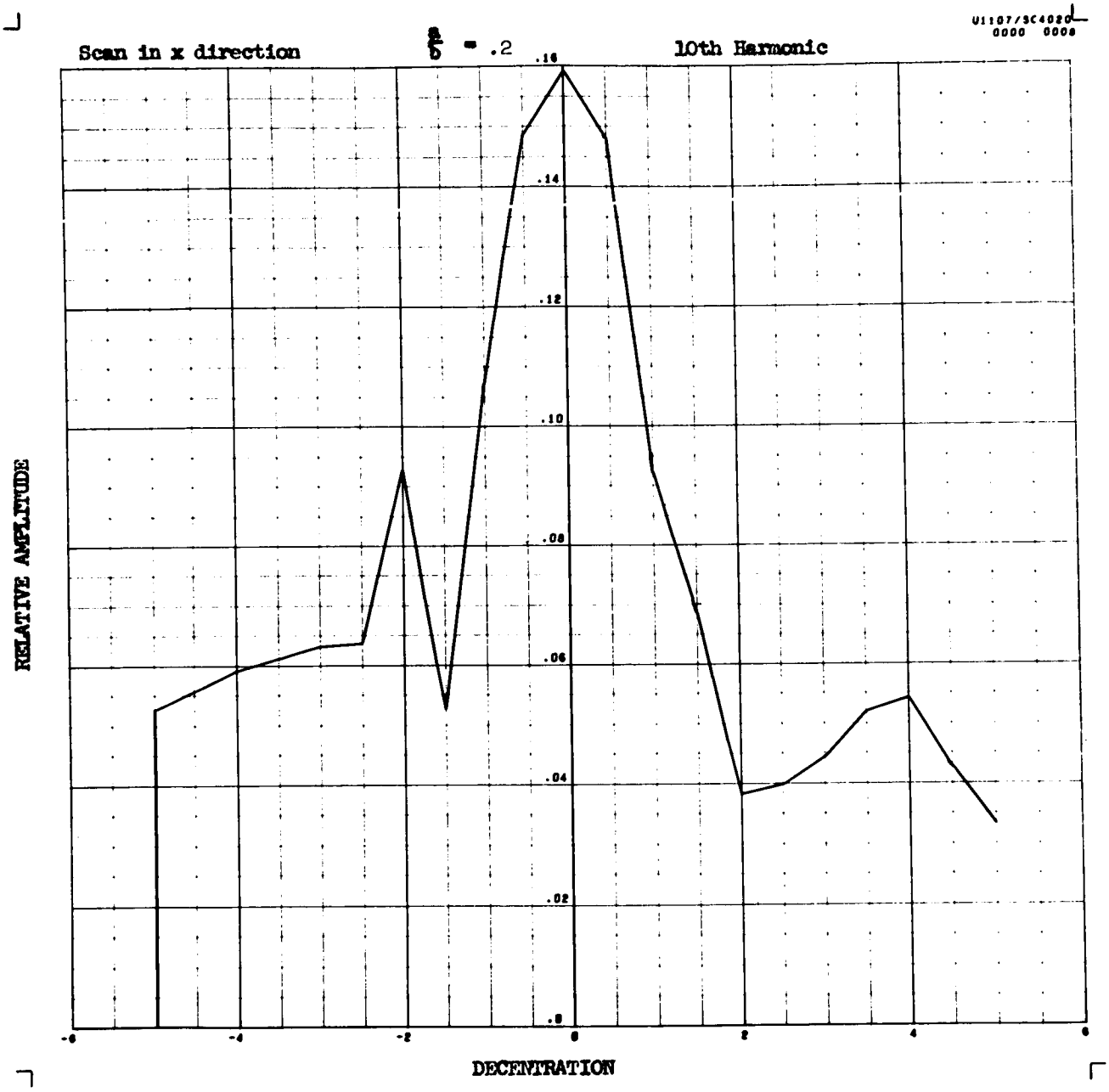
U1107/SC4020
0000 0000
Scan in x direction
a/b = .2
10th Harmonic
RELATIVE AMPLITUDE
.16
.14
.12
.10
.08
.06
.04
.02
0
-6
-4
-2
0
2
4
6
DECENTRATION

scan in x direction $\frac{a}{b} = .4$ 10th harmonic

U1107/SC4020
0000 0014

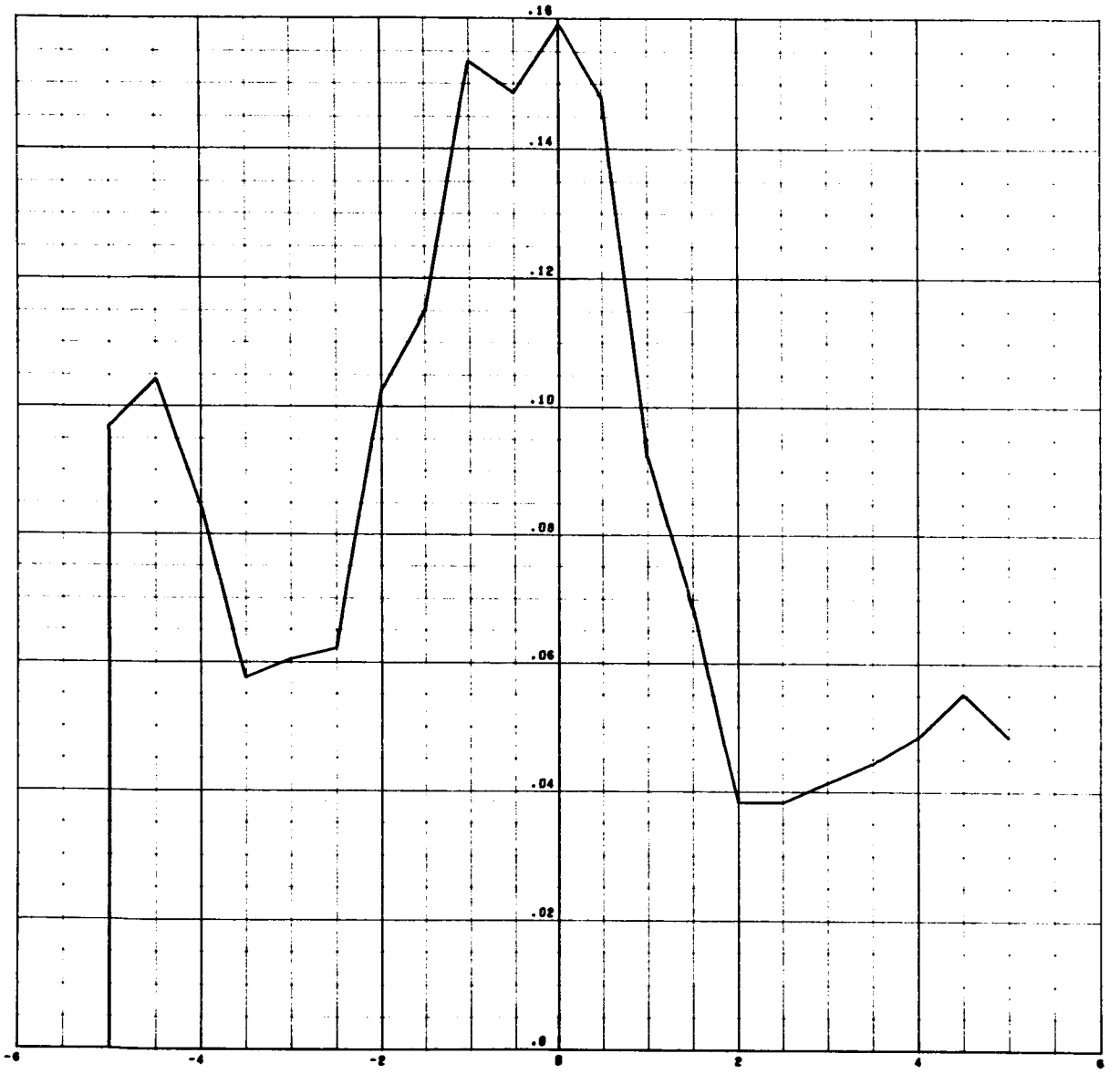

RELATIVE AMPLITUDE

DECENTRATION

Appendix

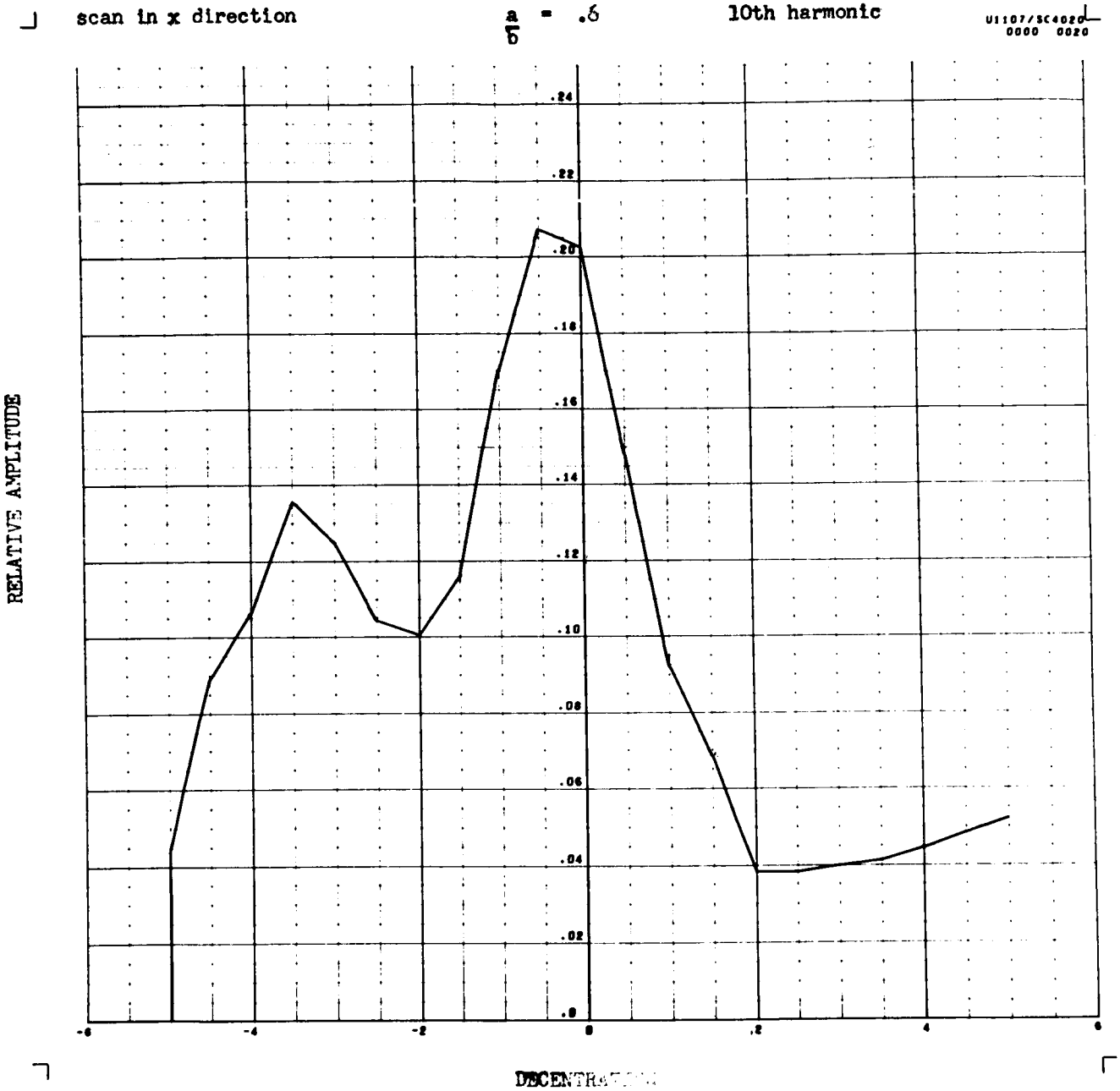
scan in x direction
a/b = .6
10th harmonic
U1107/SC4020
0000 0020
RELATIVE AMPLITUDE
.24
.22
.20
.18
.16
.14
.12
.10
.08
.06
.04
.02
.0
-6
-4
-2
0
2
4
6

Appendix

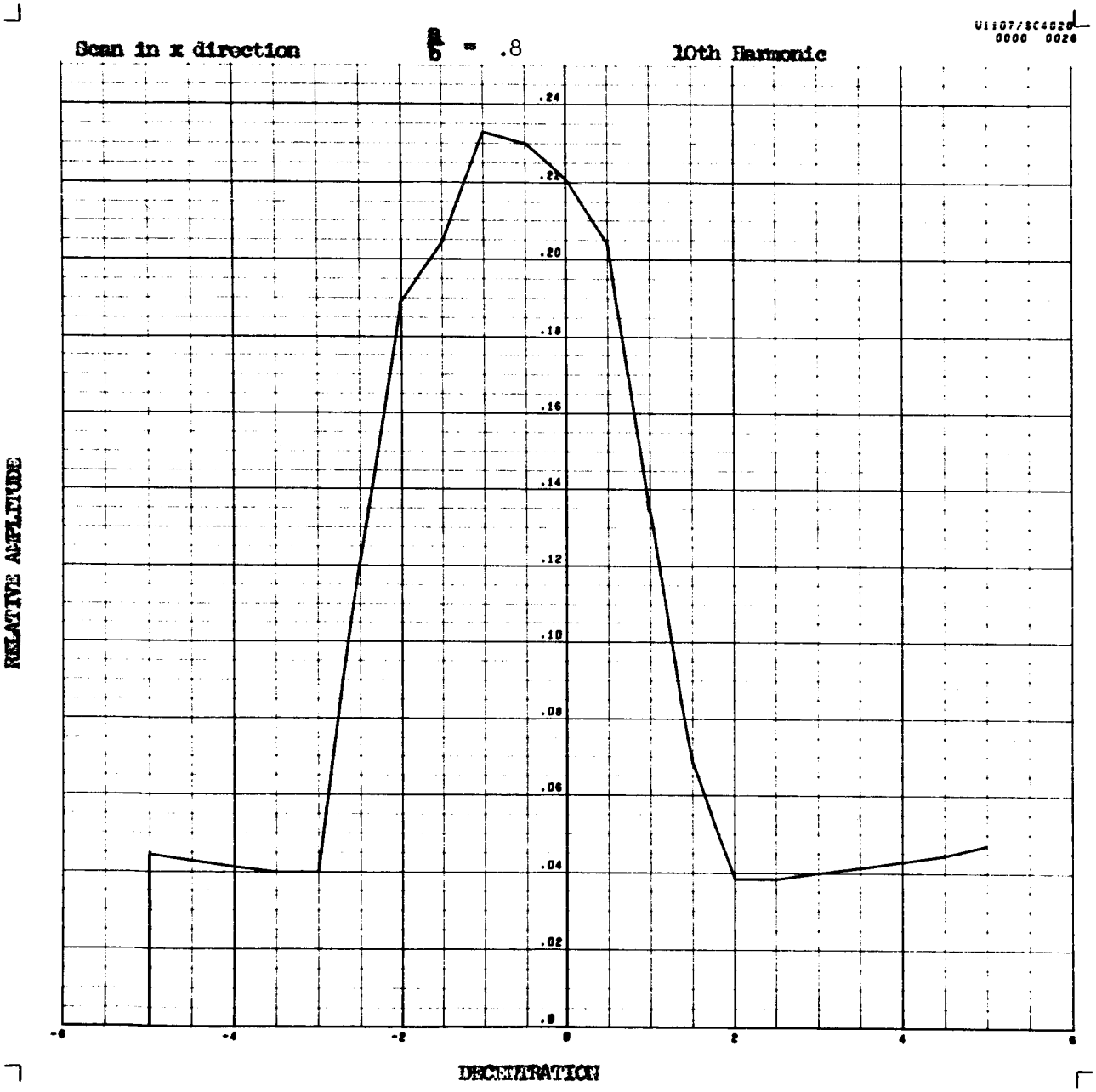
Scan in x direction
a/b = .8
10th Harmonic
RELATIVE AMPLITUDE
DECENTRATION
.24
.22
.20
.18
.16
.14
.12
.10
.08
.06
.04
.02
.0
-6
-4
-2
0
2
4
6

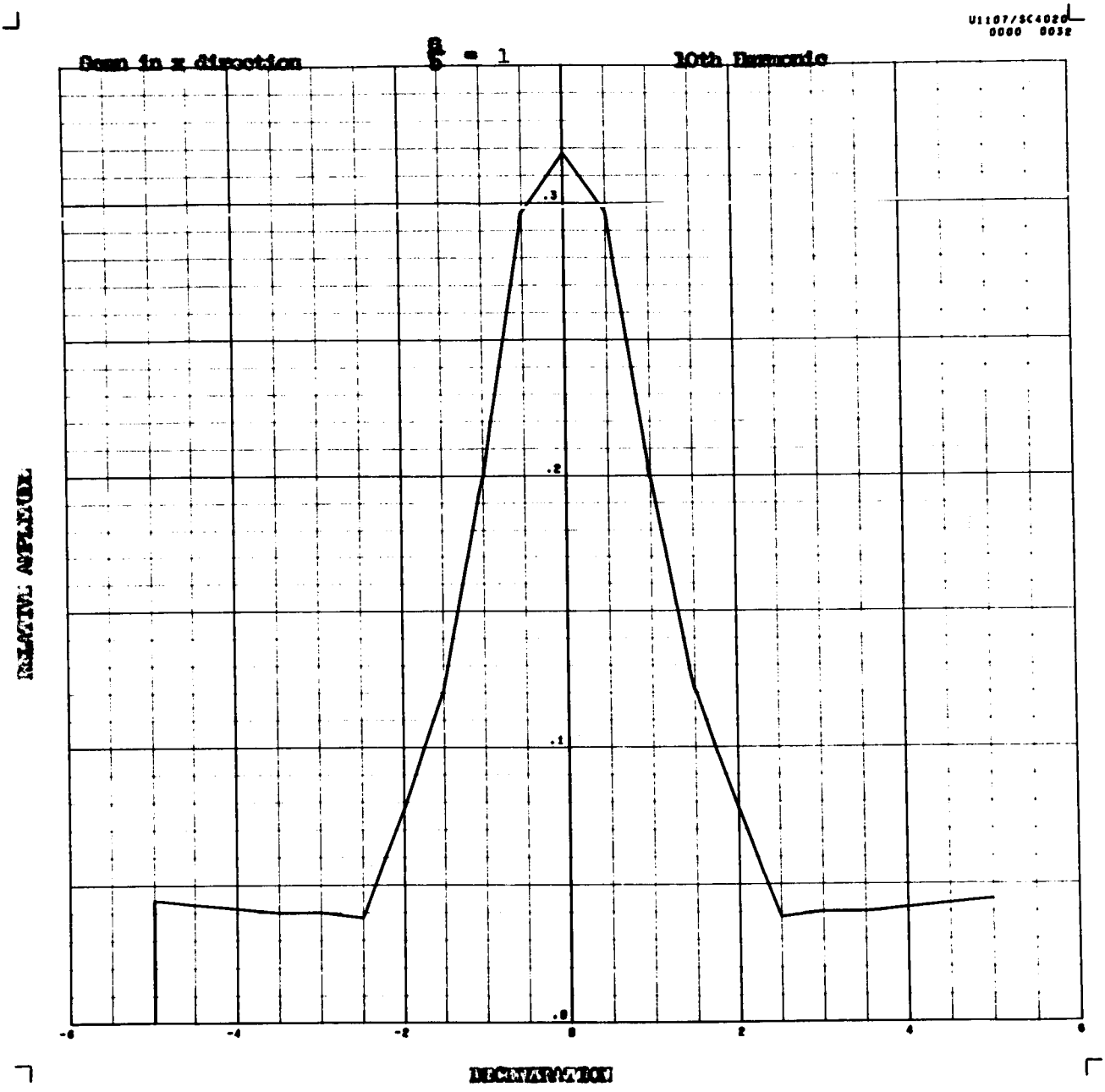
U1107/SC4020
0000 0032
Beam in x direction
$\frac{\delta}{\delta}$ = 1
10th Harmonic
.3
.2
.1
0
-6
-4
-2
0
2
4
6

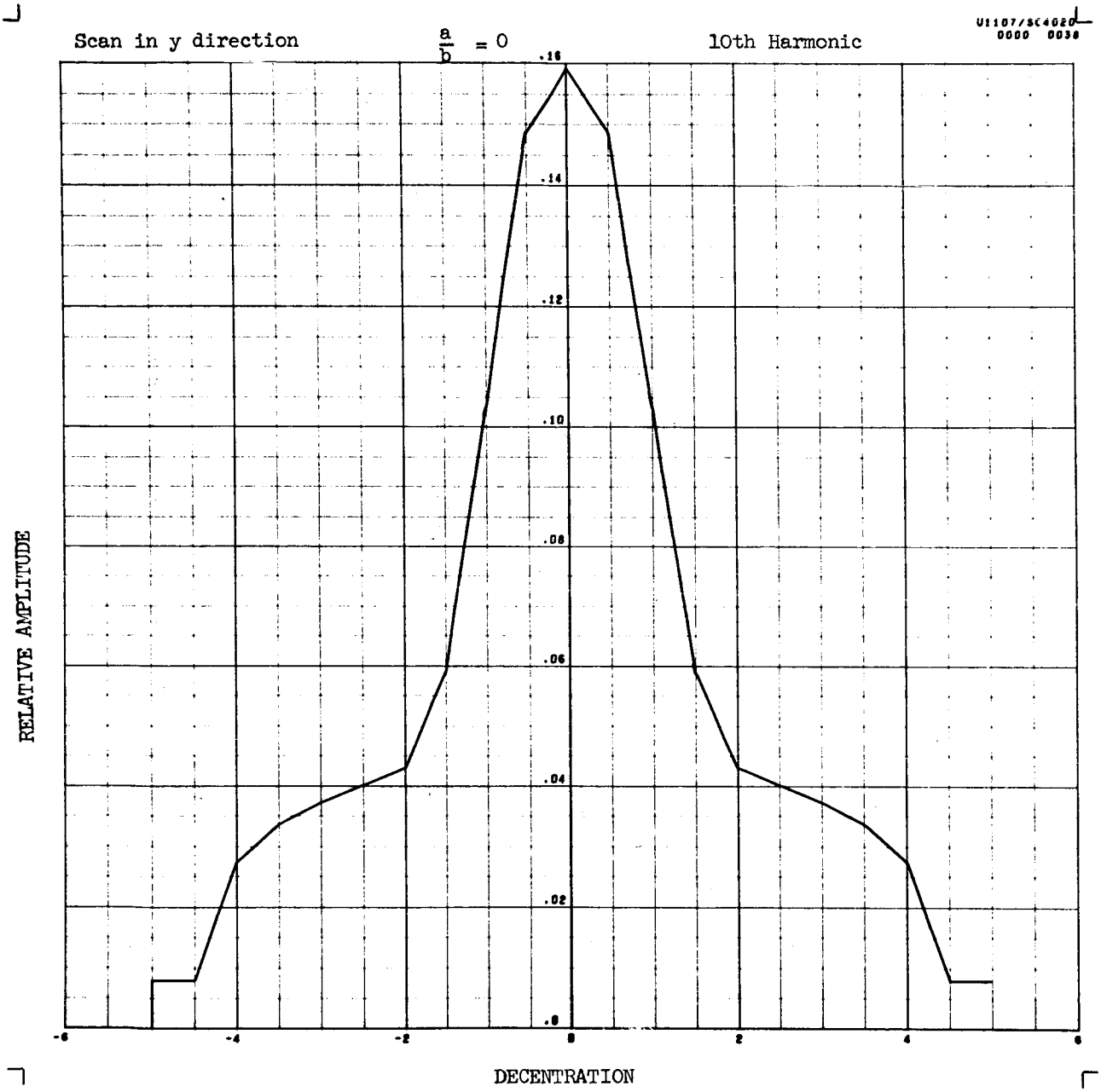
Scan in y direction
a/b = 0
10th Harmonic
U1107/SC4020
0000 0038
.16
.14
.12
.10
.08
.06
.04
.02
.0
-6
-4
-2
0
2
4
6
RELATIVE AMPLITUDE
DECENTRATION

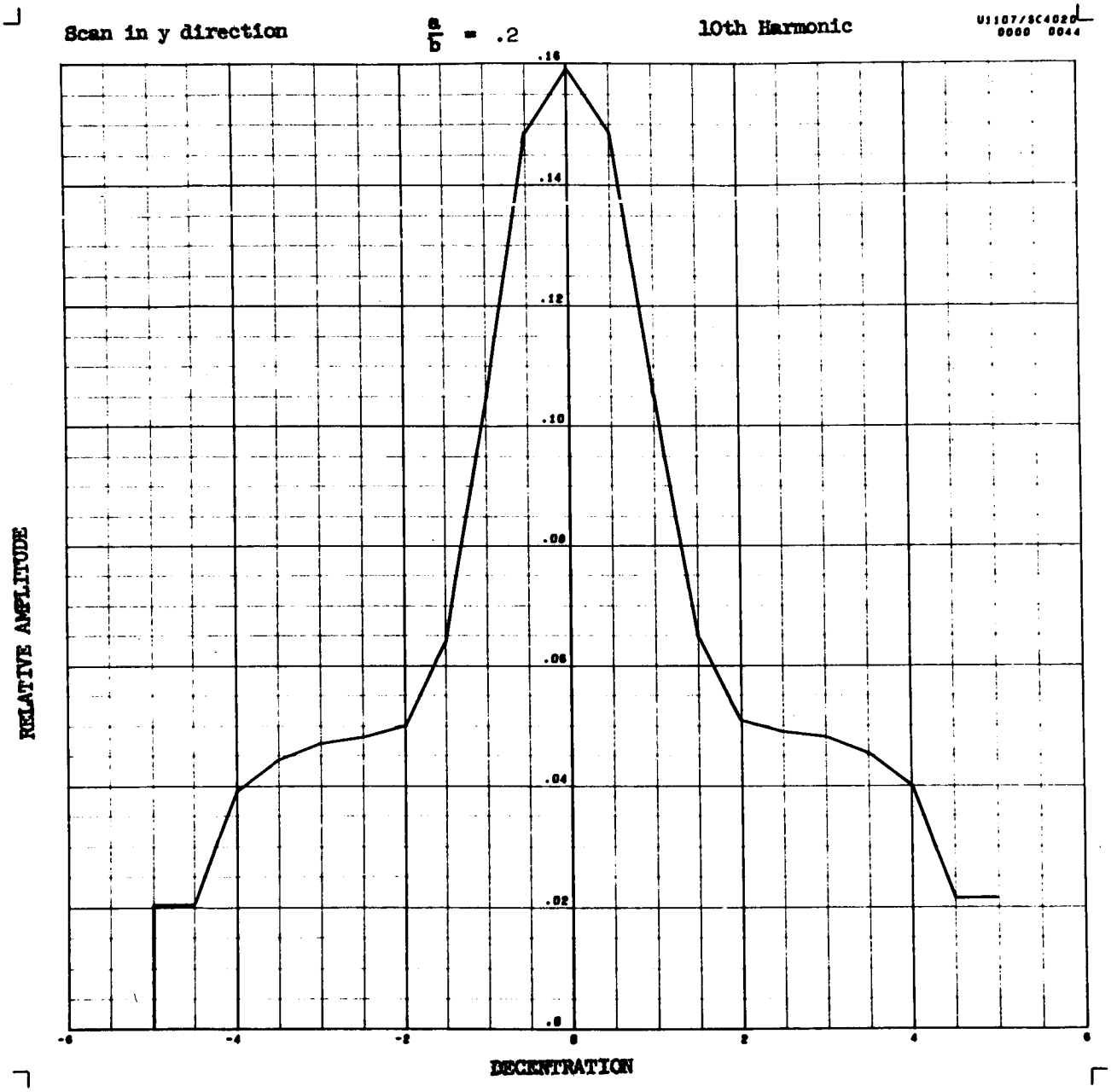
Scan in y direction
a/b = .2
10th Harmonic
U1107/SC4020
0000 0044
RELATIVE AMPLITUDE
.16
.14
.12
.10
.08
.06
.04
.02
.0
-6
-4
-2
0
2
4
6
DECENTRATION

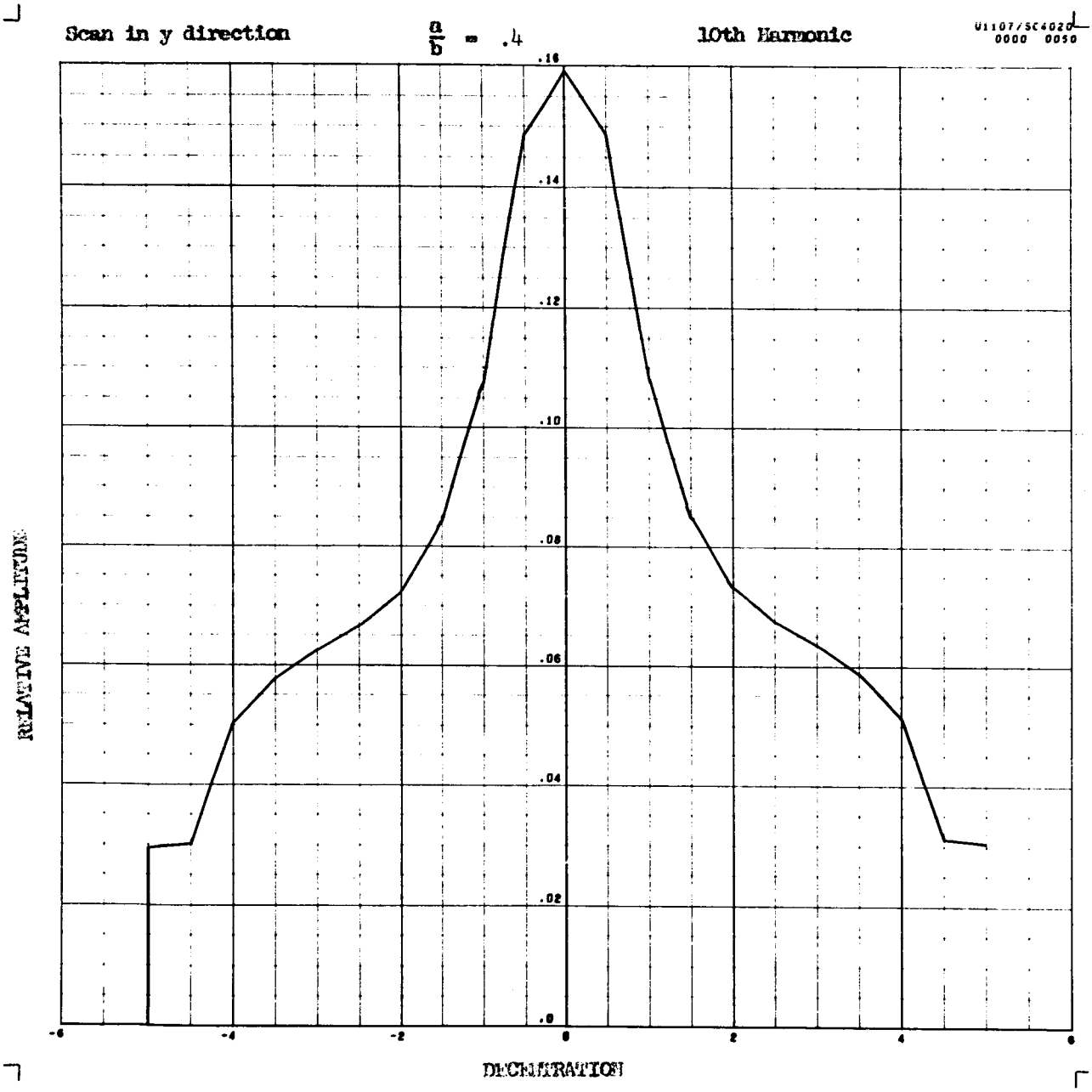
Scan in y direction
a/b = .4
10th Harmonic
U1107/SC4020
0000 0050
.16
.14
.12
.10
.08
.06
.04
.02
.0
-6
-4
-2
0
2
4
6
RELATIVE AMPLITUDE
DECLINATION

Appendix

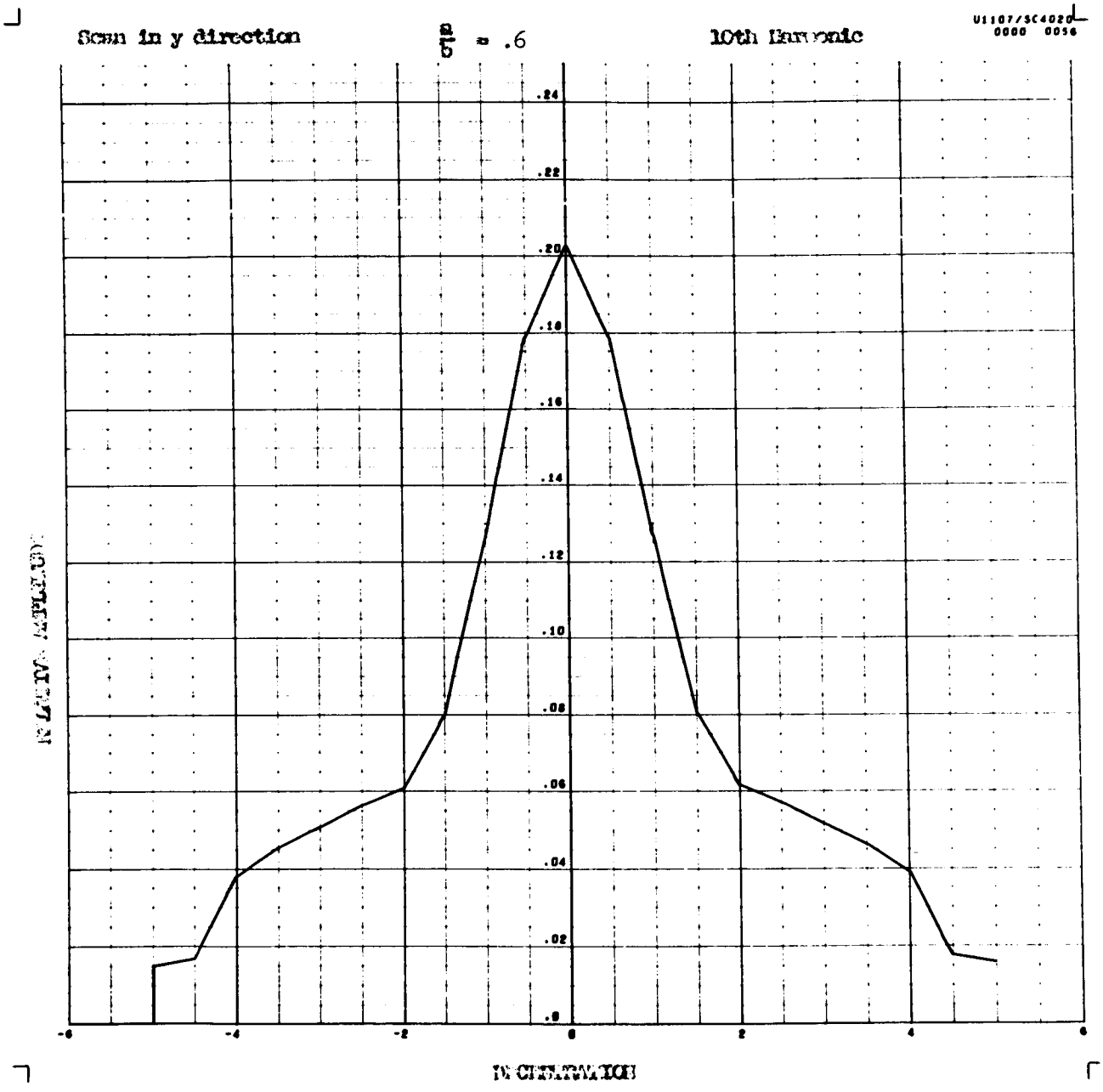
Scan in y direction
$\frac{\sin}{\sin_0}$ = .6
10th Harmonic
U1107/SC4020
0000 0056
.24
.22
.20
.18
.16
.14
.12
.10
.08
.06
.04
.02
.0
-6
-4
-2
0
2
4
6

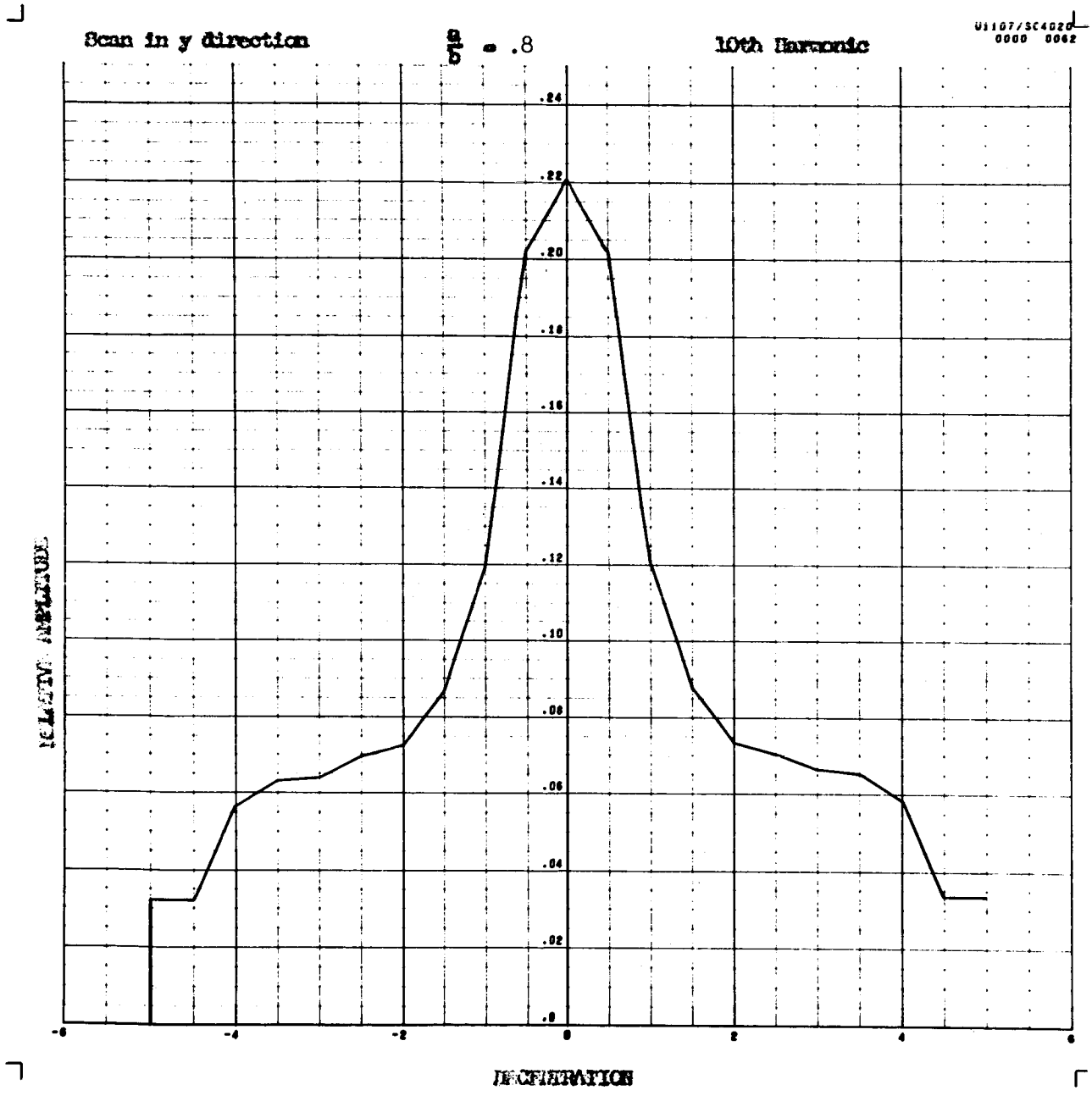
Scan in y direction
$\frac{a}{\lambda}$ = .8
10th Harmonic
01107/SC4020
0000 0062
.24
.22
.20
.18
.16
.14
.12
.10
.08
.06
.04
.02
.0
-6
-4
-2
0
2
4
6